Amalie My Olsen

Leaching and Modelling of LIB Black Mass (BM) for Metal Recovery

Graduate thesis in Chemical Engineering and Biotechnology
Supervisor: Ragnhild Elizabeth Aune
Co-supervisor: Daniel Perez Clos
August 2022

Graduate thesis

Kim Ramberghaug / NTNU

NTNU
Norwegian University of
Science and Technology

Amalie My Olsen

Leaching and Modelling of LIB Black Mass (BM) for Metal Recovery

Graduate thesis in Chemical Engineering and Biotechnology
Supervisor: Ragnhild Elizabeth Aune
Co-supervisor: Daniel Perez Clos
August 2022

Norwegian University of Science and Technology
Faculty of Natural Sciences
Department of Materials Science and Engineering

NTNU
Norwegian University of
Science and Technology

Preface

The present report is the main deliverable in the course *TMT4900 - Materials Chemistry and Energy Technology, Master's Thesis* at the Norwegian University of Science and Technology (NTNU) in Trondheim, Norway. The work presented is entitled *"Leaching and Modelling of LIB Black Mass for Metal Recovery"* and focuses on contributing to closing the loop on LIB recycling. The overall tasks performed in the present work have included:

1. Conducting a thorough literature survey.

2. Performing leaching experiments on untreated and thermally treated Black Mass (BM) samples.

3. Modelling of the experimental leaching system using commercial software (HSC Chemistry 9) and a self-designed model based on the Python framework.

4. Characterisation of the BM and Solid Residue (SR) samples by Scanning Electron Microscopy (SEM) and Energy Dispersive X-ray Spectroscopy (EDS).

5. Calculating leaching efficiencies from modelled BM compositions and Inductively Coupled Plasma Mass Spectrometry (ICP-MS) results from the leaching experiments.

6. Summarising the obtained results in a report.

The developed kinetic Phyton model is based on the framework created by Dr Daniel P. Clos for the EIT Raw Materials Project ReLieVe (*i.e.* Recycling of Li-ion Batteries for Electric Vehicles). The present author further developed the model with support from Dr Clos, the author's co-supervisor during the work.

Abstract

Numerous Li-Ion Batteries (LIBs) are being introduced into society, primarily due to the electric vehicle market's exponential growth. Both essential raw materials and potentially harmful chemicals are present in these batteries, and the established end-of-life treatment technologies available today are insufficient in view of reaching high recycling rates of the valuable materials present in this heterogeneous waste stream. Furthermore, toxic waste stream residues and high reagent usage in unoptimised recycling operations have negatively affected the environment. Consequently, end-of-life treatment improvements for LIBs have become a primary focus of environmental research.

The most conventional ways of recycling LIBs are through a combination of pyrometallurgical and hydrometallurgical unit processes. The present work addresses the leaching of both untreated and thermally treated Black Mass (BM) samples, *i.e.*, BM-U and BM-T, retrieved from ERAMET IDEAS pilot facilities in Trappes, France. To optimise the leaching process, different leaching conditions were tested to investigate the system's response, as well as metal recovery (leaching efficiency). The parameters varied were temperature, and the amounts of acid and reductant added to the system. The leaching systems were also modelled using the commercial thermodynamic software HSC Chemistry 9 and a kinetic Python model developed in the present work to predict the behaviour of different elements and thereby find the optimal leaching conditions to be used in the experimental part of the work.

A Scanning Electron Microscope (SEM) unit equipped with Energy Dispersive X-ray Spectroscopy (EDS) was used to characterise the BM-U and BM-T samples, as

well as the Solid Residue (SR) originating from industrial leaching experiments.

During the sixteen leaching experiments performed, leachate samples were extracted for further analysis by Inductively Coupled Plasma Mass Spectrometry (ICP-MS). The obtained results were used together with the calculated BM compositions from the SEM-EDS analysis to model the leaching experiments. The leaching experiment with test conditions AO7, *i.e.*, 20 mL H_2SO_4 (2.03 M), 5 mL H_2O_2 (2.5 M), and 60 °C, gave the highest leaching efficiencies for the BM-T samples with 55.7% for Lithium (Li), 51.3% for Nickel (Ni), 26.1% for Manganese (Mn), and 53% for Cobalt (Co). The corresponding leaching system for the BM-U samples, *i.e.*, test conditions AO15, also gave the highest leaching efficiencies for these samples, with 28.4% for Li, 27.7% for Ni, 28.5% for Mn, and 29.5% for Co. The overall results proved that higher temperatures and additions of reductant gave the highest leaching efficiencies for all elements, with generally higher values for the BM-T. Increasing the amount of acid did not significantly impact the leaching efficiency, possibly due to an already surplus of acid in the system.

In view of the modelling, HSC Chemistry 9 calculated 100% leaching efficiency for all elements in all leaching systems and was not considered a suitable tool for modelling the leaching experiments. The kinetic Python model showed similar trends to the actual experiments but higher leaching efficiencies. It was concluded that systematic errors in the experimental procedure were probably the reason for this deviation.

Sammendrag

På grunn av el-bilmarkedets eksponentielle vekst blir et stort antall Li-Ion-batterier (LIB-er) introdusert i samfunnet. Både essensielle råvarer og potensielt skadelige kjemikalier finnes i disse batteriene, og de etablerte teknologiene for å behandle batteriene etter bruk, er i dag utilstrekkelige for å nå høye resirkuleringsrater fra de verdifulle materialene som finnes i de heterogene avfallsstrømmene. Giftige avfallsstrømmer og høy reagensbruk i uoptimale resirkulering operasjoner har i tillegg en negativ påvirkning på miljøet. Forbedring av behandlingsmetoder etter bruk av LIB-er er derfor blitt et hovedfokus innen miljøforskning.

De mest konvensjonelle måtene å resirkulere LIB-er på, er gjennom en kombinasjon av pyrometallurgiske og hydrometallurgiske enhetsprosesser. Denne masteroppgaven tar for seg *leaching* av både ubehandlede og termisk behandlede *Black Mass* (BM) prøver, forkortet BM-U og BM-T, hentet fra ERAMET IDEAS pilotanlegg i Trappes, Frankrike. For å optimalisere *leaching*-prosessen ble forskjellige *leaching*-forhold testet for å undersøke systemets respons, samt metallgjenvinningen (*leaching*-effektiviteten). Temperatur og mengde syre og reduksjonsmiddel tilsatt i systemt, var parameterene som ble variert i forsøkene. *Leaching*-systemene ble også modellert ved hjelp av den kommersielle termodynamiske programvaren HSC Chemistry 9 og en kinetisk Python-modell utviklet i dette arbeidet, for å forutsi oppførselen til ulike elementene. Målet var finne de optimale *leaching*-forholdene som skal brukes i den eksperimentelle delen av arbeidet.

En Scanning Electron Microscope (SEM)-enhet utstyrt med Energy Dispersive X-ray Spectroscopy (EDS) ble brukt til å karakterisere BM-U- og BM-T-prøvene, i tillegg til Solid Residue (SR) prøver fra industrielle *leaching*-eksperimenter.

I løpet av de seksten *leaching*-eksperimentene som ble utført, ble det ekstrahert *leaching*-prøver for videre analyse med Inductively Coupled Plasma Mass Spectrometry (ICP-MS). Resultatene ble, sammen med de beregnede BM-sammensetningene fra SEM-EDS-analysene, brukt for å modellere *leaching*-eksperimentene. *Leaching*-eksperimentet med testbetingelsene AO7 (20 mL H_2SO_4 (2,03 M), 5 mL H_2O_2 (2,5 M), og 60 °C) ga den høyeste *leaching*-effektiviteten for BM-T-prøvene med 55,7% for Litium (Li), 51,3% for Nikkel (Ni), 26,1% for Mangan (Mn) og 53% for Kobolt (Co). Det tilsvarende *leaching*-systemet for BM-U prøvene (testbetingelsene AO15) ga også høyest *leaching*-effektivitet for disse prøvene, med 28,4% for Li, 27,7% for Ni, 28,5% for Mn, og 29,5% for Co. De samlede resultatene viste at høyere temperatur og tilsetning av reduksjonsmiddel ga den høyeste *leaching*-effektiviteten for alle elementer, med generelt høyere verdier for BM-T. Økning av mengde syre påvirket ikke *leaching*-effektiviteten i stor grad, antagligvis grunnet et overskudd av syre i systemet før tilsetning

Modelleringen beregnet i HSC Chemistry 9 ga 100% *leaching*-effektivitet for alle elementene i alle *leaching*-systemene og ble ikke ansett som et egnet verktøy for å modellere *leaching*-forsøkene. Den kinetiske Python-modellen viste lignende trender som de fakiske eksperimentene, dog høyere *leaching*-effektivitet. Det ble konkludert med at systematiske feil i den eksperimentelle prosedyren trolig var årsaken til dette avviket.

Acknowledgements

professional and cultural experience I will remember for a long time.

Lastly, I want to thank my family and friends for their encouragement and always believing in me. They have given me invaluable support during the last year and made the moments when I felt tired and unmotivated much easier.

Trondheim, August 19, 2022

Amalie My Olsen

Nomenclature

Abbrevations

LIB - Lithium Ion Battery

BM - Black Mass

BM-U - Untreated Black Mass

BM-T - Thermally treated Black Mass

SR - Solid Residue

SR-U - Solid Residue from utreated Black Mass

SR-T - Solid Residue from thermally treated Black Mass

NMC - $LiNi_{(1-y-z)}Mn_yCo_zO_2$ - Lithium nickel manganese cobalt oxide

LCO - $LiCoO_2$ - Lithium cobalt oxide

LMO - $LiMn_2O_4$ - Lithium manganese oxide

LFP - $LiFePO_4$ - Lithium iron phosphate

NiMH - Nickel-metal hydride

Methods

SEM - Scanning electron microscope

EDS - Energy-dispersive X-ray Spectroscopy

ICP-MS - Inductively Coupled Plasma Mass Spectrometry

Chemical elements and compounds

Li - Lithium

Ni - Nickel

Mn - Manganese

Co - Cobalt

Zn - Zink

C - Carbon / Graphite

Cl - Chloride

Cu - Copper

Al - Aluminium

Fe - Iron

Cl - Chlorine

F - Fluorine

CO_2 - Carbon dioxide

H_2SO_4 - Sulphuric acid

H_2O_2 - Hydrogen peroxide

$NiSO_4$ - Nickel(II) sulphate

$MnSO_4$ - Manganese(II) sulphate

$CoSO_4$ - Cobalt(II) sulphate

NaOH - Sodium hydroxide

NH_4^+ - Ammonium

Li_2CO_3 - Lithium carbonate

NH_3 - Ammonia

HCl - Hydrochloric acid

HNO_3 - Nitric acid

PVDF - Polyvinylidene fluoride

SiC - Silicon carbide

Li_2O - Lithium dioxide

$Ni_2O_3 \cdot 3H_2O$ - Nickel(III)oxide

Mn_2O_3 - Manganese(III)oxide

MnO_2 - Manganese dioxide

MnO - Manganese(II)oxide

CoO - Cobalt(II)oxide

Co$_2$O$_3$ · 3H$_2$O - Cobalt(III)oxide trihydrate

Table of Contents

List of Figures

List of Tables

1 | Introduction

Since the Industrial Revolution, mechanical labour has been out-conquered by fossil fuels. This has undoubtedly had an immensely positive effect on the development of technology. Shifting from horses and carriages to engine-driven cars, boats and trains have evolved the form, speed and opportunity of transport and trade, leading to a more global world.

Even though fossil fuels (gasoline) have been crucial to progress, it has a significant adverse effect on the climate, and climate change is now one of the biggest challenges the world is facing. It has been estimated that 1.6 billion tons of greenhouse gases are released into the air by highway vehicles every year, and one car alone can release about 6 to 9 tons [1]. To emphasise the extent of these numbers - a typical tree can absorb around 21 kg of CO2 per year [2]. These numbers make it clear that other energy alternatives are needed to avoid the consequences of global warming, which has resulted in more frequent and intense droughts, storms, heat waves, rising sea levels, melting glaciers, and increased ocean temperatures.

A much-established energy alternative to fossil fuels is electricity. Transport, different types of machines, and energy storage are becoming increasingly electrified. Among the transport types, the use of Electric Vehicles (EVs) has increased significantly during the last decade. Fobes.com [3] claims that "The electrification of transport is now one of the major trends of the 21st century", and a forecast study done by Deloitte [4] predicts that the total electric vehicle sales will grow from 2.5 million in 2020 to 11.2 million by 2035, and further increase to 31.1 million by 2030, which will make the global stock of electric vehicles to reach

245 million units by 2030. This trend is also seen in Norway, where 54% of new cars bought in 2020 were EVs, and between 2015 and 2020, the increase of EVs on Norwegian roads increased by 392% [5]. EV sales have also increased worldwide, with global sales rising strongly in 2022 with 2 million vehicles sold during the first quarter. This is up 75% from the same period in 2021 when nearly 10% of global car sales were electric, which was four times the market share in 2019 [6].

On this note, the increase in EVs also rapidly increases the need for portable electricity sources. A good option is batteries, and Li-ion batteries (LIBs) are now a typical battery found in EVs. Dorri [7] has established several issues connected with the rapid LIB growth in society:

- Long-term material supply for LIBs production.

- Environmental impacts of mining materials required for LIBs production.

- Accumulation of spent batteries at the end of life and risk associated with them due to hazardous materials.

While nearly all, 99%, of all lead batteries are recycled, few LIBs are. According to some estimates, the rate could be less than 5% due to technical, economic, and other factors [8].

This leaves us with two essential questions: "What do we do with the spent batteries?" and "How will we be able to get enough materials to continue battery production?". This present thesis will address one of these questions by investigating some of the issues related to LIB recycling.

1.1   Project objectives

Many of the existing LIB recycling methods are considered unsustainable, non-environmentally friendly, and ineffective at recycling spent LIBs with mixed chemi-

stries. In view of this, the present work will contribute to improving the recycling of LIBs through a combination of experimental work on a laboratory scale and modelling activities by investigating the optimal leaching conditions for industrial Black Masses (BMs), *i.e.*, untreated (BM-U) and thermally treated (BM-T), provided by ERAMET Ideas in Trappes, France, as part of the EIT Raw Material project ReLiVe (Recycling Li-ion Batteries for Electric Vehicles).

Figure 1.1.1 shows the scope of the present project and the order in which the activities are performed. As seen in the figure, the different BMs will be analysed by utilising the Scanning Electron Microscopy (SEM) and Energy Dispersive X-ray Spectroscopy (EDS) system, as well as Inductively Coupled Plasma Mass Spectrometry ICP-MS. The recovery of Lithium (Li), Nickel (Ni), Manganese (Mn) and Cobalt (Co) will be in focus in view of leaching efficiency. The obtained data will then be used as input data in a kinetic Python model together with data from the thermodynamic software HSC Chemistry 9 for the relevant reactions to calculate the composition of the BMs. The experimental matrix will allow for investigating the behaviour of the elements in question during different leaching conditions, *i.e.*, 10/20 mL H_2SO_4 (2.03 M), 0/5 mL H_2O_2 (2.5 M) and 40/60 °C. How accurate the models predict the experimental results will be discussed in view of available literature data and actual experimental data. In addition, the Solid Residues (SR) from the leaching trials performed at an industrial scale within the ReLiVe project will be characterised and compared with laboratory findings.
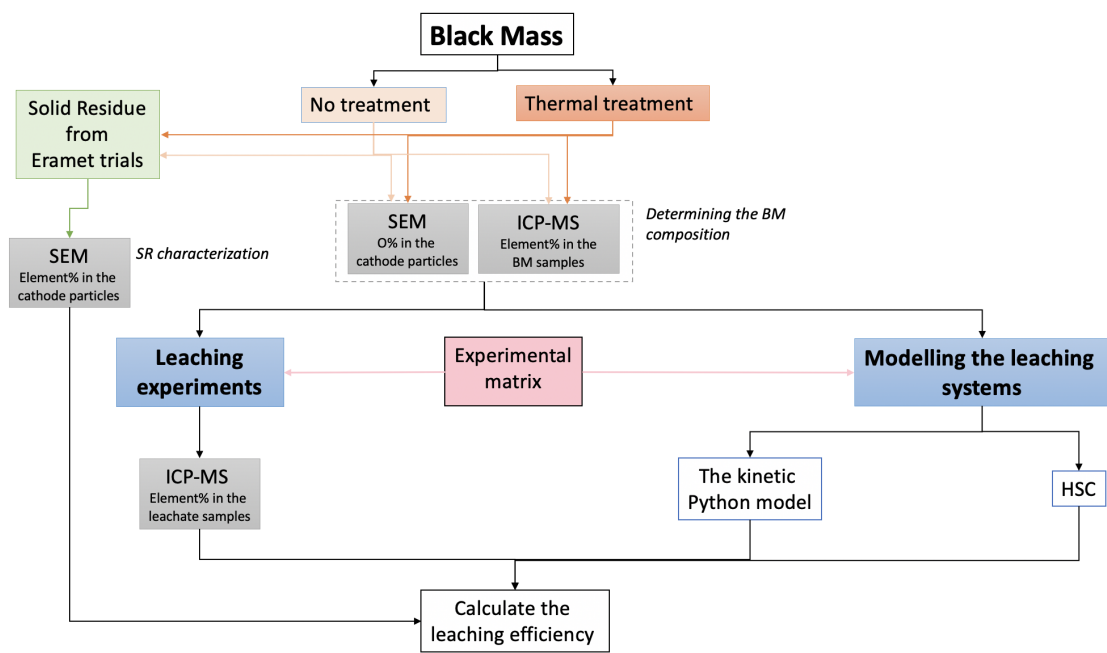
Figure 1.1.1: Flow sheet showing the scope of the present project, including all activities.

2 | Background

The present chapter is intended to give an overview of the present work's background and introduce the field. First, a brief introduction to the general idea of batteries accompanied by historical context will be given. The focus will be on EV batteries, and some existing types of EV batteries will be introduced before the chapter narrows down to describing LIBs. Furthermore, the chapter will present the essential aspects of LIB production, *i.e.*, metal mining, manufacturing, and energy consumption, followed by typical LIB recycling methods. The focus will be on pyro-, and hydrometallurgical methods, which are the dominant techniques in existing LIB recycling processes, but mechanical recycling and direct recycling will also be covered.

2.1 What is a battery?

A battery converts chemical energy into electric energy. The specific purpose of a battery is to have devices driven by electricity while still being portable. This opens up a world of possibilities for equipment that formerly relied on fossil fuels [9]. Nowadays, almost everything running on electricity contains a battery, from electrical equipment of smaller sizes, like computers and phones, to larger devices like electric vehicles, -buses, and -ferries.

Generally, the battery must have a high energy density for smaller electrical equipment such as phones and computers. However, for larger batteries, such as those used in electrical transport, higher capacities and lower weight may be prioritised over power density or lifetime [10]. A battery can come in many shapes, sizes and materials. Some components are the building blocks of a battery, *i.e.*,

the anode (negative electrode), cathode (positive electrode), electrolyte, and separator [11]. A battery is said to be spent when the ability to store and deliver electricity is significantly reduced. The reduction is due to the formation of the solid product when the lithiated anode reacts with the alkyl carbonate comprising the electrolyte solution during the charging and discharging of the battery [12].

The first demonstrator of the working principle of batteries was the galvanic cell in the 19th century. Alessandro Volta tested an experiment containing Zn- and Cu-plate lowered into a diluted H_2SO_4 solution. The Zn-plate would react with H_2SO_4 and thereby free Zn-ions, leaving the plate with a surplus of electrons. On the Cu-plate, the electrons would react with the protons in the H_2SO_4 solution and make hydrogen gas. The Zn-plate would, in other words, have a negative charge (negative electrode) and the Cu-plate a positive charge (positive electrode). Between the plates, an electron conductor was connected to facilitate the movement of electrons from the negative electrode to the positive electrode. The electrical gradient between the electrodes is the driving force of the electron movement, the electrical current in movement is the definition of electricity, and the movement of electrons generates electricity [11] [13] [14]. An illustration of Volta´s element is given in Figure 2.1.1.

2.1.1 Batteries in Electrical Vehicles

The performance of an EV battery is evaluated by the driving range, hence being a significant focus area in EV production. The main factor determining the driving range is the energy density. The type of battery typically used in EVs are LIBs. This is because LIBs have a high energy density and long lifespan. They have also gone through a significant cost reduction during the last decade [11] [15] [10].

There are mainly three other battery types used in EVs, *i.e.*, Nickel-metal hydride (NiMH) batteries, lead-acid batteries, and ultracapacitors. NiMH batteries are widely used in hybrid cars and have a longer lifespan than LIBs. However, they have a higher cost, higher self-discharge, generates heat with high temperatures, and is less efficient at recharging. Lead-acid batteries are often used as a supple-
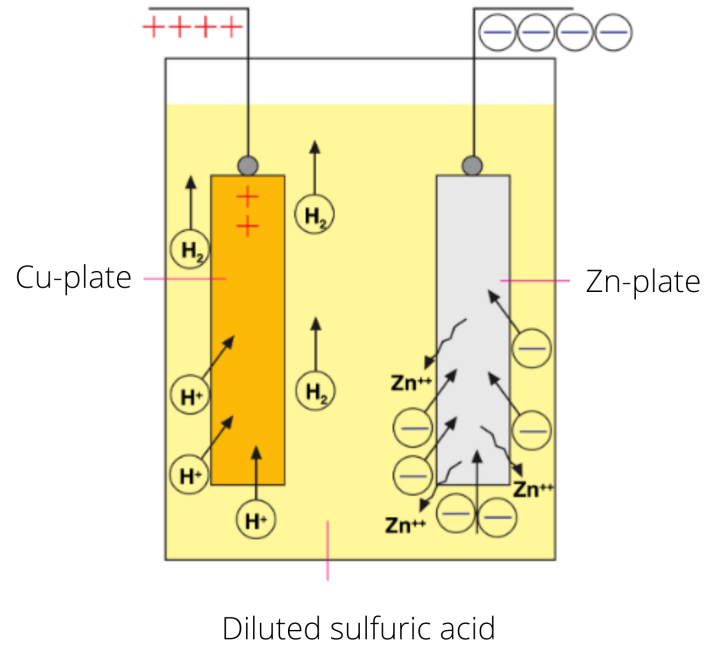
Figure 2.1.1: Illustration of Voltas element [13].

ment for other batteries in EVs. They have high power and are inexpensive, safe, and reliable, however, they have a short life span and poor performance at low temperatures. Ultracapacitors can also be used in EVs, even if they are not batteries. In EVs, they are used as secondary energy storage (like lead-acid batteries) where they store polarised liquid between the electrode and electrolyte and can help electrochemical batteries level their load. In other words, they provide the EV with extra power during acceleration and regenerative braking [2]. LIBs are dominating the current EV battery market and are therefore in focus.

The chemical composition of LIBs varies significantly depending on the type of cathode used, but all types generally implement Li. Due to electrochemical driving forces, free Li-ions move from the cathode to the anode through the electrolyte, which is called discharging of the battery. There is, however, a wide choice of electrolyte materials where the most common choice is a salt dissolved in either water or an organic solvent. The function of the electrolyte is to facilitate the movement of Li-ions between the electrodes, as well as to participate in the electrode reactions. The electrolyte and anode reaction frees electrons, giving the electrode a negative charge during discharging. On the contrary, the reaction be-
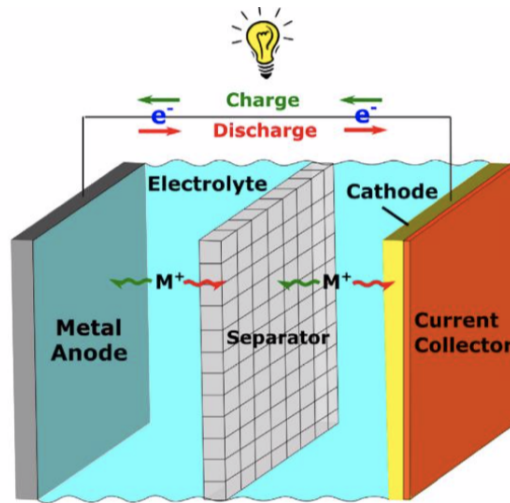
Figure 2.1.2: Illustration of the general functions in a LIB [7].

tween the cathode and the electrolyte uses electrons, inducing a positive charge in the cathode. The electron and ion exchange are illustrated with Equations 2.1.1 and 2.1.2, where "M" represents the metal in focus [7] [11] [16].

$$LiMO_2 \rightleftharpoons Li_{1-x}MO2 + xLi^+ + xe^- \tag{2.1.1}$$

$$C + xLi^+ \rightleftharpoons Li_xC \tag{2.1.2}$$
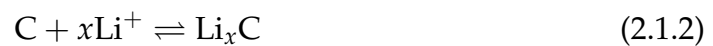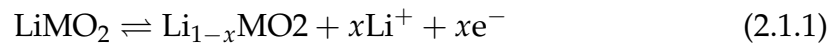
LIBs are often distinguished based on the cathode material (also called the active cathode material). The cathode is usually the largest component in the battery regarding mass and contains the most valuable materials. It is typically coated using a binder on a current collector foil. The binder is often made of PVDF, and the collector is usually Al. Section 2.1.2 describes the different LIB cathodes used in EVs in more detail. The anode is generally made of C (as graphite carbon powder), and unlike the cathode, there is less diversity between materials used for the anode. The graphite powder is bound with PVDF to the current collector (often Cu). In Figure 2.1.2 , an illustration of a LIB is presented [7] [11] [16].

2.1.2 Li-ion Batteries

Four types of LIB cathodes are widely used for EVs in the current market. The first commercialised LIB cathode was the $LiCoO_2$ (LCO), produced in 1991 by Sony. Compared to competing products at the time, it had a relatively high capacity and high nominal voltage. This LIB type was used in the Tesla Roadster sports car due to its adequate electrical performance. The preparation of the LCO LIB pack is considered to be quite easy, and it is relatively unaffected by moisture and process changes. However, a considerable disadvantage is the dependency upon Co, which makes the price of this type of LIB cathode high.

Another type of LIB cathode material is $LiMn_2O_4$ (LMO) which has a relatively low cost due to Mn's abundance in nature. It also has low toxicity to the environment and is, therefore, used commercially in cost-sensitive products that need exceptional stability upon abuse (referred to as overheating or overcharging). The LMO cathode used in the Nissan Leaf has sufficient rate capability and exceeds cycle life at ambient temperatures. However, this cathode has a lower capacity and a higher capacity loss on storage due to Mn dissolution in the electrolyte.

Moreover, $LiFePO_4$ (LFP) is described as a more reliable and safer cathode choice than the others. It is stable in overcharging and short circuit conditions and can resist high temperatures without decomposing. It has a more extensive range at operating and storage temperatures and can withstand oxidative and acidic environments. When the battery cathode is under abuse, the phosphates are not prone to thermal runaway, which means that they will not burn. The raw materials are non-toxic and available in large quantities. The LFP cathode has been used in the BYD-E6 and Mitsubishi-iMiEV.

Lastly, the $LiNi_{(1-y-z)}Mn_yCo_zO_2$ (NMC) is used in EV batteries, and the most commercialised NMC chemistries are $LiNi_{0.3}Mn_{0.3}Co_{0.3}O_2$, $LiNi_{0.5}Mn_{0.3}Co_{0.2}O_2$, and $LiNi_{0.42}Mn_{0.42}Co_{0.16}O_2$. An advantage of NMCs is their lower material cost compared to LCO with similar performance and improved thermal stability during abuse.

The industry is presently moving away from LCO cathode material due to the

high Co-price and instability, especially during abuse. LMO, LFP and NMC are all cheaper and safer alternatives, and NMC cathodes have been the focus of technological advancements in recent years due to their high energy density [16].

2.1.3   Production of Li-ion batteries

Metal mining

The first step in the primary production of LIBs is mining the different metals. Metal mining steps consist of (i) exploration, (ii) evaluation and development, (iii) design, construction and commissioning, (iv) production, and (v) project decline and closure. Economic feasibility is the main focus throughout all steps. The mine also needs a suitable infrastructure, such as transport systems, power, mineral processing facilities, waste disposal areas, mining method, and surface facilities. Hence, a mining site can take up a large area and influence nearby communities even if they are not always in production [17].

The process of extracting metals from ores varies for different metals. The reason for this is, according to Rankin *et al.* [17], that the reactivity of the metals is not the same and, therefore also, not the stability. The metals also exist in various forms, such as oxides, sulfides, and chlorides, which all behave differently. In addition, the melting- and boiling points are individual for each metal and the temperatures required for various chemical reactions to take place. Moreover, the ore mineral in an ore body is not precisely the same, and each one needs to be handled uniquely.

Consequently, each metal needs a specific extracting method. However, most metals occur as a compound and to obtain the metals in their elemental form they need to be reduced from their original compound. The decomposition of the compound and following reduction and oxidation are illustrated in Equations 2.1.3, 2.1.4, and 2.1.5 [17].

$$MO \rightarrow M^{2+} + O^{2-} \tag{2.1.3}$$

$$M^{2+} + 2e^- \rightarrow M \qquad\qquad (2.1.4)$$

$$O^{2-} \rightarrow \frac{1}{2}O_2 + 2e^- \qquad\qquad (2.1.5)$$
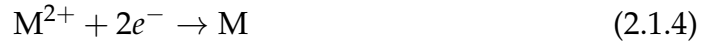
Figure 2.1.3 shows the world's largest producers of Li, Ni, Mn, Co and C [18]. As can be seen from the Figure, Australia, Argentina, and Chile are the main Li-producing countries, while Bolivia, Brazil, Canada, and Zimbabwe are among the lesser producers. Water scarcity and usage are significant issues in South American countries, which have over half of the world's Li reserves. Today's mining methods use around 2.3 litres of water to generate 1 gram of Li. Because these countries are among the driest on the planet, access to water can be a severe problem. In addition, there is a considerable risk of toxic chemicals leaking and polluting nearby rivers, groundwater and other water supplies. The soil and air near a mining site for Li are also at risk for contamination [19].
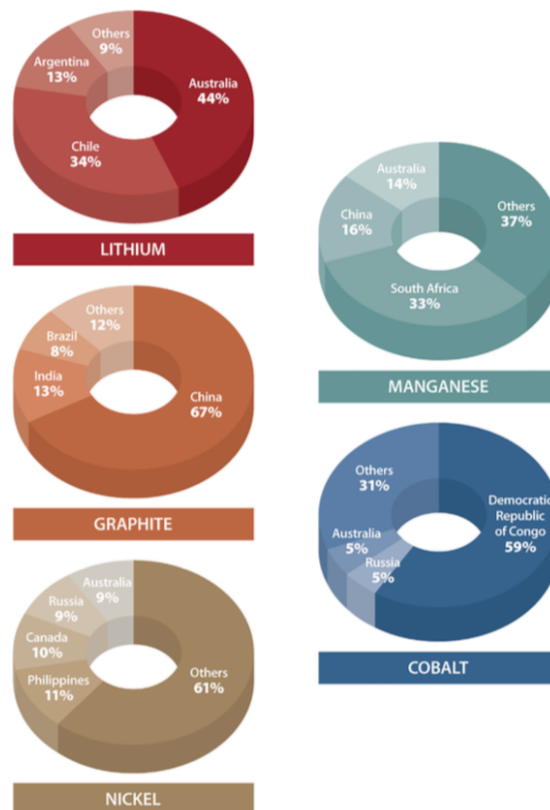
Figure 2.1.3: Overview of the countries with the highest production of Li, Ni, Mn, Co and C [18].

The social impact of the mining sector is another justification for reducing primary production and increasing the usage of secondary sources. Co, which primarily comes from Congo, is an excellent example as it provides around 60% of the total Co-production. In 2015, Amnesty International visited Congo and reported how polluted the mining area was and how residents living near the mines could not "get away from the dust". Another point raised was the government's and mining corporations' inaction in preventing pollution. Furthermore, people, including children, were working without the necessary protective equipment and were suffering from various health problems due to their job in the mines [20].

LIB manufacturing

The NMC cathode is synthesised via two steps. The first step is to produce an NMC precursor. This process begins with a reaction between stoichiometric solutions of the substrates, *i.e.*, Ni-sulphate ($NiSO_4$), Mn-sulphate ($MnSO_4$) and Co-sulphate ($CoSO_4$), and hydroxide (OH^-). Sodium hydroxide ($NaOH$) and ammonium (NH_4^+) are added to the solution, which is heated over a long period. The next step is to treat the precursor with Li. The NMC precursor is filtered and dried to a powder form before being mixed with Li-carbonate (Li_2CO_3). Finally, the Li and NMC powder are calcined until the desired oxide is produced, *i.e.*, until Ni, Mn, and Co precipitate as NMC. [21].

The manufacturing of a LIB cell consists of three processes [22]:

1. *Electrode preparation:* The cathode- and anode active materials are, for each separately, mixed with conductive additive, binder and a solvent to form a slurry. The slurry is pumped into a slot die and coated on each side on a current collector. The current collector is Al-foil for the cathode and Cu-foil for the anode. They are then dried to evaporate the solvent. Next, the physical properties, such as bonding, conductivity, density and porosity, are adjusted by calendering. The electrodes are then stamped and slit to achieve the required dimensions for the cell design. The last step of the electrode preparation is to remove the excess water in a vacuum oven.

2. *Cell assembly:* The electrodes and separators are stacked layer by layer to form the battery cell's internal structure. An Al tab is welded on the anode current collector, and likewise, a Cu tab is welded on the cathode current collector. Subsequently, the stack is transferred to the designed enclosure. The enclosure is filled with electrolytes and then sealed.

3. *Battery electrochemistry activation:* This step consists of several processes to enable operation stability. One example is forming a stable solid-electrolyte interface which can prevent irreversible consumption of the electrolyte and protect the anode from overcharging.

When the battery cell is produced, the battery system is assembled. The first step is connecting several battery cells in a series or in parallel. This is called a module and will provide a higher voltage and capacity than a single battery cell. The modules are then combined into a series, also called a pack. Lastly, one or several packs are connected in series or in parallel to form the overall battery system. The battery system does also include a cooling system [23]. Figure 2.1.4 shows an example of the path from the battery cell to the module and further on to the final battery system.

Figure 2.1.4: An illustration of the pathway for a LIB battery cell to a battery system [23].

Energy consumption

Primary LIB production uses considerable energy and produces a lot of carbon dioxide (CO_2). Golroudbary *et al.* [24] investigated how much energy is used and how much greenhouse gas is released during Li mining and production of LIBs. According to the study performed in 2020, mining produced $65 \cdot 10^6$ kg of CO_2 emissions in 2020, while LIB production produced $175 \cdot 10^6$ kg. Another study
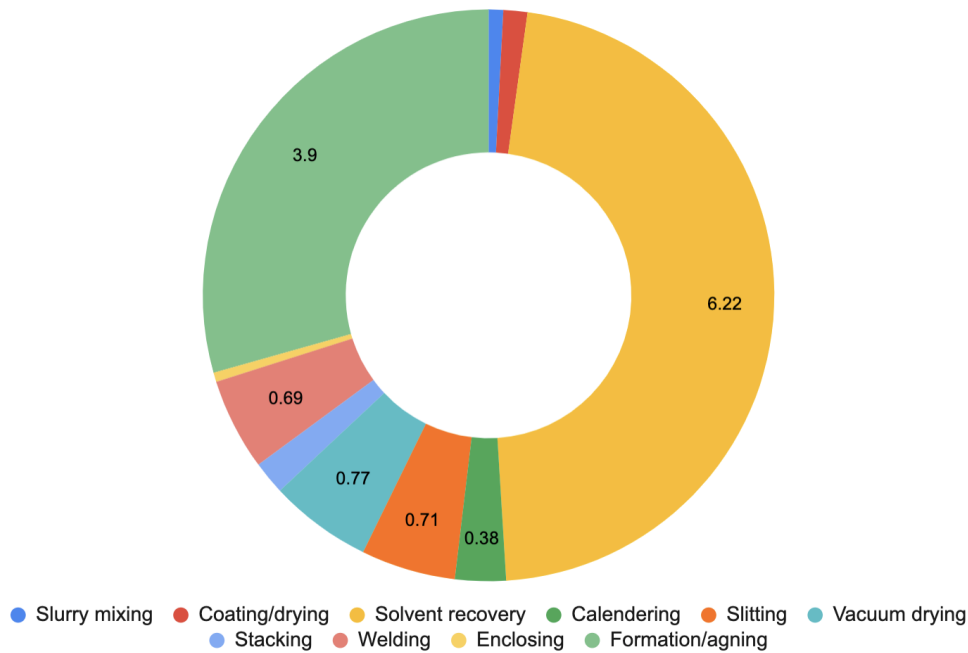
Figure 2.1.5: Pie chart with the ratio of energy consumption for the different steps in the manufacturing of LIBs. The numbers on the pie slice give the energy consumption that the respective process step in kWh per cell manufactured [22].

by Liu *et al.* [22] investigated the total energy consumption of manufacturing a LIB battery cell. Each step in the manufacturing process was considered, and in Figure 2.1.5, the percentages of each step with a total energy consumption of 13.28 kWh per battery cell are presented.

2.2   Battery recycling: State of the art

There are three main ways to handle spent batteries responsibly, also called the three Rs. That is, remanufacturing, repurposing, and recycling. Remanufacturing EV batteries consist of renovating the battery and reusing them. Usually, spent EV batteries cannot be remanufactured back to EV batteries because of the capacity, *i.e.*, the module and battery pack decrease below 80% of the original state during the process and do therefore not meet the industry criteria. Instead, they could be repurposed in less stressful applications, such as stationary energy storage. The challenges with repurposing LIBs are that the spent batteries have many different designs and performance metrics, and new battery man-
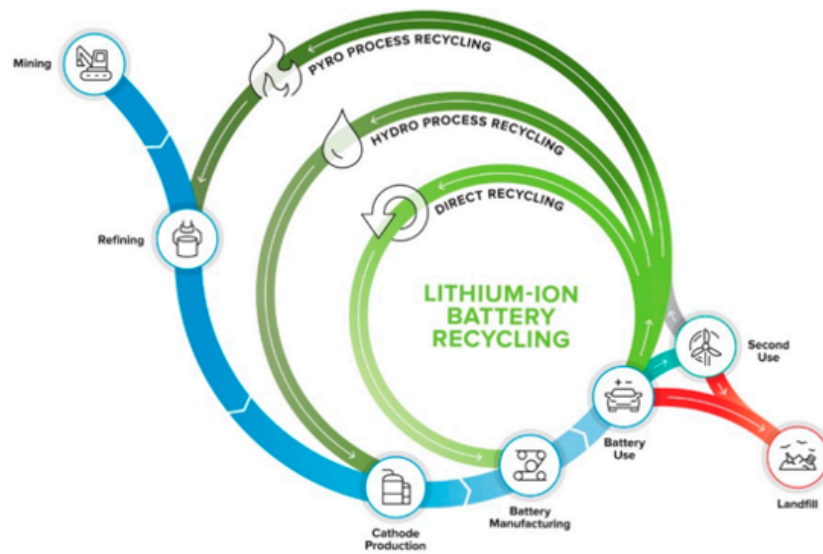
Figure 2.2.1: Overview of the different steps in the pyrometallurgical-, hydrometallurgical- and direct recycling processes [25].

agement systems need to be established as non-vehicle applications. The reconfiguration comes with additional cost and liability and competes with new and cheaper batteries. Therefore, recycling is often preferred for handling spent EV LIBs. However, LIBs have complex structures, which makes them complicated to dismantle and up-concentrate for designated waste streams. They consist of multiple modules and can contain different types of liquids. The geometry of the battery can also vary, with the most common being prismatic or cylindric. Further, the configuration with batteries in parallel can be manufactured by either welding, wire bonding, or mechanical joining. In addition, the chemical composition varies greatly. Moreover, all of these factors do vary between the different manufacturers, which results in the multiplicity of material chemistries increases the complexity of battery recycling [18].

The leading recycling technologies for batteries are pyrometallurgy, hydrometallurgy, mechanical, and direct recycling. An overview of the pyrometallurgical-, hydrometallurgical- and direct recycling process is illustrated in Figure 2.2.1. In the following sections, the respective four processes are explained.

2.2.1 Pyrometallurgy

The most common commercial treatment method for spent batteries is pyromet-allurgy. Spent batteries are treated as if they were ores, aiming to extract the valuable metals as a metal alloy [7]. In Figure 2.2.2 a general flow sheet of the pyrometallurgical process is given.

Pyrometallurgy is a high-temperature smelting process with two main steps. Step one involves smelting the LIBs, which causes the compounds to break down, and remaining organic materials, *i.e.*, plastics and separators, are burned off. In the second step, new alloys are formed through carbon reduction. The process takes place in a heated furnace with three temperature ranges. First, there is a pre-heating zone above 300 °C, where the electrolyte is evaporated. At 700 °C, plastic combustion occurs and plastic segments and the binder are burned off.

At last, the smelting and reduction of metals occur in the temperature range of 1100 - 1500 °C, which will also ensure that the remaining compounds containing carbon will burn off. The output from the process is slag, various gases, and alloys containing valuable metals. In most pyrometallurgical processes, only Co, Ni, and Cu are recovered with high efficiency for economic reasons. Li will have to be recovered through subsequent steps, which often are hydrometallurgical steps intending to separate the remaining metal alloys to recover pure materials. Adding steps to the process comes with additional cost and energy usage. In addition, some compounds are used as fuel in the process, naturally making their recovery more complicated. These are the anode, electrolyte, and plastics as they are oxidised and thereby supply energy to the process. Further, the burning of Al and C (graphite) has a reducing effect that will decrease the process's energy need [7] [18].

An advantage of pyrometallurgical treatments of spent LIBs is that the process is well-established and reliable. It has high productive capacity and simplicity and has been used for a long time worldwide. It can recover the material in a wide range of spent batteries without the need for sorting, size reduction, mechanical pretreatment and disassembly. That means that it is possible to recycle a mixture

Figure 2.2.2: General flow sheet over the pyrometallurgical process [18].

of LIBs and NiMHs together, which is a considerable advantage for countries without the infrastructure and/or storage space needed for battery sorting. Further, the process output can be synthesised to new cathodes with many different chemistries, *i.e.*, there is no dependency related to the previous battery, which gives it high flexibility [7] [16] [18].

Pyrometallurgical treatments also have disadvantages. The most critical is the high energy consumption during smelting and the formation of CO_2. Due to the process being very energy-intensive, pyrometallurgy has a relatively high environmental impact, adding to global warming and air pollution. In addition, many materials in the LIB are not recovered at all, which leads to the requirement of further processing of the alloys, which increases the recycling cost. Furthermore, since the pyrometallurgical business model depends on economic benefits, the cost of recycling the remaining metals is not a priority in view of additional costs. In the future, this process might also be incompatible with recycling LIBs as LIB product design for EVs trends toward lower Co content. Moreover, the output gas from the process contains hazardous substances like chlorine (Cl) and fluorine (F) from the electrolyte and binder [18] [7].

2.2.2   Hydrometallurgy

Hydrometallurgy uses aqueous chemical reactions to extract and separate the metals in ore or an alloy. For LIB recycling, the hydrometallurgical treatments are performed on BM produced from spent batteries, but the technique has applications in several fields. With water, acid, and other parameters like reductant, temperature, stirring speed, etc., the BM is leached. This means that the active cathode material from the battery is dissolved in an acidic solution to break the crystal structure. The metals are later recovered through precipitation processes. Considering metal recovery, hydrometallurgical processes are favourable, however, there are still a few recycling plants that use hydrometallurgical processes independently of pyrometallurgical processes even if combining them has proved to be successful. The steps in hydrometallurgical battery recycling are pre-treatment, leaching, purification, and material recovery [18] [7]. In Figure

2.2.3 a general flow sheet of the hydrometallurgical process is given.

For leaching of battery cathodes, the raw material in the process can be BM or a metal alloy depending on where the raw material comes from. If the hydrometallurgical process is a subsequent step after a pyrometallurgical process, the raw material for the leaching would be a metal alloy. The metal alloy from a pyrometallurgical process contains reduced metals separated through smelting. If the hydrometallurgical process is used independently, the raw material is BM [18] [7].

The objective of pre-treatment is to change the physical or chemical structure of the material to facilitate the extraction of valuable materials and achieve higher recovery rates by up-concentration. Often the pre-treatment involves pyrometallurgical processing, also called thermal treatment. Thermal treatment facilitates the leaching process, increasing the material recovery up to 95 %. For instance, it can remove parts that interfere with the leaching chemicals. The C and the binder in the battery are removed or decomposed. The active metal is reduced, increasing the solubility in the leaching process. The other main ways of pre-treatment are chemical and physical processes or a combination of the different methods. Chemical pre-treatment aims to remove the segments of the batteries that slow down the leaching reactions, for example, the binder and current collectors in the battery. Physical pre-treatment most often involves mechanical or manual sorting of the batteries, shredding and crushing. The BM used in leaching is produced through mechanical pre-treatment or in combination with thermal treatment [7] [17].

There are different ways the BM can be leached. One way is alkali leaching, a selective method that can reduce the need for separation and purification, which can be expensive. Alkali leaching is often based on an ammonia (NH_3) system, where NH_3 will form complexes with the metals. Bioleaching is another alternative where acid production is used during microorganisms' metabolism. This method is potentially more environmentally friendly. The most common leaching system for LIB recycling is acid leaching. Many types of inorganic acid and organic acids can be used, such as HCl, H_2SO_4, HNO_3, citric acid, ascorbic acid,

Figure 2.2.3: General flow sheet over the hydrometallurgical process [18].

oxalic acid, and formic acid. At a large scale, leaching with H_2SO_4 is most common. From this point on, the term leaching refers to the acid type of leaching. In addition to acid, a reductant can be used to improve the leaching process by reducing the metals. With a lower valance, the metals will dissolve in the acid more efficiently. The most common reducing agent is s H_2O_2 [18] [7].

Separation and purification aim to isolate the desired metals from the impurities and can be done in several ways. One way is through solvent extraction, in which the driving force for the mechanism is the different solubilities of the metal ions and the liquid. Another way is through chemical precipitation. With chemical precipitation, the pH of the solution is strategically tuned to precipitate out the metals. Some metals are challenging to precipitate in isolation due to similar properties, such as Ni, Mn, and Co. Therefore, one possible approach is to coprecipitate them and directly make new NMC cathodes [18].

Hydrometallurgy has several advantages as the recovered materials are of high purity, and the metal recovery rate can be high. However, the process takes place at lower temperatures, reducing energy usage, and CO_2 emissions are also low. The environmental safety is increased for disposing of hazardous elements due to material handling at the recycling plant, additionally, there is no production of toxic gases and particles [18] [7].

Disadvantages of hydrometallurgical processes are often directly connected to water usage and the inflexibility of the process. The process is dependent on water supply and will produce wastewater. The wastewater needs to be treated so as not to pollute nearby rivers and lakes, which is an added cost. Further, pre-treatment processes are necessary for the metal recovery to be sufficient.

Overall, the hydrometallurgical recycling process is more complex than the pyrometallurgical processes, and the recycling rates for BMs of mixed battery types are low. Therefore, the process is also dependent on sorting the batteries before recycling. This can be a problem in view of storage space and additional cost, making the process more complicated. As previously mentioned, some elements are also challenging to separate due to their similarity in properties, *i.e.*, Ni, Mn, Co, Fe and Al. Separating these elements will give additional costs [18] [7].
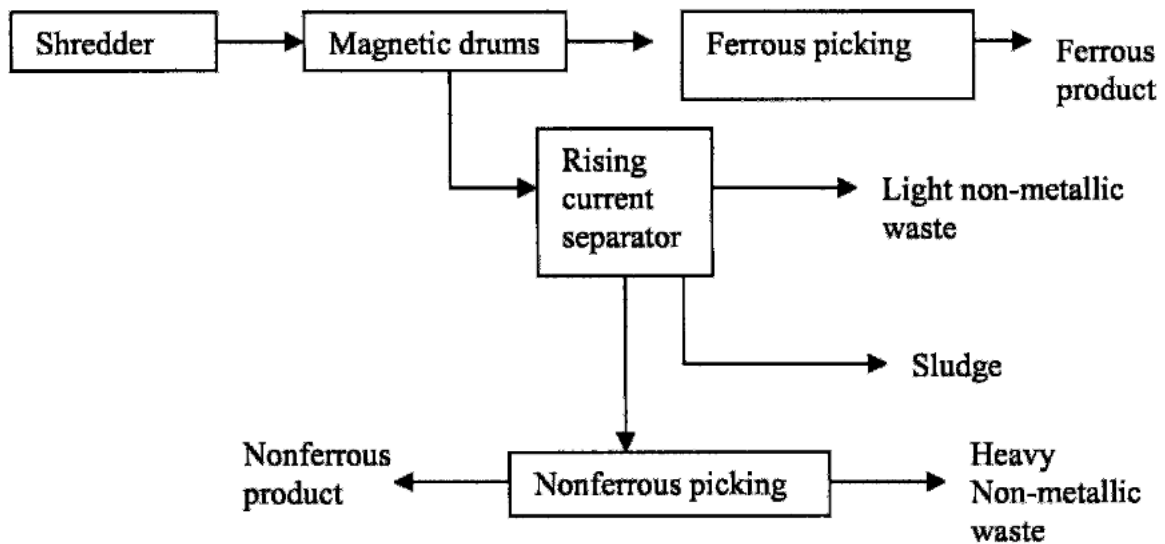
Figure 2.2.4: General flow sheet over a shredding system [26].

2.2.3   Mechanical recycling

Mechanical recycling (can also be called physical pre-treatment) techniques are based on utilising the specific physical properties of the materials, *e.g.*, gravity, magnetic properties, and electrical conductivity.

Physical processes, most often shredding, can also be used in combination with thermal treatment in the production of BM. The shredding system is often used to process vehicles and other domestic equipment because the material needs to be shredded and fragmented to release ferrous metals. The shredding system can be either wet or dry. A general flow sheet of the shredding system is given in Figure 2.2.4.

Another form of physical separation can, *e.g.*, be separation by picking. This method was used to beneficiate C (coal) by sorting for quality in the mineral industry. Separation by picking is based on visual recognition. However, alongside the technology development, this method has become more automatic with the help of sensors, computers, and cameras.

Gravity separation is another physical process that exploits the compounds' specific mass differences in the recycling system. It has been widely used to separate minerals from ores in mineral processing for a long time. The technique is often used in water since both density differences and particle size can be utilised for

separation. Examples of gravity separation processes are (i) shaking table, (ii) Bartles-Mozley concentrator, (iii) pneumatic table, and (iv) jigs.

Magnetic separation is yet another type of physical process. This process is often used when Fe is present in the system because of its magnetic properties. The property of a material that determines the response to a magnetic field is magnetic susceptibility. If a material is paramagnetic, it is attracted to a magnetic field. If it is diamagnetic, on the other hand, the material is repelled. A material can also be strongly paramagnetic and is then called ferromagnetic.

Furthermore, one can utilise the difference in electrical conductivities to sort the material, also known as electrostatic separation. One example is the Eddy current separator.

The adsorptive bubble separation techniques can also be used and exploit the difference in surface activity when gas bubbles recover solid particles. The bubbles rise through a liquid surface, and the solid particles attach to the bubbles. There are many different examples of adsorptive bubble separation techniques, e.g., (i) froth flotation, (ii) dissolved air flotation, and (iii) precipitation flotation [26].

2.2.4 Direct recycling

The direct recycling process aims to harvest and recover the active material while retaining the original composition and structure. In other words, the components should be recycled without breaking the crystal structures of the active materials. The whole structure of active material is exploited instead of extracting the elements individually, and the recycled material can be used directly to manufacture a new battery. The battery components are first separated through, *e.g.*, physical- or magnetic separation or moderate thermal processing while avoiding the chemical breakdown of the active materials. Then the active material is purified, either through re-lithiation or hydrothermal processes, and the surface or bulk defects are restored. Like hydrometallurgical recycling, direct recycling cannot recover mixtures of different chemistries, which leads to the need for battery sorting, which is not always economically or technically feasible [18] [7]. A general flow sheet of the direct recycling process is given in Figure 2.2.5.

Figure 2.2.5: General flow sheet over a shredding system [18].

With a homogeneous battery feed, the process is relatively simple. Another advantage is that the active material is directly reused after regeneration. The emissions are also significantly lower than the other recycling processes, and there is less secondary pollution. However, as previously mentioned, this method requires thorough sorting and pre-processing, dependent on exact active material chemistry. It is susceptible to the input stream and is a very stringent process. The battery industry requires a given standard for the batteries, and direct recycling can guarantee consistently high purity only under specific conditions. Still, direct recycling is an unproven technology because it has only been tried on a laboratory scale [18].

2.2.5 Examples from the industry

Different companies use different methods for recycling spent LIBs. In a study done by Chen *et al.* [18], several pyrometallurgical and hydrometallurgical methods are described, some of which are presented below.

There are numerous of ways that LIBs are handled through pyrometallurgy. Some companies using pyrometallurgical recycling methods are Umicore, Accurec, Sony, Sumitomo, Inmeteco, and Glencore. The methods of Umicore and Accurec are in the present work used as examples.

Umicore is one of the leading companies in heavy metal recovery and specialises in recycling almost all battery types. In addition, they are said to have the most sophisticated battery recycling plant to date [10]. It uses an ultra-high temperature method that generates both a high-value alloy (containing Co, Ni and Co) and a slag. The slag can later be used as additives in construction. For further separation and purification, Umicore uses hydrometallurgical methods to produce new cathode materials, *e.g.*, LCO and NMC cathodes. This process allows Umicore to handle 7000 metric tons of spent LIBs per year [27]. A flow sheet over Umicore´s smelter and refinery is given in Figure 2.2.6.

Accurec combines hydrometallurgy and pyrometallurgy in a vacuum thermal recycling method. First, the electronic fractions and plastic covers are removed by physical processes before distillation and pyrolysis is employed to extract the
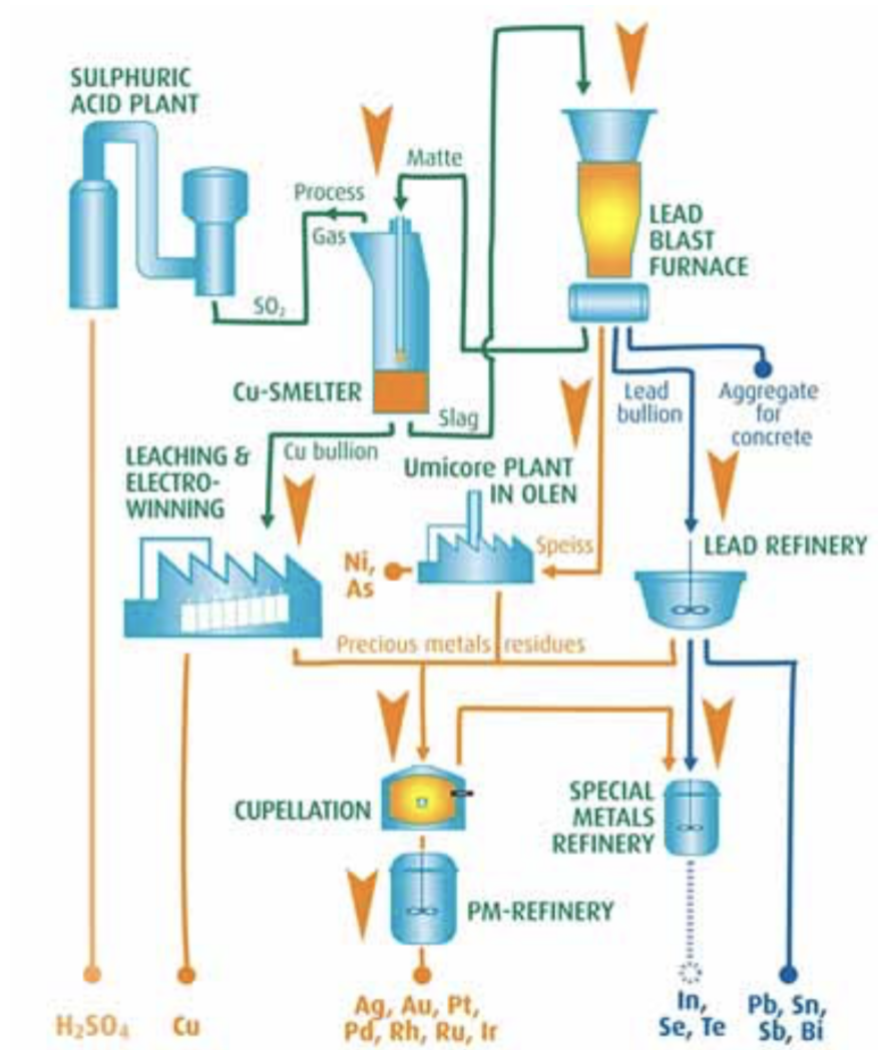
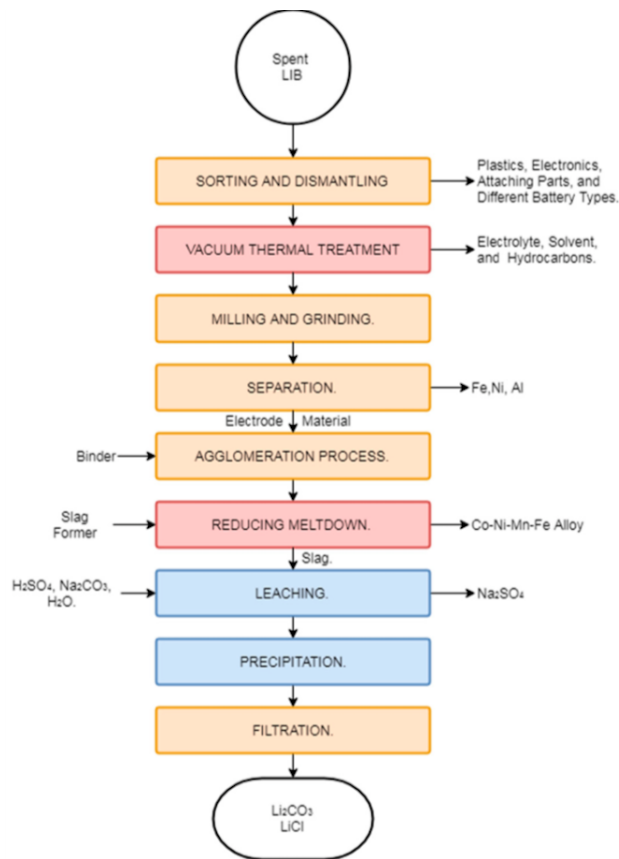**Figure 2.2.6:** Flow sheet over Umicore's integrated metals smelter and refinery [28].

Figure 2.2.7: Flow sheet presenting Accurec´s recycling process [29].

electrolyte. The next step is to crush, categorise, and sort the remains of Al, Cu and steel to recover them by mechanical recycling, *i.e.*, specifically sieving, magnetic separation, and air separation. Electrode materials are then agglomerated into pellets with a binder before being converted to a Co-based alloy by smelting. Lastly, Li-slag is acid-leached and converted to Li_2CO_3 or Cl for recovery. Figure 2.2.7 shows a flow sheet over Accurec´s recycling process.

Several companies work with hydrometallurgical recovery of LIBs, including Retriev, Baterc Industrie AG, Recupyl, and The LithoRec project. The method of Retriev and Baterc Industrie AG is in the present work used as examples.

Retriev uses physical processes before hydrometallurgical recycling of the spent LIBs. The battery packs are first manually dismantled and then crushed by a flooded hammer mill immersed with Li brine. The crushing lowers the battery reactivity, prevents gas emissions, and neutralises the electrolyte. Figure 2.2.8 shows a flow sheet over Retriev´s recycling process.
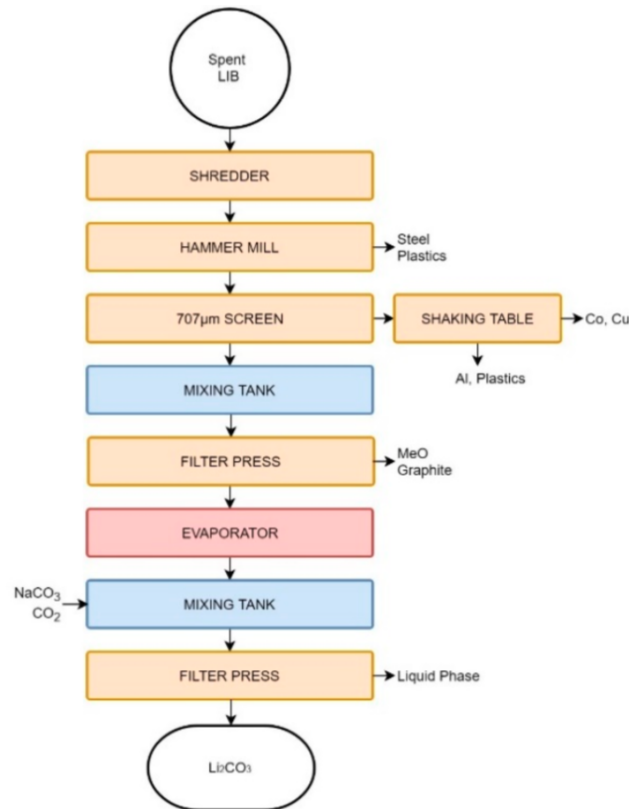
Figure 2.2.8: Flow sheet over Retriev´s recycling process [29].

Retrieved methods produce three streams of materials:

1. Metal solids - BM, Cu-foil and Al-foil.

2. Metal enriched liquid - Li ions that can be precipitated and filtered out.

3. Plastic fluff.

Retrievs methods recover Li as Li_2CO_3, but they are not currently focusing on recovering the other metals. Therefore, the metal solids are sold for metal recovery by other companies such as Glencore.

Batrec Industrie AG sorts and crushes the spent LIBs in the CO_2 atmosphere, which releases Li. Moist air is utilised to neutralise the released Li. The remaining materials are then leached in acid, and the leachate and solid residue are separated and purified.

3 | Methods - Experimental and Modelling

The following chapter will elaborate on the experimental approach, as well as the different analytical techniques used to evaluate the result. It will also give an overview on how the different techniques interact, as illustrated in Figure 3.0.1.
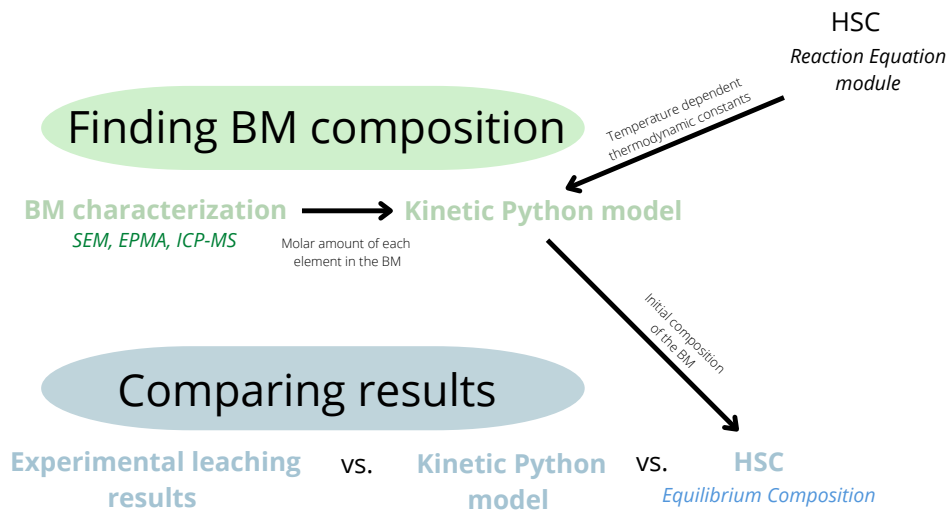

Figure 3.0.1: Flow sheet of the experimental approach.

In total sixteen leaching experiments were performed. The testID for these experiments is abbreviated as AO1 - AO16. Two additional leaching experiments were performed to test the reproducibility of the experiments, *i.e.*, AO17 and AO18.

To assess the effectiveness of the leaching step, the leachate from the experiments was analysed with Inductively Coupled Plasma Mass Spectrometry (ICP-MS) with the help of ALS Global (Luleå, Sweden). Scanning Electron Microscope (SEM) equipped with an Energy Dispersive X-ray Spectroscopy (EDS) unit was

used to characterise the untreated and thermally treated Black Mass (BM). In addition, the Solid Residues (SRs) from the experiments performed by ERAMET IDEAS (Trappes, France) in their pilot facility, as well as some of the SRs from the leaching experiments performed in the present work, were also characterised.

The software HSC Chemistry 9 by Metso Outotec (Sala, Sweden) and a kinetic Python model were used to model the leaching system and predict the leaching efficiencies.

3.1   Leaching experiments

The BMs used in the leaching experiments in the present work originated from a pilot experiment conducted by ERAMET IDEAS. The BM samples received was two different type of samples, *i.e.*, before and after thermal treatment. For simplicity, the untreated - and thermally treated BM is abbreviated as BM-U and BM-T, respectively.

Eight experiments were conducted on each BM to figure out how the different leaching conditions affect the metal recovery in each case. The parameters varied in the leaching systems were the temperature and the used amounts of acid and reductant, all of which had their respective high and low values. The amount of water in the system was adjusted to ensure a solid/liquid ratio of 50g/L. In Table 3.1.1 the high and low values of the applied parameters are presented.

Table 3.1.1: The high and low values of the experimental parameters used during the leaching experiments.

Parameter	Low	High
Acid	10 mL	20 mL
Reductant	0 mL	5 mL
Temperature	40 °C	60 °C

During the leaching experiments, a leachate sample was extracted at different time intervals to determine the metal recovery as a function of time. The time intervals used were 10, 30, 60, 120, 180 and 1380 minutes for every experiment,

resulting in a total of 96[1] leachate samples. In addition, the experimental reproducibility likability was tested (testID AO13 were repeated twice, leading to the additional tests AO17 and AO18). An overview of all the leaching experiments performed is given as an experimental matrix in Table 3.1.2.

---

[1]For the last experiment, the lab ran out of test tubes, so a one-time interval was disregarded, hence the actual total was 95 leachate samples.

Test ID	BM type	Temperature [°C]	Time [min]	Acid [mL]	Reductant [mL]	Water [mL]
$AO1_1$	BM-T	40	10	20	0	20
$AO1_2$	BM-T	40	30	20	0	20
$AO1_3$	BM-T	40	60	20	0	20
$AO1_4$	BM-T	40	120	20	0	20
$AO1_5$	BM-T	40	180	20	0	20
$AO1_6$	BM-T	40	1380	20	0	20
$AO2_1$	BM-T	40	10	10	0	30
$AO2_2$	BM-T	40	30	10	0	30
$AO2_3$	BM-T	40	60	10	0	30
$AO2_4$	BM-T	40	120	10	0	30
$AO2_5$	BM-T	40	180	10	0	30
$AO2_6$	BM-T	40	1380	10	0	30
$AO3_1$	BM-T	40	10	20	5	15
$AO3_2$	BM-T	40	30	20	5	15
$AO3_3$	BM-T	40	60	20	5	15
$AO3_4$	BM-T	40	120	20	5	15
$AO3_5$	BM-T	40	180	20	5	15
$AO3_6$	BM-T	40	1380	20	5	15

$AO4_1$	BM-T	40	10	10	5	25
$AO4_2$	BM-T	40	30	10	5	25
$AO4_3$	BM-T	40	60	10	5	25
$AO4_4$	BM-T	40	120	10	5	25
$AO4_5$	BM-T	40	180	10	5	25
$AO4_6$	BM-T	40	1380	10	5	25
$AO5_1$	BM-T	60	10	20	0	20
$AO5_2$	BM-T	60	30	20	0	20
$AO5_3$	BM-T	60	60	20	0	20
$AO5_4$	BM-T	60	120	20	0	20
$AO5_5$	BM-T	60	180	20	0	20
$AO5_6$	BM-T	60	1380	20	0	20
$AO6_1$	BM-T	60	10	10	0	30
$AO6_2$	BM-T	60	30	10	0	30
$AO6_3$	BM-T	60	60	10	0	30
$AO6_4$	BM-T	60	120	10	0	30
$AO6_5$	BM-T	60	180	10	0	30
$AO6_6$	BM-T	60	1380	10	0	30
$AO7_1$	BM-T	60	10	20	5	15

$AO7_2$	BM-T	60	30	20	5	15
$AO7_3$	BM-T	60	60	20	5	15
$AO7_4$	BM-T	60	120	20	5	15
$AO7_5$	BM-T	60	180	20	5	15
$AO7_6$	BM-T	60	1380	20	5	15
$AO8_1$	BM-T	60	10	10	5	25
$AO8_2$	BM-T	60	30	10	5	25
$AO8_3$	BM-T	60	60	10	5	25
$AO8_4$	BM-T	60	120	10	5	25
$AO8_5$	BM-T	60	180	10	5	25
$AO8_6$	BM-T	60	1380	10	5	25
$AO9_1$	BM-U	40	10	20	0	20
$AO9_2$	BM-U	40	30	20	0	20
$AO9_3$	BM-U	40	60	20	0	20
$AO9_4$	BM-U	40	120	20	0	20
$AO9_5$	BM-U	40	180	20	0	20
$AO9_6$	BM-U	40	1380	20	0	20
$AO10_1$	BM-U	40	10	10	0	30
$AO10_2$	BM-U	40	30	10	0	30

AO10$_3$	BM-U	40	60	10	0	30
AO10$_4$	BM-U	40	120	10	0	30
AO10$_5$	BM-U	40	180	10	0	30
AO10$_6$	BM-U	40	1380	10	0	30
AO11$_1$	BM-U	40	10	20	5	15
AO11$_2$	BM-U	40	30	20	5	15
AO11$_3$	BM-U	40	60	20	5	15
AO11$_4$	BM-U	40	120	20	5	15
AO11$_5$	BM-U	40	180	20	5	15
AO11$_6$	BM-U	40	1380	20	5	15
AO12$_1$	BM-U	40	10	10	5	25
AO12$_2$	BM-U	40	30	10	5	25
AO12$_3$	BM-U	40	60	10	5	25
AO12$_4$	BM-U	40	120	10	5	25
AO12$_5$	BM-U	40	1380	10	5	25
AO13$_1$	BM-U	60	10	20	0	20
AO13$_2$	BM-U	60	30	20	0	20
AO13$_3$	BM-U	60	60	20	0	20
AO13$_4$	BM-U	60	120	20	0	20

$AO13_5$	BM-U	60	180	20	0	20
$AO13_6$	BM-U	60	1380	20	0	20
$AO14_1$	BM-U	60	10	10	0	30
$AO14_2$	BM-U	60	30	10	0	30
$AO14_3$	BM-U	60	60	10	0	30
$AO14_4$	BM-U	60	120	10	0	30
$AO14_5$	BM-U	60	180	10	0	30
$AO14_6$	BM-U	60	1380	10	0	30
$AO15_1$	BM-U	60	10	20	5	15
$AO15_2$	BM-U	60	30	20	5	15
$AO15_3$	BM-U	60	60	20	5	15
$AO15_4$	BM-U	60	120	20	5	15
$AO15_5$	BM-U	60	180	20	5	15
$AO15_6$	BM-U	60	1380	20	5	15
$AO16_1$	BM-U	60	10	10	5	25
$AO16_2$	BM-U	60	30	10	5	25
$AO16_3$	BM-U	60	60	10	5	25
$AO16_4$	BM-U	60	120	10	5	25
$AO16_5$	BM-U	60	180	10	5	25

AO16$_6$	BM-U	60	1380	10	5	25
AO17$_1$	BM-U	60	10	20	0	20
AO17$_2$	BM-U	60	30	20	0	20
AO17$_3$	BM-U	60	60	20	0	20
AO17$_4$	BM-U	60	120	20	0	20
AO17$_5$	BM-U	60	180	20	0	20
AO17$_6$	BM-U	60	1380	20	0	20
AO18$_1$	BM-U	60	10	20	0	20
AO18$_2$	BM-U	60	30	20	0	20
AO18$_3$	BM-U	60	60	20	0	20
AO18$_4$	BM-U	60	120	20	0	20
AO18$_5$	BM-U	60	180	20	0	20
AO18$_6$	BM-U	60	1380	20	0	20

Table 3.1.2: The experimental matrix of the leaching experiments.

3.1.1   Experimental preparation

The preparation necessary before starting the experiments were weighing the BMs and making the acid- and reductant solutions. First, the BM was weighed to approximately 1 g in a weighing cabinet. The exact weights are given in Table A.1.1 in Appendix A.1. Then the H_2O_2 solution was prepared by diluting 54 mL of 98.1 g/mol H_2SO_4 solution which further was diluted by 446 mL distilled water to produce a 2.03 M H_2SO_4 solution (see Appendix A.2 for the calculations for how the solutions should be prepared). Thereafter, the reduction solution was prepared by diluting 51 mL of 30% H_2O_2 with 149 mL of distilled water, resulting in a molarity of 2.5 M (see Appendix A.3 for the calculations for how the solutions should be prepared). The volume of the respective solution added to the acid- and reductant concentrations in the leaching system was at all time controlled.

3.1.2   Experimental setup

A 100mL round flask with three necks and an IKA RET basic hotplate with magnetic stirring was used for the leaching experiments in combination with an IKE ETS-D5 to control the temperature, see Figure 3.1.1. A water bath was used to achieve an even temperature in the leaching solution. The water bath was further placed on the hot plate, and the round flask was placed in the water bath. The magnetic stirrer ensured an even stirring speed of $\sim$ 400 rpm. When each sample was collected, the pH was also measured using a PHM210 standard pH meter, see Figure 3.1.2.
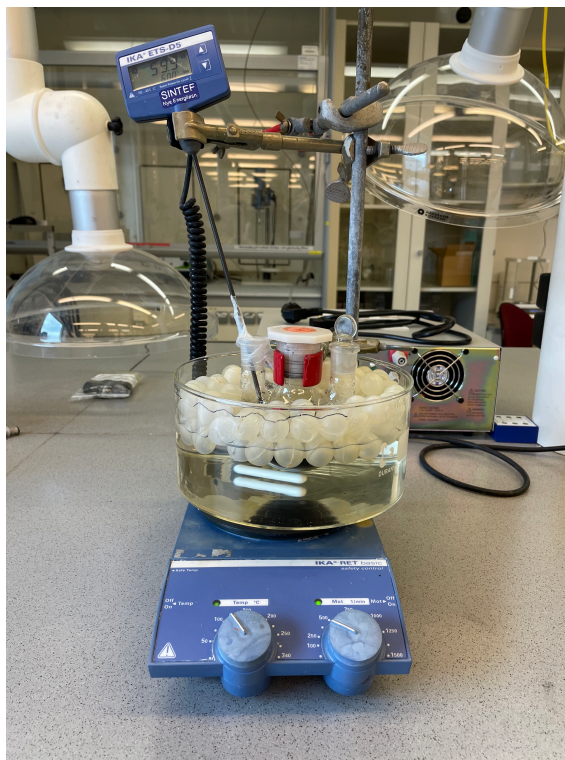
Figure 3.1.1: Experimental set-up for the leaching experiments.
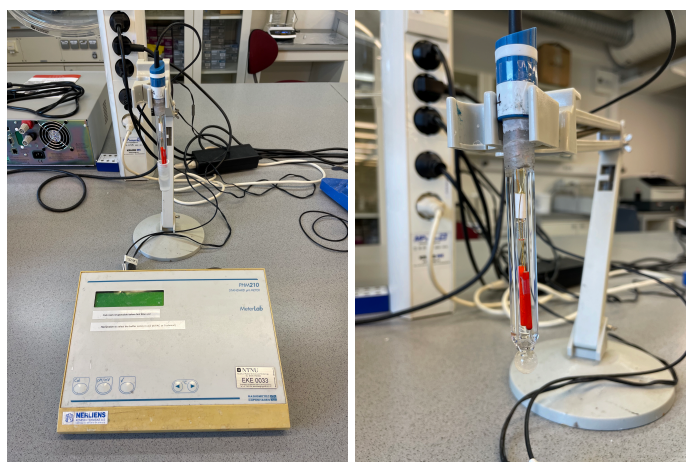
(a) PHM210, standard pH meter. **(b)** A closeup of the pH wand.

Figure 3.1.2: A standard pH meter used to measure the pH in the leaching solution.

A 5 mL NORM-JECT Luer syringe was used to extract the leachate samples for analysis. The leachate was then filtered using a 25 mm syringe filter (w/0.45 µm Polyethersulfone Membrane) placed in a MetalFree tube, see Figure 3.1.3.
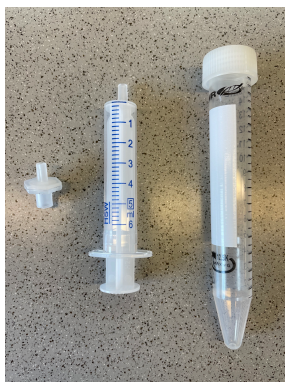
Figure 3.1.3: Image of the type of filters, syringes, and tubes used to extract each sample.

A Butchner funnel and 70 mm Whatman Filter Papers were used to filter the remaining leachate after each experiment, as illustrated in Figure 3.1.4.
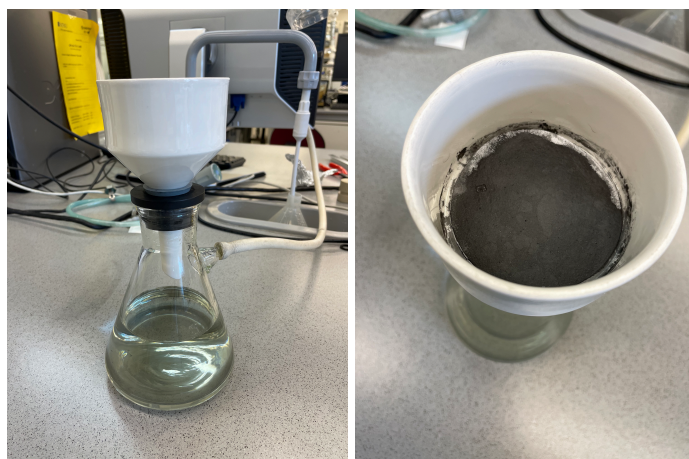
(a) Set-up of the Büchner funnel and Büchner flask.

(b) Birds eye view of the Büchner funnel.

Figure 3.1.4: Image of the Büchner funnel setup and in situ filtering of the solid residue (SR).

3.1.3   Experimental procedure

The first step of the experiments was to set up the equipment, according to Figure 3.1.1, followed by adding distilled water, acid, reductant, and a magnetic stirrer to the round flask. The BM was added when the solution reached the desired temperature. The magnetic stirrer was turned to a lower speed to avoid foaming of the BM with the acid. When the BM had been mixed into the solution, the stirring rate was again increased to approximately 400 rpm. The solution was then set to leach for 23 hours (1380 min) with the given temperature and stirring

speed so that the leaching system reached assumed equilibrium. The leachate samples were collected at their respective time intervals, and the temperature and pH were noted for every extraction. The temperature and pH evolution during leaching are presented in Appendix B. After 23 hours, the last leachate sample was collected, and the heat and stirring were turned off. The remaining leachate was filtered to collect the SR.

3.1.4   Leachate analysis

ICP-MS analyses were used to characterise the leachate samples using an *Element2 - Finnigan MAT* unit at the laboratory facilities of ALS Global. With the ICP-MS technique, low concentrations of elements can be detected. The elements are ionised through a plasma source before they are sorted, and their mass is accounted for. The results from the ICP-MS are given in µg/L.

3.2   Characterisation of BM and SR

3.2.1   Sample preparation

Before characterising the BMs and SRs by SEM, they had to undergo sample preparation consisting of several steps to ensure that the powder was not sucked into the vacuum pumps during the analysis. During the sample preparation, the BM was transferred to a sample holder and placed inside a metal ring to prevent the powder from scattering when the liquid epoxy was added.

The epoxy was prepared by mixing EpoFix Resin and EpoFix Hardener in a 1:7 weight-based ratio, and was thoroughly mixed for ca. 2 minutes to secure that one phase was obtained. A vacuum chamber set to reach 10 bar was used to remove any air bubbles formed during the mixing. After bubble removal, the epoxy mixture was slowly poured onto a sample holder and mixed with the powder inside a metal ring, eventually covering the bottom of the sample holder for stabilisation. The sample holder was set aside for at least 8 hours for the epoxy to harden.

When the epoxy had hardened, the sample was polished using a Strugers TergaForce 5 polishing machine. The polishing procedure consisted of four steps with varying polishing surfaces and lubricants/suspensions. The first polishing step was performed with a SiC grinding paper and water as a lubricant for 15 seconds, which secures the removal of the outer surface of the particles in the sample. Between the polishing steps, the samples were placed in an ultrasonic cleaner. The following steps aim to eliminate the grinding tracks from the first polishing steps, using finer surfaces and diamond suspensions. The three last steps had a total polishing time of 11.5 minutes.

When the sample preparation was finished, the samples were put in a heating cabinet for surplus fumes and moisture to evaporate.

3.2.2   Characterisation with Scanning Electron Microscope (SEM)

A SEM unit can be used to characterise the materials and surfaces of the samples. The electron beam can either be stationary or scan the surface. Different signals can be detected with SEM, *e.g.*, secondary and backscattered electrons. The different signals give different information about the sample [30].

In the present work, a Zeiss-Supra 55VP-FEG-SEM (Trondheim, Norway) unit was used to characterise the cathode particles in the BM, as well as the SR, to determine the overall ratio of metals to O in the analysed BMs. The oxidation state of the metals could be deduced from that ratio, and thereby also the efficiency of the reduction process from the thermal pre-treatment.

A combination of individual particles and metal oxide species was later used to model the cathode particles with the average values from the characterisation. However, it should be noted that the cathode particles were found to have a structure that included multiple transition metals and Li. Since the O content and morphology were not homogeneous, the method is only a simplification that neglects this complexity.

During the present SEM-EDS characterisation, the beam was stationary and characterised six spots on each sample, and the signal was secondary electrons. The

six spots were analysed by EDS to find the element composition in the cathode particles. All images were taken with the magnification of x 1 K, and the accelerating voltages were set to 10 kV.

3.3 Modelling

3.3.1 HSC Chemistry 9

The computer software HSC Chemistry 9 is in most cases used to perform thermodynamic calculations and simulate chemical processes. In the present work the software was used to model the leaching process of the BMs, as well as to find the equilibrium compositions in view of the given initial composition of each of the BMs, the reactants, and the leaching conditions. This was accomplished by using the HSC Chemistry 9 modules *"Equilibrium Composition"* and *"Reaction Equations"*. Each module is described below.

Equilibrium Composition

The *"Equilibrium Composition"* module simulates the composition of a heterogeneous multi-component system when equilibrium is reached, which in the present work is the leaching system. To use the software, the chemical reaction system needes to be defined, *i.e.,* all phases and species in the raw material, as well as all species expected to be present in the leaching system. The amount of each raw material had to be given, as well as the temperature used during each leaching experiment. The module uses the Gibbs energy minimising method to calculate the equilibrium compositions. The method focuses on the chemical potential of the species involved, and numerical solutions are obtained by minimising the total potential (or Gibbs free energy) of the system. The molal standard Gibbs free energy function is used to determine the equilibrium composition, and can for a system with a mixture of n chemical species and x_i moles of specie i be expressed as [31] [32]:

$$F(X) = \Sigma_n^{i=1} f_i \qquad (3.3.1)$$

In the experimental work performed in the present thesis, sixteen leaching experiments were performed and modelled using the *"Equilibrium Composition"* module. The input amounts are based on the average composition of the BMs, *i.e.*, of the BM-U and BM-T compositions, which were analysed by SEM-EDS and ICP-MS. To ensure that equilibrium was reached in the each of the experiments, a 23-hour time interval was set, which made it possible to compare the experimental and modelled results.

Reaction Equations

The *"Reaction Equations"* module in the HSC Chemistry 9 software allows for the calculation of the enthalpy, entropy, heat capacity, and Gibbs free energy of both chemical reactions and pure substances. In addition, the corresponding thermodynamic constants of the responses can also be calculated.

In the present work, the module was used to model the dissolution and reduction of the metals in the BMs in reaction with acid and reductant. Equations 3.3.2, 3.3.3 and 3.3.4 below are presented below as a general representation of these reactions where "M" signify the metal in focus:

$$M(s) + 2\,H^+ \rightarrow M^{2+} + H_2(g) \tag{3.3.2}$$

$$M(s) + H_2O_2 + H^+ \rightarrow M^{2+} + H_2O \tag{3.3.3}$$

$$MO(s) + H^+ \rightarrow M^{2+} + H_2O(g) \tag{3.3.4}$$
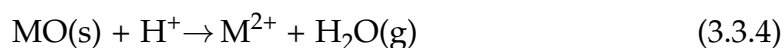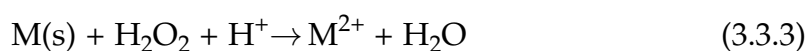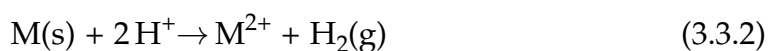
The reactions taking place in the leaching system were identified, and by using the present module, the thermodynamic constants were extracted. The results were later used as input data in the kinetic Python model.

3.3.2   Kinetic Python model

Python is a general-purpose programming language that can be used to solve a wide range of issues [33]. In the present work the Python model was used to

model the leaching system of the BMs, as well as for comparing the obtained results with experimental and HSC Chemistry 9 results.

The present approach was chosen to provide a better understanding of the overall system, as well as the specific reactions that would occur. It was also believed to be the most effective way to improve the leaching efficiency.

Compared to the modelling performed by using the HSC Chemistry 9 software, the Python model was designed to consider the kinetics of the processes in the system in question, resulting in a more precise prediction of the leaching efficiency. For this to be possible, some essential factors need to be established, *i.e.*:

- model equations

- system reactions

- temperature-dependent kinetic constants of the reactions and coefficients of the species in question

- temperature-dependent thermodynamic constants

The equations expressing the global kinetic model are the (i) chemical reaction rate, (ii) specie concentration, (iii) solid specie concentration, (iv) initial surface area, (v) number of particles, and (vi) change in surface area, and these terms will be described below.

The chemical reaction rate is expressed in Equation 3.3.5 and given as the time derivative of the species ($\frac{dC_i}{dt}$) involved in the given reaction divided by the stoichiometric coefficient (ν_{r_i}). It is also proportional to the reactions´ kinetic constant (k_{kin}) multiplied by the concentration of the reactions ($C_{i,t-1}$) to the power of their kinetic orders ($\nu_{kin_{i,j}}$). The reactants´ kinetic coefficients are dependent on the mechanisms of the reaction:

$$v = \frac{1}{\nu_{r_i}} \frac{dC_i}{dt} = k_{kin} \cdot \Pi_{i=1}^{sp_l} C_{i,t-1}^{\nu_{kin_{i,j}}} \qquad (3.3.5)$$

The specie concentration (see Equation 3.3.6) is obtained after variables separation and integration when all reactions in the system are considered:

$$C_i(t) = C_{i,t+1} + \Sigma_j^{n_{reac}}(v_{r_{i,j}} \cdot k_{kin,j}) \cdot \Pi_{i=1}^{sp_l}(C_{i,t-1}^{v_{kin_{i,j}}} \cdot \Delta t) \tag{3.3.6}$$

Equation 3.3.7 describes the solid specie concentration, which is expressed as a function of the particles´ surface area of the species (A_i) multiplied by the species surface concentration ($C_{i,area}$) divided by the aqueous volume (V):

$$C_{i,sol} = \frac{A_i C_{i,area}}{V} \tag{3.3.7}$$

Further, the sphere surface formula is used to calculate the initial surface area (A_i), as given in Equation 3.3.8.

$$A_i = n_p 4\pi \hat{r}_{vol_{PSD}}^2 \tag{3.3.8}$$

where n_p describes the number of particles and $\hat{r}_{vol_{PSD}}^2$ is the mean particle size when volumetric percent particle size is considered.

The number of particles (see Equation 3.3.9) was calculated from the initial mass of the specie (m_{BM}), the density of the specie (ρ_i), and devided by the volume of a spherical particle ($\frac{4}{3r^3}$) where the radius is given by the mean size ($\hat{r}_{vol_{PSD}}$):

$$n_p = \frac{m_{BM} w_i^t}{\rho_i} \frac{3}{4\hat{r}_{vol_{PSD}}^3} \tag{3.3.9}$$

Lastly, the change in the surface area used the initially known particle size distribution derived from the particle´s mass change, which was calculated from the change in leachate concentration or measurements of SR mass and composition. The change in surface area is given by 3.3.10.

$$\frac{dA}{dM} = \frac{dA}{dr}\frac{dr}{dM} = n8\pi r(n4\pi r^2 \rho)^{-1} = \frac{2}{\rho r} = \frac{2}{\rho}\frac{4n_p \pi \rho}{3M}^{\frac{1}{3}} \tag{3.3.10}$$

where M is the mass of the particle and n_p is the number of particles with initial size r^0 that satisfies the initial mass of the BM.

To use the equations above, all the system reactions taking place in the system in question needed to be identified. Due to kinetic effects and precipitation reactions competing with the dissolution reactions, the cathode might not achieve complete dissolution. Identifying those reactions was, therefore, crucial to making a kinetic model.

The kinetic constants of the reactions and the kinetic coefficients of the species needed to be determined experimentally, however, due to the complexity of the leaching system, each reaction could not be assessed individually to find these. Still, constants from previous studies can be used as representative values even if the leaching conditions are not identical. To manage this issue, the global kinetic Phyton model was run as a non-linear regression model against experimental data.

To find the temperature-dependent thermodynamic constants, the system reactions and species were evaluated in the HSC Chemistry 9 module *"Reaction Equations"*, which provided the thermodynamic constant at each temperature in a temperature interval of interest.

4 | Results

In the present chapter, the obtained results of the project will be presented, *i.e.*, (i) the determined BM compositions obtained through modelling and characterisation, (ii) the analysed leaching efficiencies of the performed laboratory experiments, (iii) the characterised solid residues from the industrial samples, and (iv) the modelled leaching system.

The main elements in focus during both the experimental part of the work, as well as the numerical simulations, have been Li, Ni, Mn, Co, and O, and the results presented will therefore be directly linked to these elements.

4.1 Black Mass (BM) composition

The BM powders were analysed using ICP-MS (ALS Global, Element2 - Finnigan MAT, Sweden) and further characterised using an SEM-EDS unit (NTNU, Zeiss-Supra 55VP-FEG-SEM, Norway) to provide insight into the chemical composition of each sample. The obtained results were further used as input data to the kinetic Python model, which calculated the chemical composition for both the BM-U and the BM-T samples. The obtained results will be discussed below.

4.1.1 SEM-EDS characterisation

Six micrographs of each BM, *i.e.*, six micrographs of the BM-U samples and six of the BM-T samples, were taken using SEM and further analysed using EDS. In Figure 4.1.1 and Figure 4.1.2, representative micrographs of the two BMs are presented. As seen in Figure 4.1.1, the oxide particles present in the BM-U sam-

ples (seen as white spots in the SEM micrographs) are smaller and appear more often than in the case of the BM-T samples seen in Figure 4.1.2, which are more prominent and less in numbers.
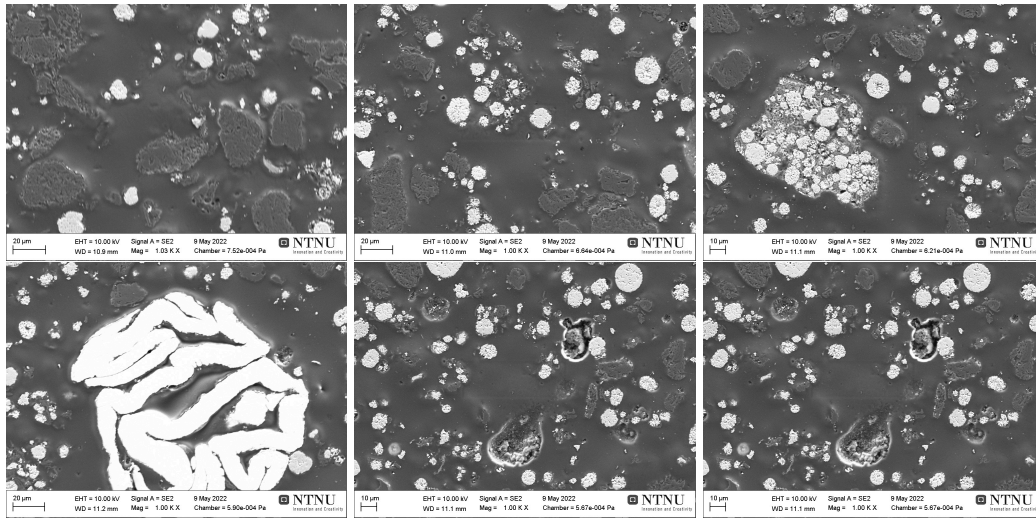
Figure 4.1.1: Representative SEM images of BM-U. Magnification x 1K
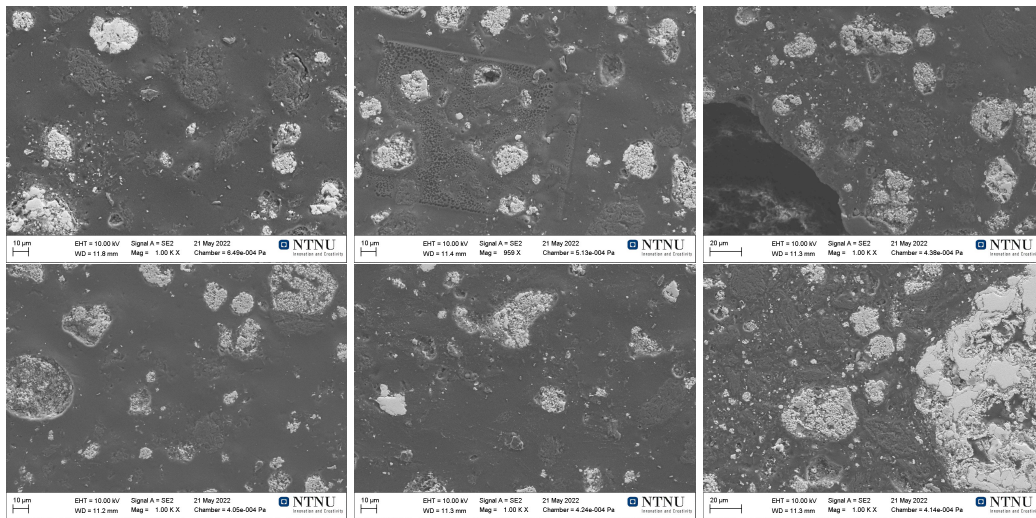
Figure 4.1.2: Representative SEM images of BM-T. Magnification X 1K

Figure 4.1.3 and Figure 4.1.4 shows an representation of the EDS analysis for the BM-U and BM-T samples. The remaining EDS analysis are given in Appendix D. As seen from the Figures, the chemical mapping demonstrates that the BM-U samples, on average, had a higher O concentration in the particles than the BM-T samples. The average O concentration was calculated to be 35.4 % and 24.9% for, respectively, the BM-U and BM-T.
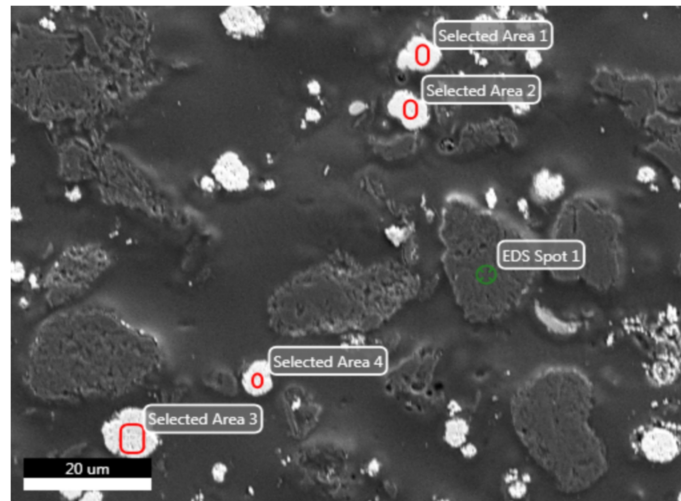
(a) Overview of Selected Areas and EDS Spots.
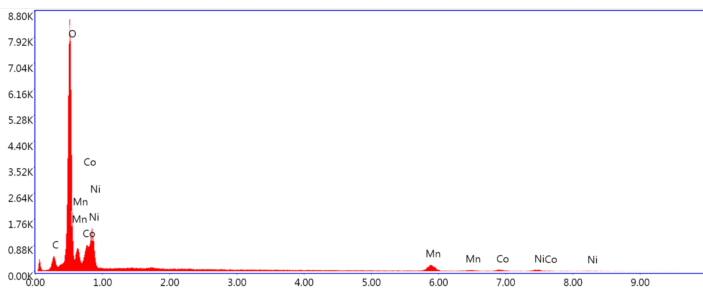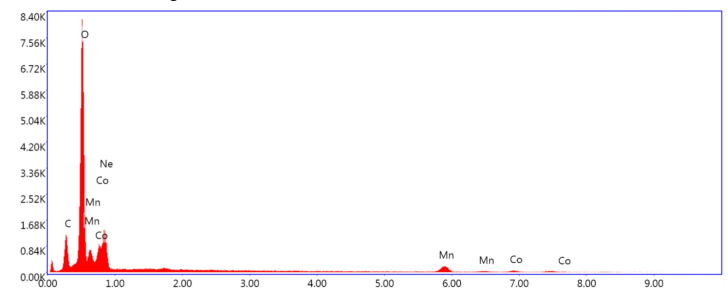
(b) Mass specter: Selected Area 1

(c) Mass specter: Selected Area 2
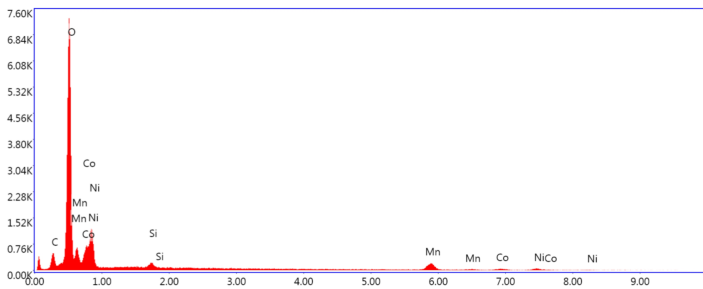
(d) Mass specter: Selected Area 3
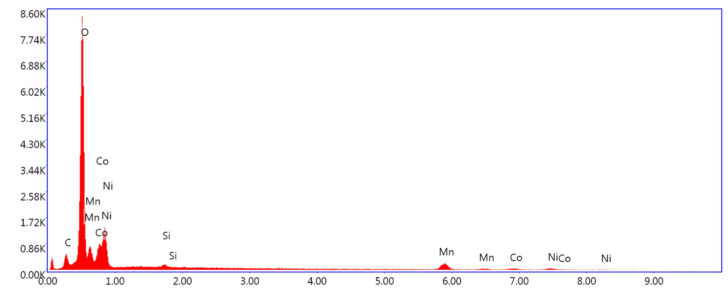
(e) Mass specter: Selected Area 4
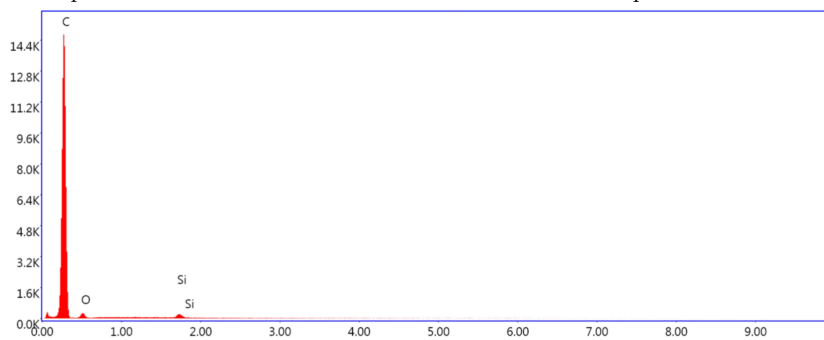
(f) Mass specter: EDS Spot 1

Figure 4.1.3: Representative chemical mapping by EDS of a BM-U sample
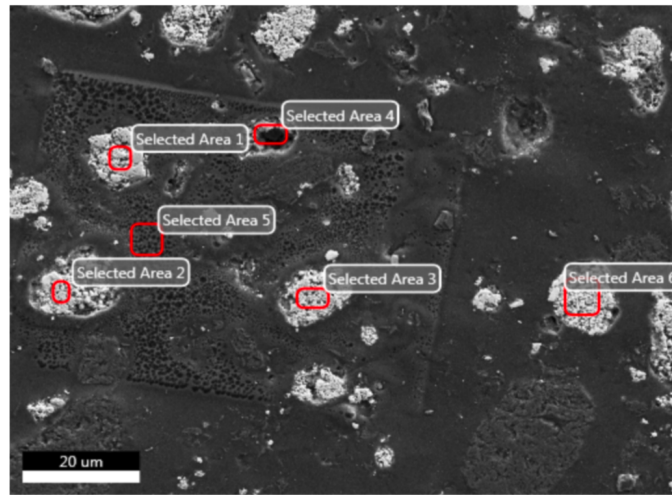
(a) Overview of Selective Areas and EDS Spots.
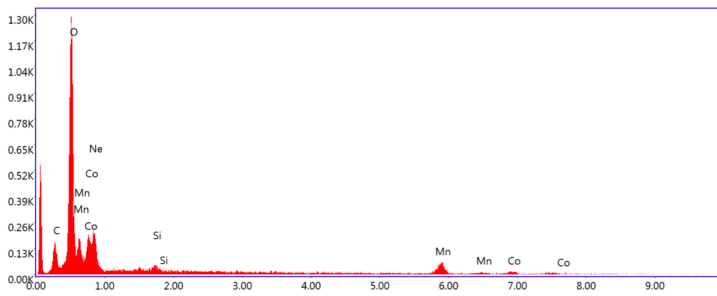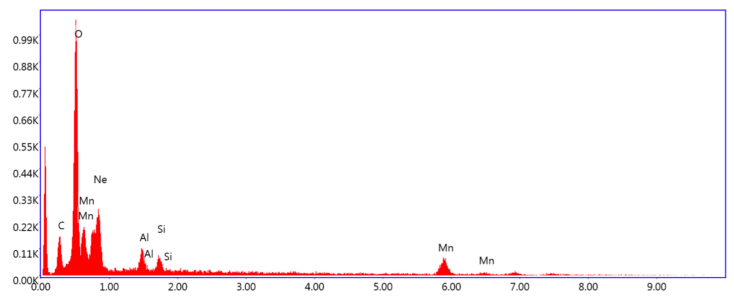
(b) Mass specter: Selected Area 1

(c) Mass specter: Selected Area 2
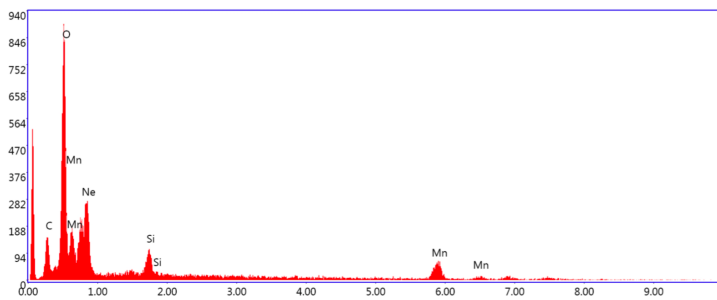
(d) Mass specter: Selected Area 3
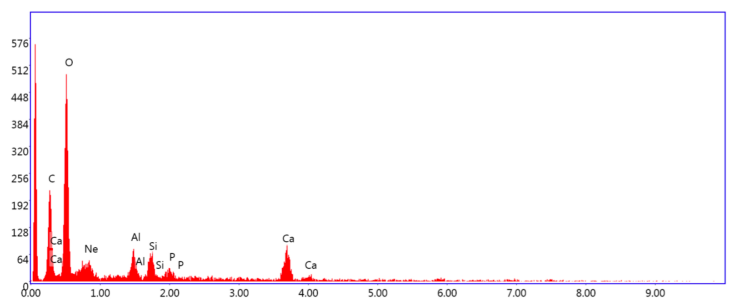
(e) Mass specter: Selected Area 4
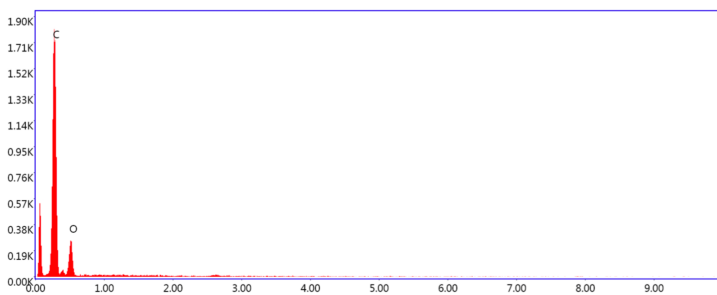
(f) Mass specter: Selected Area 5
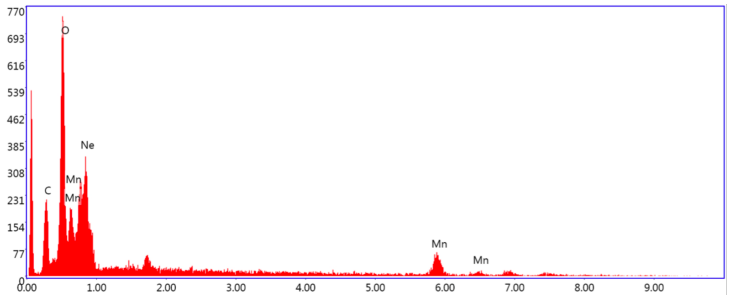
(g) Mass specter: Selected Area 6

Figure 4.1.4: Representative chemical mapping by EDS of a BM-U sample

4.1.2 ICP-MS analyses

The ICP-MS results of the BMs in view of the elements Li, Ni, Mn, and Co are shown in Table 4.1.1. As seen from the table, the chemical composition of the BM changes after thermal treatment. In the BM-T samples, the content of Li, Ni, Mn, and Co are approximately 1-4% higher than in the case of the BM-U samples.

Table 4.1.1: ICP-MS results of the BM-U and BM-T samples.

BM	Element	Results [mg/kg]	Calculated percentage [%]
	Co	71500	7.15
	Li	43800	4.38
BM-U	Mn	107000	10.7
	Ni	138000	13.8
	Co	90400	9.04
	Li	53400	5.34
BM-T	Mn	133000	13.3
	Ni	173000	17.3

4.1.3 Modelling of chemical compositions

The ICP-MS results from Table 4.1.1, as well as the O analyses from the SEM-EDS characterisation, were used as input data in the developed kinetic Python model to calculate the chemical compositions of the BM samples, see Table 4.1.2.

Table 4.1.2: Modelled BM compositions.

Specie	BM-T [mol]	BM-U [mol]
Li_2O	0.00385	0.00316
Ni	0.00139	0
NiO	0.00154	0
$Ni_2O_3 \cdot 2H_2O$	0	0.00117
MnO	0.00239	0
Mn_2O_3	0	0.00006
MnO_2	0	0.00183
CoO	0.00154	0
$Co_2O_3 \cdot 2H_2O$	0	0.00060

As seen from the table, the BM-U samples were reduced during the thermal treatment according to the following reactions:

$$Ni_2O_3 \cdot H_2O \longrightarrow 4\,NiO + O_2 + 2\,H_2O \tag{4.1.1}$$

$$2\,NiO \longrightarrow 2\,Ni + O_2 \tag{4.1.2}$$

$$2\,Co_2O_3 \cdot H_2O \longrightarrow 4\,CoO + O_2 + {}_2H_2O \tag{4.1.3}$$

$$2\,Mn_2O_3 \longrightarrow 4\,MnO_2 + O_2 \tag{4.1.4}$$

$$2\,MnO_2 \longrightarrow 2\,MnO + O_2 \tag{4.1.5}$$
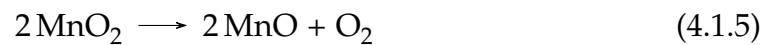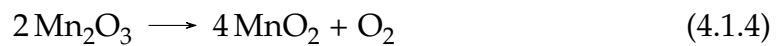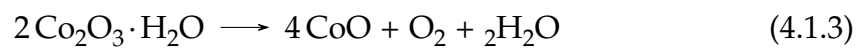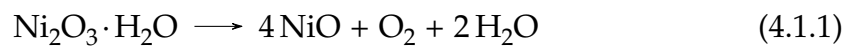
4.2   Experimental leaching efficiency

To determine the leaching efficiency of the BMs the leachate samples were analysed by ICP-MS.

4.2.1 Leaching efficiency of BM-U

An overview of the parameters used during the leaching experiments of the BM-U samples is shown in Table 4.2.1, *i.e.*, the temperature and the used amounts of acid/reductant. The calculated leaching efficiencies are shown in Figure 4.2.1.

Table 4.2.1: Overview of the parameters temperature and used amounts of acid/reductant during the leaching experiments of the BM-U samples.

Leaching conditions	Temperature [°C]	Acid [mL]	Reductant [mL]
AO9	40	20	0
AO10	40	10	0
AO11	40	20	5
AO12	40	10	5
AO13	60	20	0
AO14	60	10	0
AO15	60	20	5
AO16	60	10	5

As seen from the figure, Li has the highest leaching efficiency in nearly all the experiments (20-30 %) except in the case of tests AO9 and AO12 where the performance was 6 % and 13 %, respectively. The remaining elements, Ni, Co, and Mn, reveal similar leaching efficiencies in almost all experiments, with the majority between 15 % and 25 %, with only one exception for Mn in test AO9 with a value of 4 %.

(a) Experiment with Leaching conditions AO9

(b) Experiment with Leaching conditions AO10

(c) Experiment with Leaching conditions AO11

(d) Experiment with Leaching conditions AO12

(e) Experiment with Leaching conditions AO13

(f) Experiment with Leaching conditions AO14

(g) Experiment with Leaching conditions AO15

(h) Experiment with Leaching conditions AO16

(i) Labels

Figure 4.2.1: Calculated leaching efficiencies for the elements Li, Ni, Mn and Co present in the BM-U samples for the parameters temperature and used amounts of acid/reductant.

Overall, the best leaching parameters proved to be those of test AO15, where all the elements had a leaching efficiency slightly below 30 %, as well as test AO16 with leaching efficiencies of around 25 %. The parameters of these tests can be summarised as being performed at high temperatures and with an increased amount of reductant.

Furthermore, it can also be seen in Figure 4.2.1 that there was an overall increasing trend in the leaching efficiencies during the first 180 minutes, and after that, it flattened out.

In Figure 4.2.2 the leaching efficiencies for Li, Ni, Mn and Co as a function of (a) temperature, (b) used amount of acid, and (c) used amount of reductant are shown. The lines in the graphs are trend lines provided by Microsoft Excel (version 16.54), which calculated the average efficiencies based on the high and low parameter values. As seen in Figure 4.2.2a, it was evident that the leaching efficiency for all the elements increased with increasing temperature. The same trend can be seen for increasing amounts of reductants (see Figure 4.2.2c), except in the case of Li where almost no difference was observed. Regarding adding of an increased amount of acid, the leaching efficiency was observed to decrease for Li and increase for all the other elements, however, to a lesser degree for Mn (see Figure 4.2.2b).To illustrate the trends, Figure 4.2.2 is only plotted for leaching efficiencies between 10 % and 30 %.

4.2.2 Leaching efficiency of BM-T

An overview of the parameters used during the leaching experiments of the BM-T samples is shown in Table 4.2.2, *i.e.*, the temperature and the used amounts of acid/reductant. The calculated leaching efficiencies are shown in Figure 4.2.3. It should be noted that the y-axis does not have the same maximum value in all experiments due to the higher leaching efficiencies in some tests, *i.e.,* tests AO5 and AO6 with a maximum at 35 %, test AO7 at 60 %, and all the remaining tests at 30 %.

(a) Parameter study on temperature

(b) Parameter study on acid

(c) Parameter study on reductant
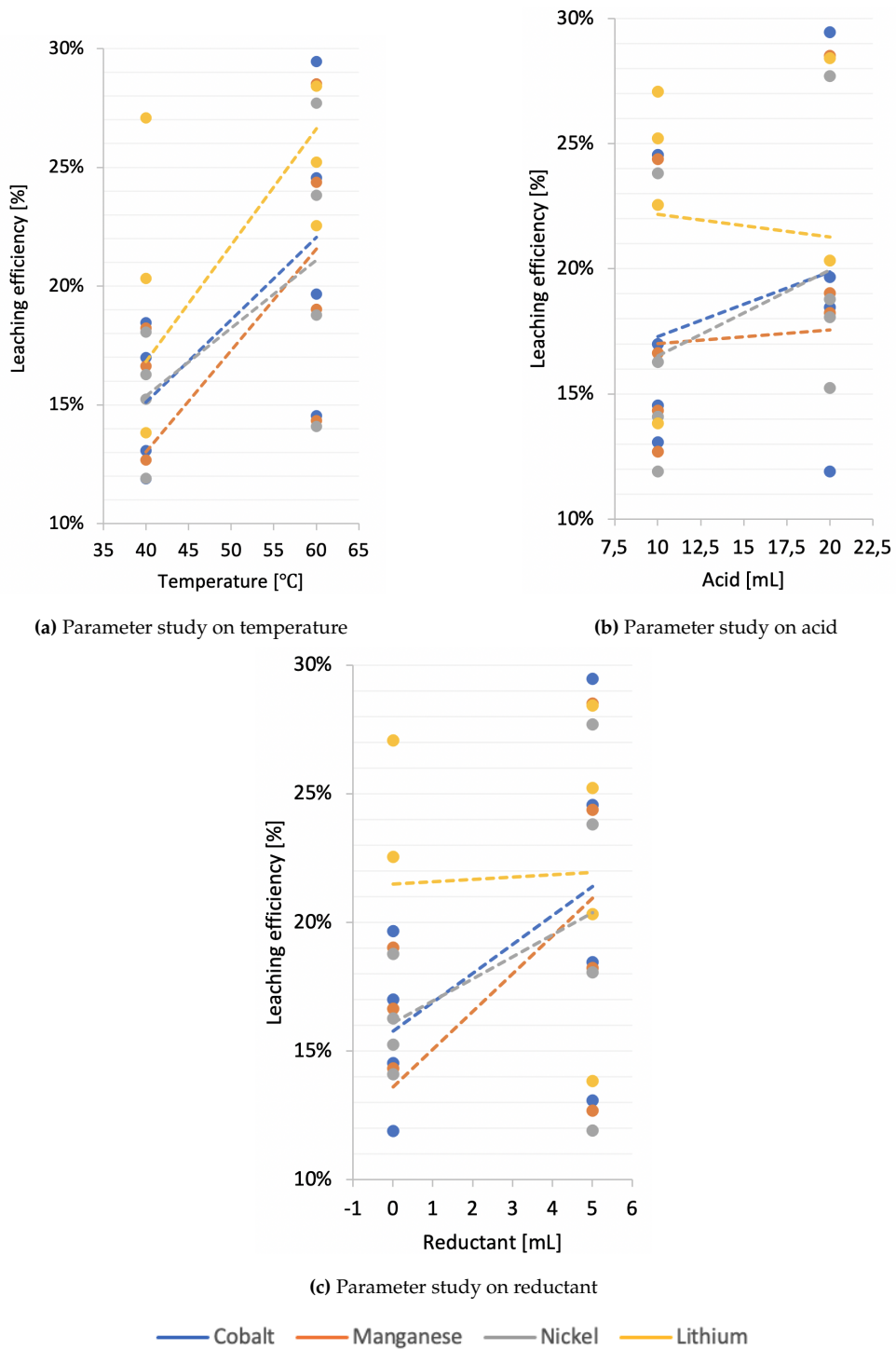
Figure 4.2.2: Leaching efficiency of the elements Li, Ni, Mn and Co in BM-U samples as a function of (a) temperature, (b) used amount of acid, and (c) used amount of reductant

Table 4.2.2: Overview of the parameters temperature and used amounts of acid/reductant during the leaching experiments of the BM-T samples.

Leaching conditions	Temperature [°C]	Acid [mL]	Reductant [mL]
AO1	40	20	0
AO2	40	10	0
AO3	40	20	5
AO4	40	10	5
AO5	60	20	0
AO6	60	10	0
AO7	60	20	5
AO8	60	10	5

(a) Experiment with Leaching conditions AO1

(b) Experiment with Leaching conditions AO2

(c) Experiment with Leaching conditions AO3

(d) Experiment with Leaching conditions AO4

(e) Experiment with Leaching conditions AO5

(f) Experiment with Leaching conditions AO6

(g) Experiment with Leaching conditions AO7

(h) Experiment with Leaching conditions AO8

(i) Labels
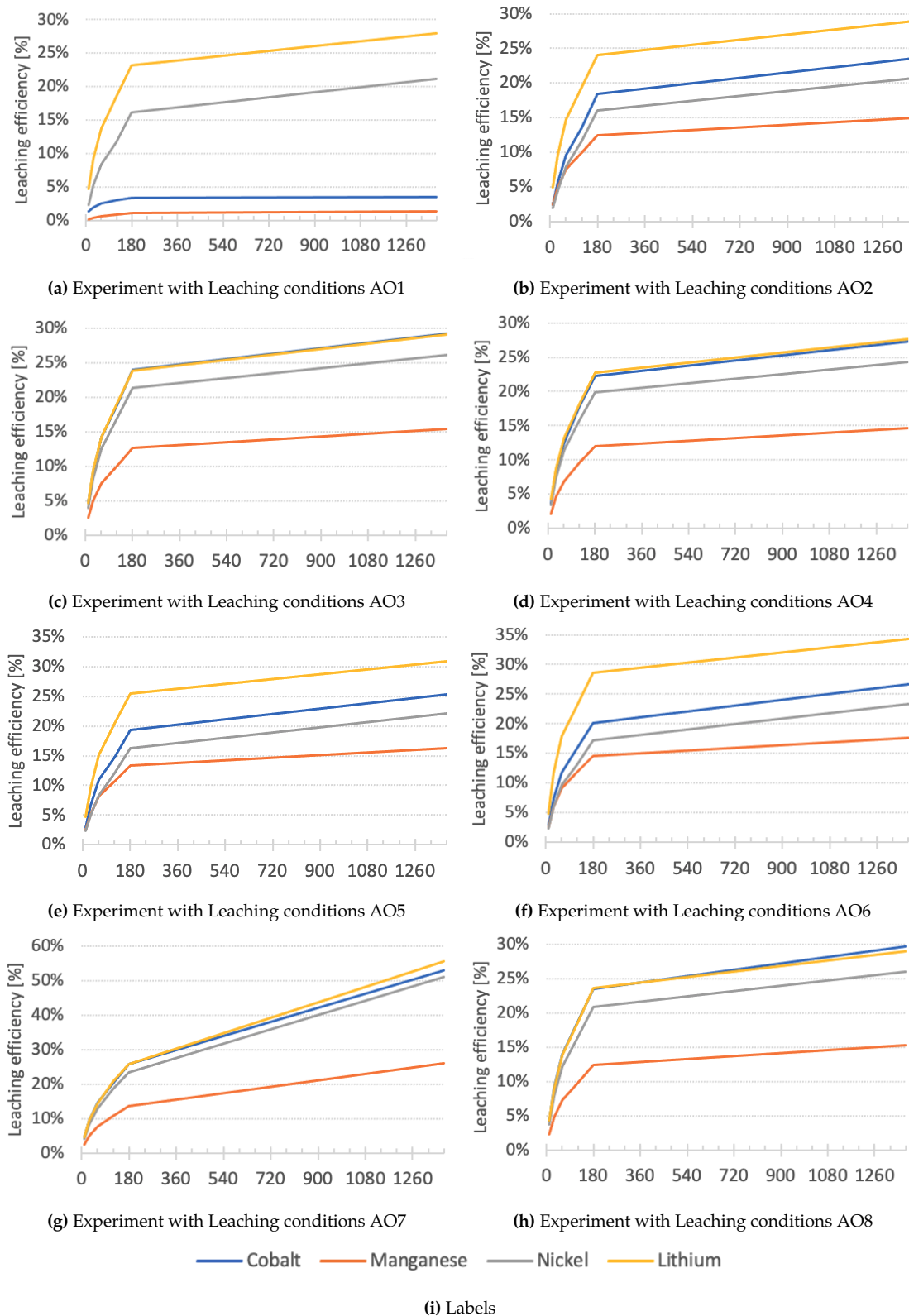
Figure 4.2.3: Calculated leaching efficiencies for the elements Li, Ni, Mn and Co present in the BM-T samples for the parameters temperature and used amounts of acid/reductant.

As seen from the Figure, even in this case, Li has the highest leaching efficiency

in all experiments (30 %), except for test AO7, which was observed to be even higher (56 %). Co was observed to have leaching efficiencies in the range of 24-29%. In the case of tests AO3, AO4, AO7, and AO8, where an increasing amount of reductant was used, the same leaching efficiencies as for Li were observed. Mn, however, was observed to have significantly lower leaching efficiencies (15 %), with tests AO1 and AO7 deviating from the trend with leaching efficiencies of 1 % and 26 %, respectively. Ni was observed to have leaching efficiencies between 20 % and 26 % in all experiments, except for test AO7, which was 51 %. It should, however, be mentioned that Ni was observed to have higher leaching efficiencies in the experiments where the reductant was present.

Overall, the leaching experiments performed on the BM-T samples showed only minor variations in the leaching efficiencies for each element. However, tests AO1 and AO7 clearly deviate from this trend. The lowest leaching efficiencies were observed for test AO1 in the case of Co and Mn with values below 5 %. The highest leaching efficiency was reached in test AO7, where Li, Co, and Ni showed a leaching efficiency above 50 %. Even if AO7 offered the best test conditions for Mn, the leaching efficiencies were notably lower at 26 %.

Similarly to the BM-U samples, it can also be seen in Figure 4.2.3 that there was an overall increasing trend in the leaching efficiencies during the first 180 minutes, and after that, it flattened out.

In Figure 4.2.4, the leaching efficiencies for Li, Ni, Mn and Co as a function of (a) temperature, (b) used amount of acid, and (c) used amount of reductant are shown. In this case, as well, the lines in the graphs are trend lines provided by Microsoft Excel (version 16.54), which calculated the average efficiencies based on the high and low parameter values. To illustrate the trends, Figure 4.2.4 is only plotted for leaching efficiencies between 10 % and 40 %.

(a) Parameter study on temperature

(b) Parameter study on acid

(c) Parameter study on reductant
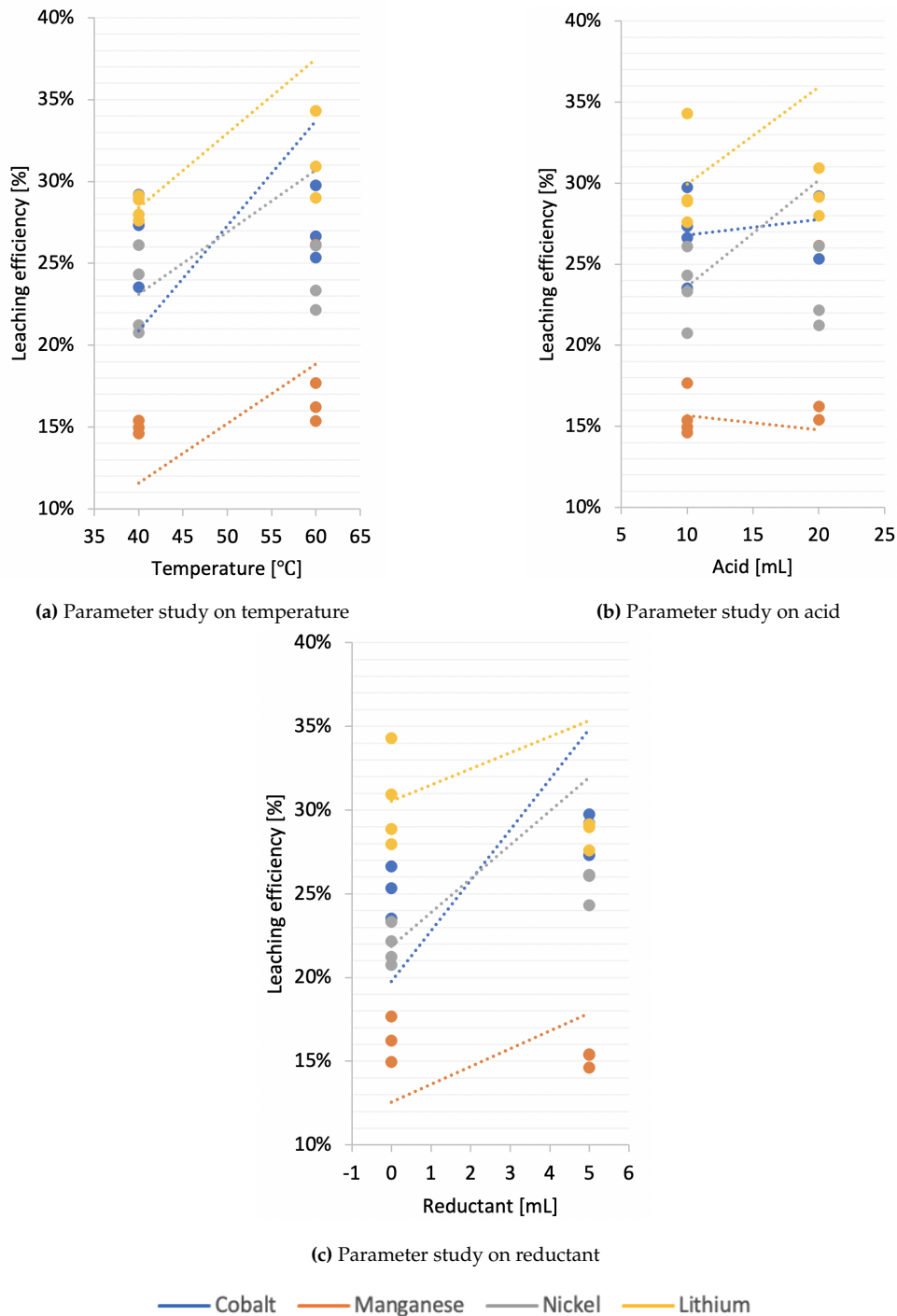
Figure 4.2.4: Leaching efficiency of the elements Li, Ni, Mn and Co in BM-T samples as a function of (a) temperature, (b) used amount of acid, and (c) used amount of reductant.

As seen in Figure 4.2.4a, it was apparent in this case that the leaching efficiencies for all the elements increased with increasing temperature from 40°C to 60°C. The same observation was made when the reductant amount was increased (Figure 4.2.4c). Regarding the addition of an increased amount of acid, the leaching

efficiency was observed to increase for all elements, except for Mn, where it decreased (see Figure 4.2.4b).

4.2.3 Comparison of BM-U and BM-T results

To evaluate the impact that the thermal treatment had on the leaching efficiencies for Li, Ni, Mn and Co as a function of the experimental conditions, the obtained results in both cases were plotted together in Figure 4.2.5. The red lines in the figure represent the BM-U samples and the blue lines the BM-T samples.

(a) Lithium

(b) Nickel

(c) Manganese

(d) Cobalt
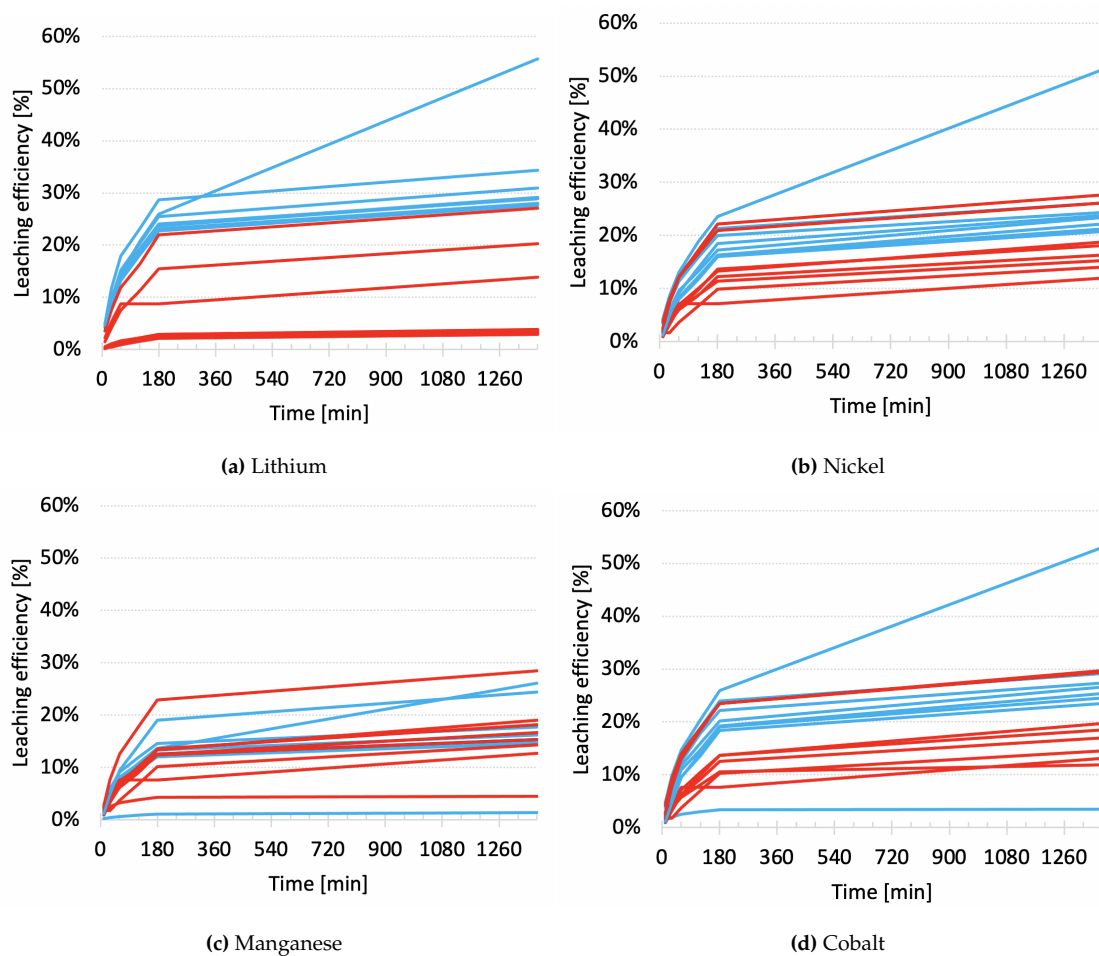
Figure 4.2.5: Comparison of the leaching efficiency of (a) Li, (b) Ni, (c) Mn and (d) Co for test conditions for both the BM-U (red lines) and BM-T (blue lines) samples.

As can be seen from Figure 4.2.5, the BM-T samples have generally higher leaching efficiencies than the BM-U samples, even though it is not obvious for every element. For Li, *e.g.*, it is evident that the thermal treatment resulted in higher

leaching efficiencies since all the blue lines lie above the red lines, see Figure 4.2.5a. However, this is not as obvious in the case of Co, Mn, and Ni. For the elements Co and Ni, several of the experiments performed on the BM-T samples revealed higher leaching efficiencies (see Figure 4.2.5d and Figure 4.2.5b) than in the case of the BM-U samples. For Mn it was, however, observed to be the opposite, *i.e.*, several of the BM-U samples revealed higher leaching efficiency values than in the case of the BM-T samples. The overall lowest leaching efficiency ($\sim$ 1 %) was obtained for the BM-T samples in view of the leaching of Mn during AO1 test conditions, followed by Co ($\sim$ 3 %) during the same leaching conditions. In addition, for the AO15 and AO16 test conditions, all the investigated elements had a leaching efficiency in the range of Li, *i.e.*, 28.4 % and 25.2 % for Li, 27.7 % and 23.8 % for Ni, 28.5 % and 24.4 % for Mn, and 29.5 % and 24.6 % for Co, respectively.

This comparison shows that the leaching efficiency is not higher for the experiments with the BM-T samples regardless of parameters and elements.

4.2.4 Reproducibility

To evaluate the reproducibility of the results, one experiment was randomly chosen, *i.e.*, test conditions AO13, and performed two times on BM-U samples following the same experimental procedures as in the earlier experiments, *i.e.*, tests conditions AO17 and AO18.

In Figure 4.2.6, the leaching efficiencies of Li, Ni, Mn and Co from the BM-U samples during the identical tests AO13 (blue line), AO17 (red line), and AO18 (grey line) are shown. As seen from the Figure, the observed results for test AO13 are overall higher than for the identical tests AO17 and AO18 (1-2 %). Good agreement is, however, observed between the results of tests AO17 and AO18. The standard deviation between the leaching efficiencies for each element is calculated and presented in Table 4.2.3. A standard deviation below 1 is considered low, and as seen in the table, all standard deviations are below 0.1 and, thereby, low.

(a) Lithium (Li).

(b) Nickel (Ni)

(c) Manganese (Mn).

(d) Cobalt (Co).

(e) Labels
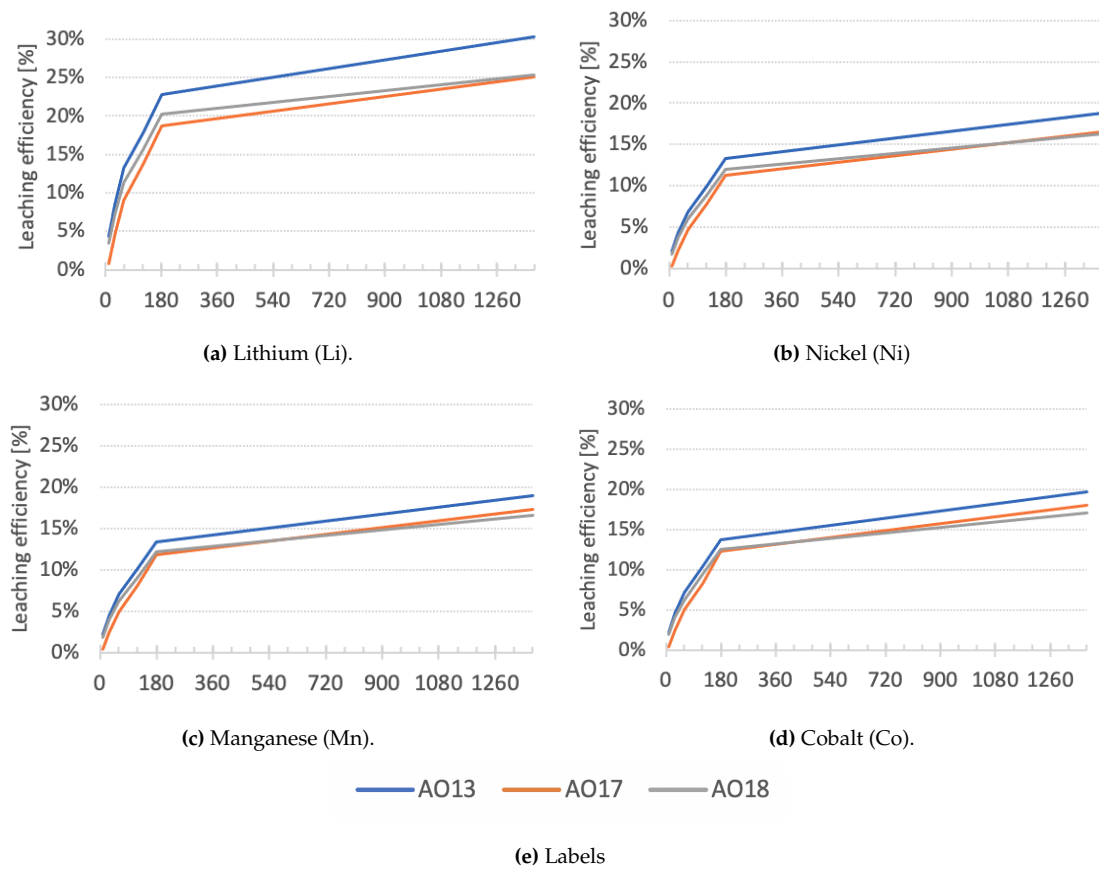
Figure 4.2.6: Comparison of the leaching efficiency for Li, Ni, Mn and Co from the BM-U samples during tests AO13 (blue lines), AO17 (red lines), and AO18 (grey lines).

Table 4.2.3: Standard deviation of the leaching efficiencies for Li, Ni, Mn and Co from BM-U samples during identical test conditions.

	Standard deviation			
Time	Cobalt	Manganese	Nickel	Lithium
10	0.010	0.010	0.009	0.019
30	0.011	0.011	0.011	0.020
60	0.010	0.010	0.011	0.021
120	0.011	0.010	0.011	0.021
180	0.007	0.008	0.010	0.021
1380	0.013	0.012	0.014	0.029

4.3   Solid residue (SR) characterisation

The SR from the leaching experiments performed at ERAMET pilot facilities were characterised and used for comparison. The exact leaching parameters are unknown, however, the experiments are performed on a larger scale than those performed in the present work and at a much higher temperature.

In 4.3.1 and 4.3.2, the SR is shown after leaching the BM-U and BM-T samples. As seen in Figure 4.3.1, the SR from the BM-U (SR-U) sample leaching experiments appears to consist of smaller particles than in the case of the SR from the BM-T (SR-U) sample experiments.

In Figure 4.3.3 and Figure 4.3.4, the EDS analysis for a high atomic concentration of O in the SR-T samples is shown. It was, however, established that the oxides detected were not originating from the $LiNi_{(1-y-z)}Mn_yCo_zO_2$ (Lithium Nickel Manganese Cobalt Oxide (NMC)) cathode particles investigated in the present work. The elements detected were Silicon (Si), Calcium (Ca), Magnesium (Mg), Aluminium (Al), Thulium (Tm), Bromine (Br), and small amounts of other elements. Moreover, the same elements were also found to exist in the SR-U samples, just to a lesser degree. As these elements were not within the scope of the present work, they were not further investigated. The complete chemical mapping of the SRs with SEM-EDS is given in Appendix D.
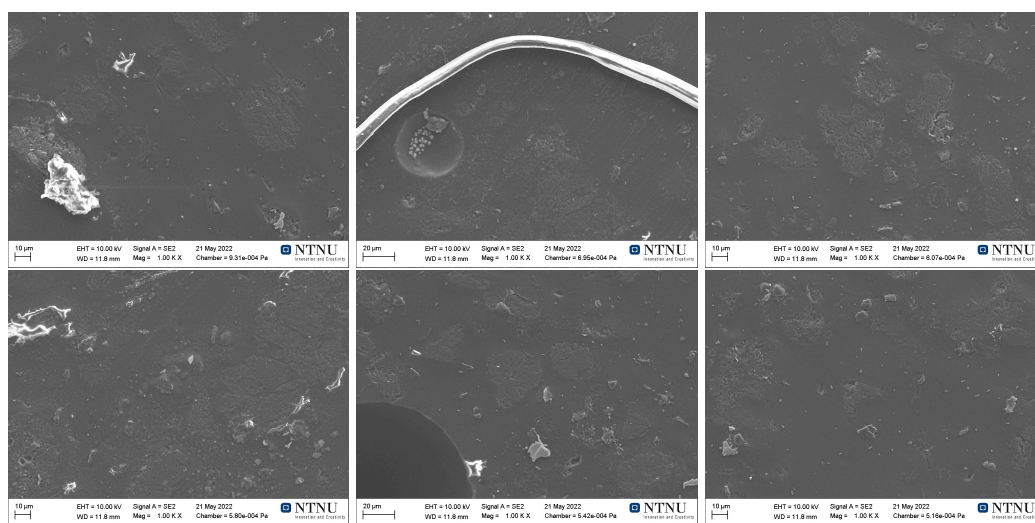
Figure 4.3.1: SEM-EDS analysis of the SR-U samples originating from the leaching experiments performed at ERAMETS pilot facilities.
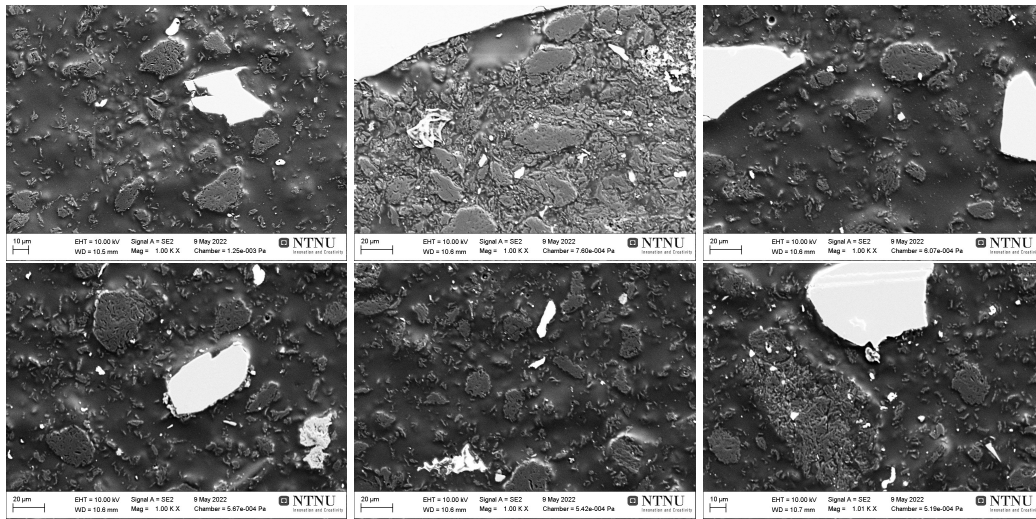
Figure 4.3.2: SEM-EDS analysis of the SR-T samples originating from the leaching experiments performed at ERAMETS pilot facilities.
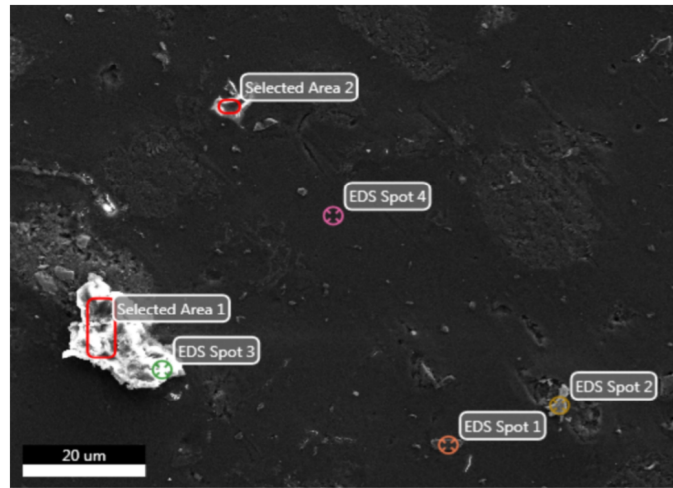
(a) SR-U: Area 1. Overview of Selected Areas and EDS Spots.
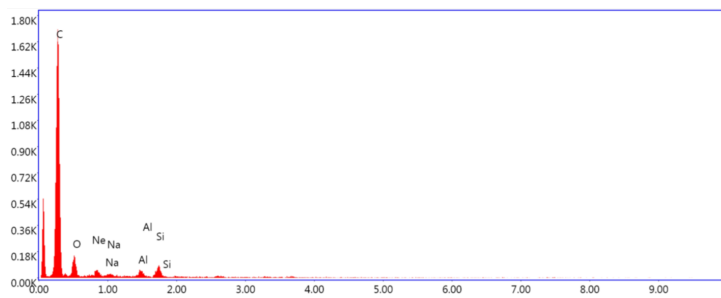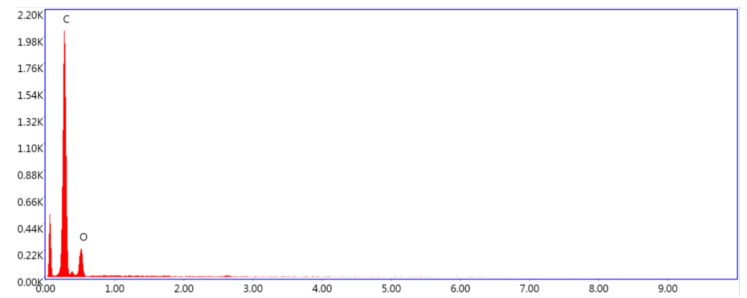
(b) Mass specter: Selected Area 1
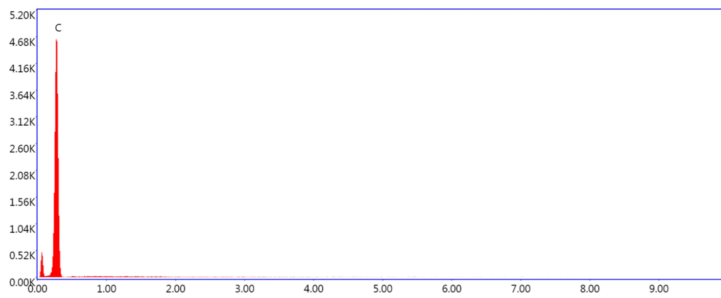
(c) Mass specter: Selected Area 2
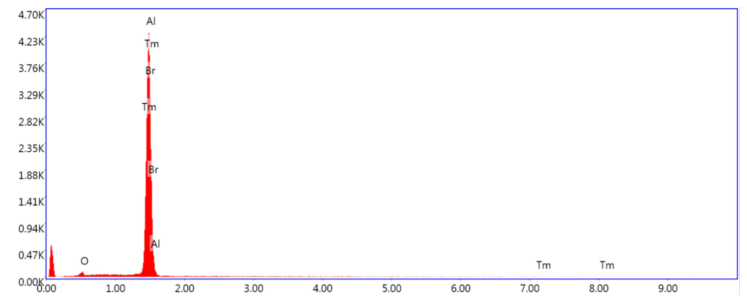
(d) Mass specter: EDS Spot 1
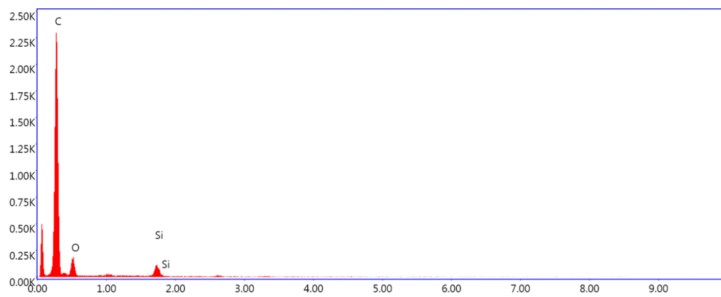
(e) Mass specter: EDS Spot 2
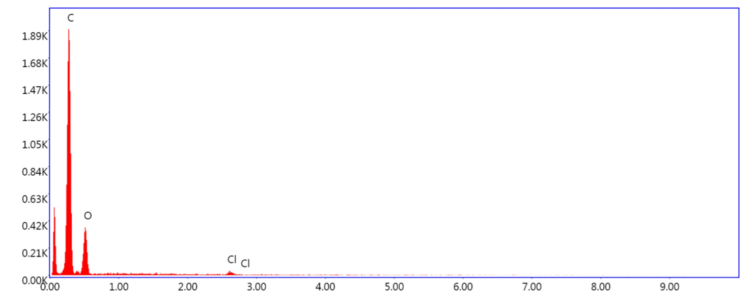
(f) Mass specter: EDS Spot 3

(g) Mass specter: EDS Spot 4

Figure 4.3.3: Representative chemical mapping by EDS of a SR-U sample
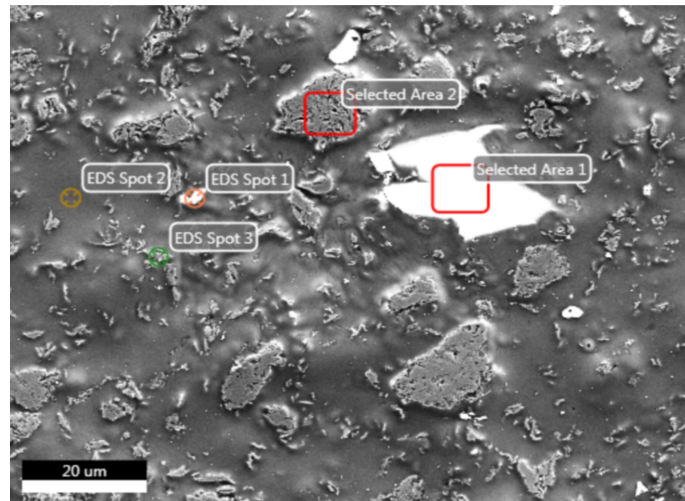
(a) SR-T: Area 1. Overview of Selected Areas and EDS Spots.
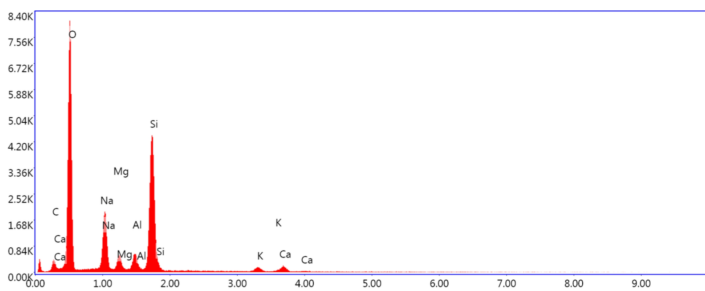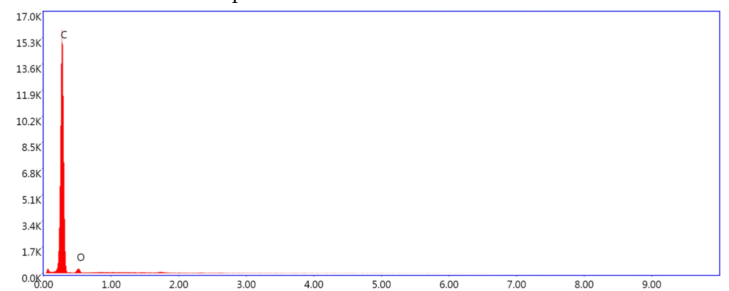
(b) Mass specter: Selected Area 1

(c) Mass specter: Selected Area 2
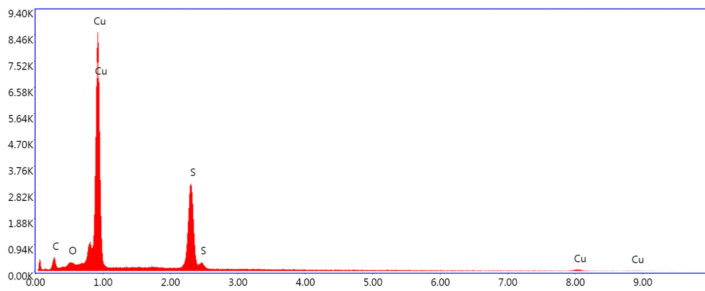
(d) Mass specter: EDS Spot 1
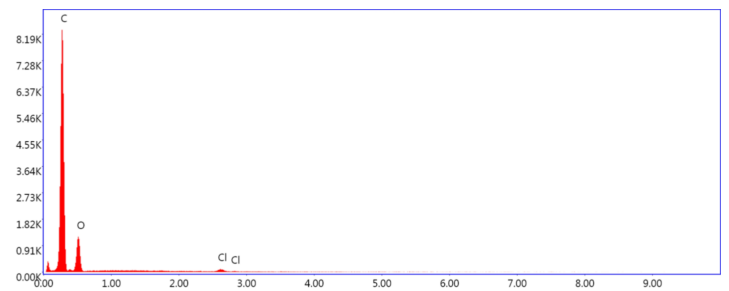
(e) Mass specter: EDS Spot 2
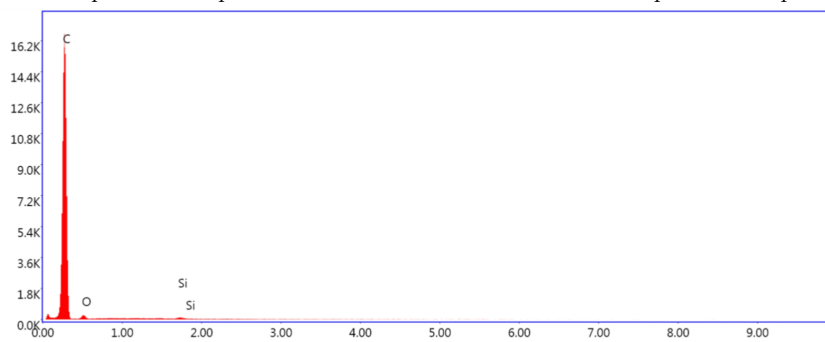
(f) Mass specter: EDS Spot 3

Figure 4.3.4: Representative chemical mapping by EDS of a SR-T sample

4.4 Modelling of the leaching system

In the present section, the leaching system was modelled using a kinetic Python model with input of thermodynamic data modelled and calculated using the HSC Chemistry 9 software and the data experimentally generated in the present work. The results from the model are presented below.

4.4.1 HSC Chemistry 9 calculations

The module *"Equilibrium Composition"* in the HSC Chemistry 9 software was used to calculate the leaching system. The input data was the respective BM compositions modelled with the use of the Python framework and the parameters used in the laboratory experiments.

For every leaching experiment performed, the HSC Chemistry 9 software calculated the corresponding leaching systems to reach 100% leaching efficiency at equilibrium. The obtained values proved to deviate significantly from the experimental results, where the highest leaching efficiencies at equilibrium were experimentally established to be 55.7% for Li, 51.3% for Ni, 26.1% for Mn, and 53% for Co (see Figure 4.2.3g).

4.4.2 Kinetic Python model

Sixteen leaching systems were evaluated in the kinetic Python model, corresponding to the leaching experiments performed in the present work. The input data were (i) the composition of the respective BM, (ii) the temperature, (iii) the used amount of acid, and (iv) the used amount of reductant (see Table 3.1.2).

In Figure 4.4.1, the modelling results for the BM-U samples are shown, and in Figure 4.4.2, for the BM-T samples. The leaching system´s change in concentration was calculated every second for 60 minutes of modelled leaching. It should be noted that the data given in Figure 4.4.1 and Figure 4.4.2 have the concentration given in the molarity (M) of each element in question on the y-axis and not the leaching efficiency (%) as in the case of most of the earlier Figures presented.
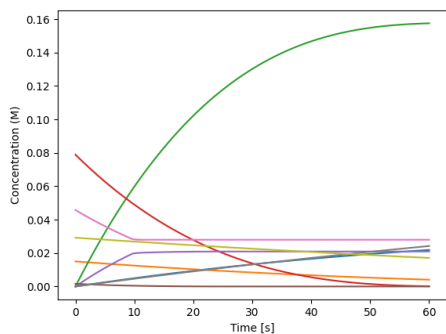
(a) Modelled leaching system with TestID AO9
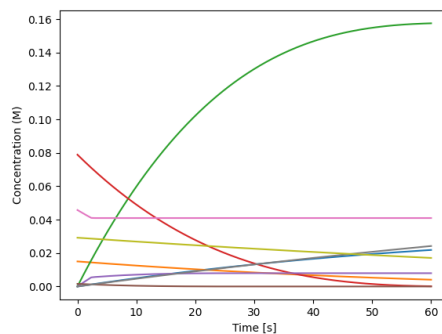
(b) Modelled leaching system with TestID AO10
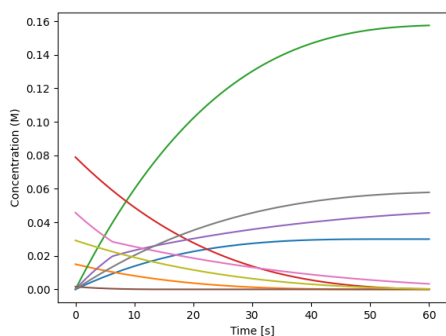
(c) Modelled leaching system with TestID AO11
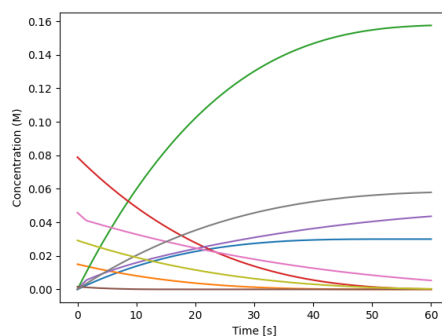
(d) Modelled leaching system with TestID AO12
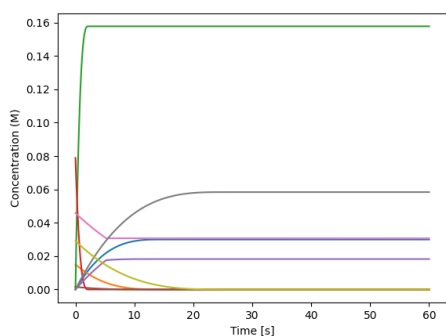
(e) Modelled leaching system with TestID AO13
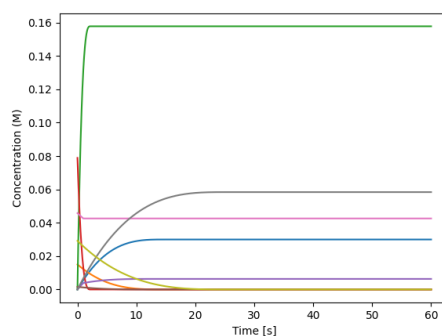
(f) Modelled leaching system with TestID AO14
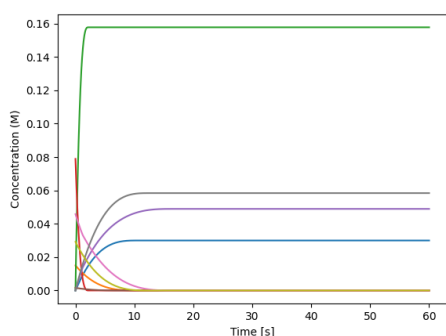
(g) Modelled leaching system with TestID AO15
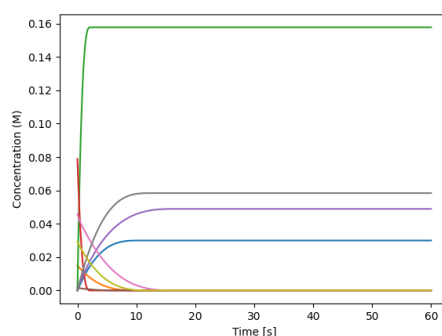
(h) Modelled leaching system with TestID AO16
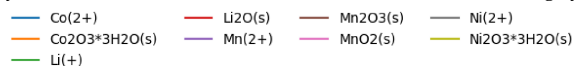
(i) Labels

Figure 4.4.1: Modelled concentrations in molarity (M) of each specie in the leaching system versus time in seconds for the BM-U samples.

(a) Modelled leaching system with TestID AO1

(b) Modelled leaching system with TestID AO2

(c) Modelled leaching system with TestID AO3

(d) Modelled leaching system with TestID AO4

(e) Modelled leaching system with TestID AO5

(f) Modelled leaching system with TestID AO6

(g) Modelled leaching system with TestID AO7

(h) Modelled leaching system with TestID AO8

(i) Labels
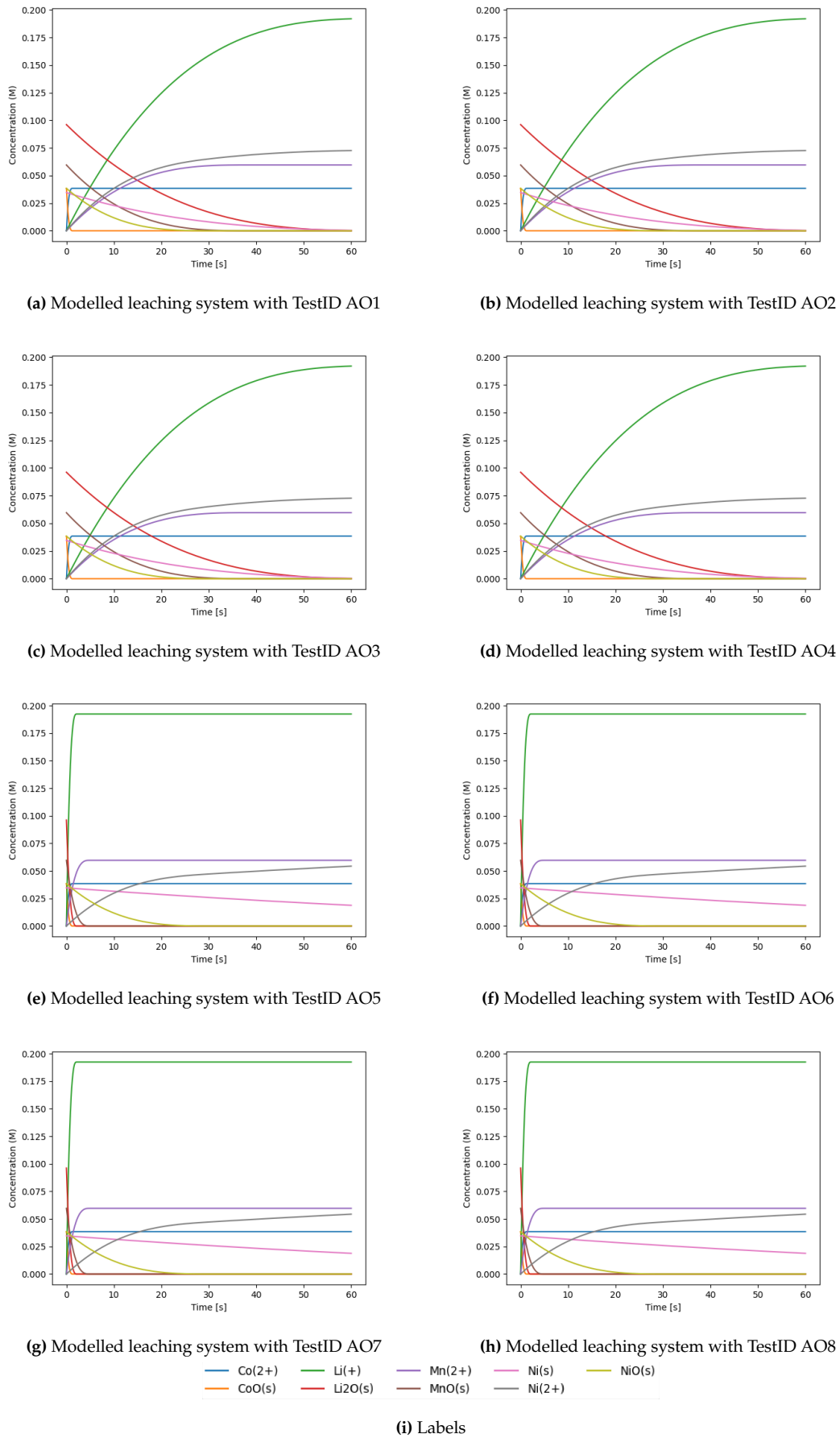
Figure 4.4.2: Modelled concentrations in molarity (M) of each species in the leaching system versus time in seconds for the BM-T samples.

Modelling of the systems with BM-U samples

As seen in Figure 4.4.1, the modelled leaching experiments performed with the test conditions AO9, AO10, AO11 and AO12 at 40 °C and 60 °C showed different results. In the case of Li, the used amounts of acid and reductant were not observed to influence the dissolution rate. The rate of dissolution of the other elements, *i.e.*, Co, Mn and Ni, was to a varying degree observed to be influenced by the used amount of reductant and, in the case of the Mn, even by the acid. The temperature was, however, clearly the dominating parameter in view of reaching complete dissolution (100 % leaching efficiency) for all the investigated elements.

The Li-containing specie of the BM-U samples was experimentally established to be Li_2O. In Figures 4.4.1a, 4.4.1b, 4.4.1c and 4.4.1d, it can be observed that during the modelling of tests AO9, AO10, AO11 and AO12 at 40 °C, the dissolution rate of Li_2O was slower than at 60 °C. In the four test conditions mentioned above, only $\sim$ 99 % dissolution was reached after 60 min. The rate of dissolution of LiO_2 at 60 °C, however, reached complete dissolution after only 128 seconds. Modelling attempts were made with additions of both acid and reductant, but as mentioned above, they were not observed to influence the rate of dissolution at any of the modelled temperatures.

The Ni-containing species of the BM-U samples were experimentally established to be $Ni_2O_3 \cdot 3H_2O$. When modelling the test conditions, AO9 and AO10, Ni was primarily influenced by the temperature and reached complete decomposition at 60 °C. However, adding a reductant affected the decomposition rate when modelling the system at 40 °C, which increased the leaching efficiency from 41 % during tests AO9 and AO10 to 99 % during test conditions AO11 and AO12.

The Mn-containing species of the BM-U samples were experimentally established to be Mn_2O_3 and MnO_2. When modelling the different test conditions at both 40 °C and 60 °C, they were observed to behave quite differently from the other species present. Complete dissolution was observed for Mn_2O_3 during modelling at all the different test conditions (AO9, AO10, AO11, and AO12) at both 40 °C and 60 °C, while not for MnO_2. The dissolution rate of both species was, however, not only influenced by the temperature but also by adding a reductant (tests

AO11 and AO12), which increased the rate. Additions of acid were observed not to have any significant impact on the rate of dissolution of Mn_2O_3 but to decrease the rate in the case of MnO_2 (the leaching efficiency decreased from $\sim$ 39 % to 11 % when modelled at 40 °C and from 33 % to 12 % when modelled at 60 °C). MnO_2 was, however, observed to have reached complete dissolution at 60 °C with additions of a reductant and with a higher acid concentration (tests AO15 and AO16).

The Co-containing species of the BM-U samples were experimentally established to be $Co_2O_3 \cdot 3H_2O$. In the case of Co, the used amounts of reductant were crucial for leaching at 40 °C. When modelling tests AO9 and AO10, Co was observed not to leach completely, however, when modelling tests AO11 and AO12, with additions of the reductant $Co_2O_3 \cdot 3H_2O$, complete dissolution was observed after 3212 seconds. Increasing the modelling temperature to 60 °C secured complete dissolutions for all the test conditions, with an apparent increase in the dissolution rate for the test conditions where a reductant was added. However, the amount of acid was not observed to influence the modelled results.

Modelling of the systems with BM-T

As seen in Figures 4.4.2 4.4.2a, 4.4.2b, 4.4.2c and 4.4.2d, the modelled leaching experiments performed with the test conditions AO1, AO2, AO3 and AO4 were observed to have nearly identical results regardless of the used amounts of acid and reductant. The temperature, however, was observed to have an essential impact on the system. This was also established to be the case for the modelled leaching experiments with the test conditions AO5, AO6, AO7 and AO8 in Figures 4.4.2e, 4.4.2f, 4.4.2g and 4.4.2h, where the changes in concentration also were observed to be independent of the amount of acid and reductant.

The Li-, Ni-, Mn- and Co-containing species of the BM-T samples were experimentally established to be Li_2O, Ni, NiO, MnO and CoO. It can be seen from Figure 4.4.2 that when the system was modelled with the test conditions AO1, AO2, AO3 and AO4 at 40 °C, Co and Mn reached complete dissolution after 74 seconds and 2318 seconds respectively. Li and Ni, however, never reach complete dissolution, and by the end of the 60 minutes, the modelled leaching efficiency

reached $\sim$ 99 % for LiO_2, 100 % for NiO and $\sim$ 99 % for Ni(s).

When modelling the same system at 60 °C the dissolution rate increased rapidly for Li and Mn, which reached 100 % after, respectively, 127 seconds and 292 seconds. Co reached 100 % dissolution in at both temperatures, *i.e.,* 74 seconds. Ni, however, was observed to have a slower dissolution rate and Ni(s) only reached $\sim$ 46 % dissolution. It should be noted that NiO(s) was modelled to reach complete dissolution after 1832 seconds.

5 | Discussion

The present chapter will discuss the results obtained in view of the parameters tested during the leaching of the different BMs. First, general notes about the results will be made before a more in-depth discussion on the leaching efficiency of Li, Mn, Ni and Co is evaluated based on both the experimental- and modelling approaches chosen.

5.1 Parameters´ influence on the experimental trends

From previous studies, knowledge about what theoretically should occur has been gathered, and an overall increase in all the parameters presently investigated, *i.e.*, leaching temperature, used amount of acid and reductant, and longer leaching times, should generally increase the leaching efficiency of the elements present in an average BM [34][35][36]. He *et al.* [34] , Yang *et al.* [35] , and Viecelie *et al.* [36] all experienced that adding acid to the leaching solution increased the leaching efficiency. This was also observed in the present experiments, where some elements (Li and Ni) were more influenced by increasing the amount of acid added to the leaching solution than others. Yang *et al.* [35] suggested that the reason for this could be the more frequent collisions taking place between the leaching agent and the particles in the BM. However, not all metal oxides react similarly due to different bonding lengths and binding energies between the metal and the O atom. Vieceli *et al.* [36] proposed, based on this, that when the BM is thermally treated, and the high oxidation oxides are reduced, a significant increase in leaching efficiency could be observed even with only small amounts of acid in the system. Hence, increasing the amount of acid even further proved

not to give any significant difference in the results, as also observed in the present experiments where a surplus of acid existed. Similarly, the reductant will facilitate the leaching by reducing the oxidative state of the metals in the oxides. The addition of reductant gave notable to significant increases for the elements investigated.

Further, when the temperature increases, the leaching efficiency increases, possibly due to the leaching reactions being endothermic. The reactions are thus more favourable in systems with higher temperatures. In addition, the dissociation constant and ion transfer in the acid increases with higher temperatures. Another factor is that the average kinetic energy increases when the temperature increases, leading to more frequent and energetic collisions, accelerating the reactions [35]. In the present experiments, the temperature was a parameter that significantly impacted the experimental leaching efficiencies.

Leachate samples were extracted at different time intervals, and from the ICP-MS analysis, the resulting ion concentrations showed minor changes after 3 hours, as illustrated by the flattening curves in the leaching efficiency figures (see Figure 4.2.1 and Figure 4.2.3). This seems to indicate that the leaching reaction was finishing. A similar flattening of the leaching was discovered by Yang *et al.* [35], which found no significant change after 60 minutes.

As presented in Chapter 4, the present experiments did not always behave exactly as in previous studies or as modelled, and the deviations will be discussed in the following sections.

5.2   Behaviour of the elements

In the following section, the obtained experimental and modelling results will be presented, and the behaviour of each element discussed separately. The relevant leaching reactions in each individual case, as well as the calculated equilibrium constant, will also be presented and further discussed to evaluate thermodynamic favourability in view of the different leaching parameters investigated. The *"Reaction Equations"* module in the HSC Chemistry 9 software was used to calculate

the equilibrium constant for each reaction at 40 °C and 60 °C.

It is worth noticing that the equilibrium constants decrease slightly with increasing temperatures for all the reactions (see Table 5.2.1, Table 5.2.2, Table 5.2.3 and Table 5.2.4). However, a notable increase in leaching efficiency was observed for all elements both in the BM-U and BM-T (see Figure 4.2.2a and Figure 4.2.4a). It is believed that the previously explained effects of increasing the temperature have a more significant impact on the system than the relatively low decrease in the equilibrium constant.

The overall analysis of the BMs showed that the weight % of each element investigated in the present work, *i.e.*, Li, Mn, Ni and Co, increased by 1-4%. This was also reported by Yang et al. [35] and Viecelie et al. [36] and explained by them based on a decrease in C content during thermal treatment.

During the discussion, there will be a mention of *"an average increase/decrease in leaching efficiency"* related to increasing the parameters, which refers to the present studies performed on BM-U and BM-T samples (see Figure 4.2.4 and Figure 4.2.2).

5.2.1 Lithium (Li)

As presented in Chapter 4, Li has proved to have the highest leaching efficiency. This was an expected result since Li only has one oxidation state and is reactive in acidic environments. The bond between Li-ions and the O-ion in Li_2O is, in other words, more accessible to break than the bonds in the additional metal oxides present in the system. Li is also more stable as a cation than in metallic form, meaning it will not be reduced back to metallic Li under the present conditions [37].

The reaction of interest for Li in the present leaching system is presented in Equation 5.2.1, and the calculated equilibrium constants at 40 °C and 60 °C are presented in Table 5.2.1.

$$Li_2O(s) + 2\,H^+(aq) \rightarrow 2\,Li^+(aq) + H_2O \qquad (5.2.1)$$
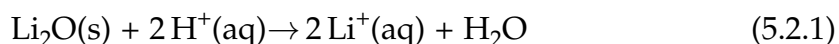
Table 5.2.1: Equilibrium constants for the relevant reactions in the leaching system of Li at 40 °C and 60 °C

Reaction	Equilibrium constant	
	40 °C	60 °C
Reaction 5.2.1	$6.659 \cdot 10^{43}$	$2.543 \cdot 10^{41}$

Equation 5.2.1 describes the reaction between acid and lithium dioxide, and as shown in Table 5.2.1, the equilibrium constant for dissolution of lithium dioxide in acid is high and, therefore, thermodynamically favourable. As observed in the experiments, with the addition of 10 mL acid, there was an average increase in the leaching efficiency of Li by > 5% in the experiments with the BM-T samples. However, in the experiments with the BM-U samples, there was an average decrease in leaching efficiency by $\sim 1\%$. The decrease in leaching efficiency was not expected, however, a 1% decline is relatively limited and can also originate from errors in the experimental measurements.

Li proved to not participate in the reaction with H_2O_2 due to their identical oxidation state, *i.e.*, (+1), on both sides of the reaction. Figures 4.2.2c and 4.2.4c show a slight increase of 1 - 4 % in leaching efficiency when the reductant was added. However, it is believed that the increase was not the direct result of the addition of the reductant but from some other source which is unknown at present.

Another interesting finding is that Li showed the most significant increase in leaching efficiency after pre-treatment of the BM, with an average equilibrium leaching efficiency of 33 % for the BM-T samples and 10 % for the BM-U samples. This was unexpected as Li_2O was the Li containing oxide in both the BMs. In other words, the leaching of Li for both the BM-T and BM-U samples should give the same result.

Vieceli *et al.* [36] reported that the leaching of Li decreased with an increasing pre-treatment temperature. In their experiments, Li was leached to over 90 % after 60 minutes for both their untreated and pre-treated BMs when the pre-treatment temperature was between 400 - 600 °C. However, when the BM was pre-treated at 700°C, the leaching efficiency notably decreased to slightly above 80 %. This

was explained based on a decrease in the C content, which constrained the carbothermic reduction and decreased the leaching efficiency. Since the BM in the present project was pre-treated at 800°C, an even more significant decline in efficiency was expected. However, the BM-T samples had a notably higher leaching efficiency than the BM-U samples. Since the overall leaching efficiencies were lower than the ones reported by Viecelie *et al.* [36], there are clearly other factors that limit the reaction, which at present is unknown.

From the modelling activities, neither acid nor reductant proved to impact the equilibrium calculations. However, an increase in temperature clearly influenced the system, speeding up the reactions, *e.g.*, 100% leaching efficiency was reached within 10 minutes at 60°C for Li, and only 99% after 60 minutes at 40°C. These findings also matched with the trends obtained in the experimental part of the present projects.

Even though Li has a higher leaching efficiency than the other elements in the present leaching systems, the leaching efficiency was low considering what was expected from previous studies and the modelling results. In the earlier studies reported in the literature, the general leaching efficiencies for Li were reported by Vieceli *et al.* [36], Yang*et al.* [35] and Makuza *et al.* [38] to be > 80% under similar conditions as those in the present study. The kinetic Python modelling revealed a leaching efficiency of over 99 % in all leaching systems for Li. The considerably lower experimental results are believed to be due to a systematic error during the execution of the leaching experiments, which will be elaborated on later in the present chapter (see section 5.3).

5.2.2 Nickel (Ni)

In the BM-U samples, Ni was modelled as Nickel(III)oxide trihydrate ($Ni_2O_3 \cdot 3H_2O$) and in the BM-T samples as metallic Nickel (Ni(s)) and Nickel(II)oxide (NiO). The relevant reactions for Ni in the present leaching systems are presented in Equation 5.2.2 - Equation 5.2.6, where the first four (Equations 5.2.2, Equation 5.2.3 and Equation 5.2.4) represent the BM-T and the two following the BM-U samples (Equation 5.2.5 and Equation 5.2.6).

$$Ni(s) + 2\,H^+(aq) \rightarrow Ni^{2+}(aq) + H_2(g) \tag{5.2.2}$$

$$Ni(s) + H_2O_2(aq) + 2\,H^+(aq) \rightarrow Ni^{2+}(aq) + 2\,H_2O \tag{5.2.3}$$

$$NiO(s) + 2\,H^+(aq) \rightarrow Ni^{+2} + H_2O \tag{5.2.4}$$

$$2\,Ni_2O_3 \cdot 3\,H_2O + 8\,H^+(aq) \rightarrow 4\,Ni^{2+}(aq) + O_2(g) + 10\,H_2O \tag{5.2.5}$$

$$Ni_2O_3 \cdot 3\,H_2O + H_2O_2(aq) + 4\,H^+(aq) \rightarrow 2\,Ni^{2+}(aq) + O_2(g) + 6\,H_2O \tag{5.2.6}$$
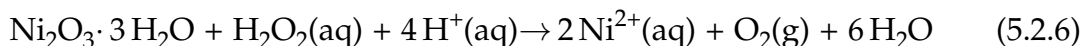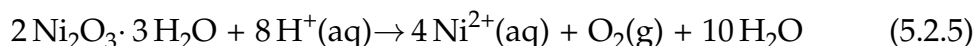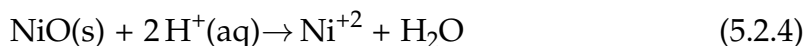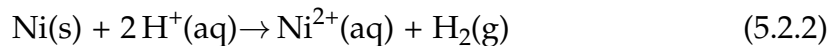
In Table 5.2.2, the calculated equilibrium constants for the reactions at 40°C and 60°C are presented. As can be seen from the table, the dissolution of metallic Ni and Nickel(II)oxide (NiO) with H_2O_2 have higher equilibrium constants and are, therefore, more thermodynamic favourable reactions than the reactions with just acid. This is believed to be the reason for the higher leaching efficiency of Ni in the experiments with additions of reductant compared to the ones without. However, an average increase in leaching efficiency of ~ 6 % with an increasing amount of acid indicated that the acid concentration is essential for the leaching of Ni. However, if the leaching system were already in surplus of acid, adding even further amounts of acid would not result in a significant increase.

According to the equilibrium constant, the reaction without reductant is supposed to be more thermodynamically favourable in view of the BM-U sample (see Table 5.2.2, Reaction 5.2.5 (without reductant) and Reaction 5.2.6 (with reductant)). However, the leaching efficiency increased from an average of ~ 16 % to ~ 20 % when adding 5 mL H_2O_2. Both the change in leaching efficiency and the difference between the equilibrium constants were, however, relatively small, making it difficult to evaluate whether it was a trend or a systematic error in the experiments.

Both in the leaching experiments and the modelling activities, the leaching of Ni from the BM-T samples had a higher leaching efficiency than in the case with the BM-U samples. From the experiments, the average equilibrium leaching efficiency was 27 % for the BM-T samples and 18 % for the BM-U samples. A possible explanation for this increase in view of the thermal treatment can be that Nickel(II)oxide trihydrate consists of Ni in a higher oxidation state, *i.e.*, Ni^{3+}, which is more difficult to dissolve than the Ni^{2+} from the metallic Ni and Nickel(II) oxide.

Table 5.2.2: Equilibrium constants for the relevant reactions in the leaching system of Ni at 40 °C and 60 °C

Reaction	Equilibrium constant	
	40 °C	60 °C
Reaction 5.2.2	$3.623 \cdot 10^7$	$9.971 \cdot 10^6$
Reaction 5.2.3	$9.996 \cdot 10^{63}$	$4.448 \cdot 10^{59}$
Reaction 5.2.4	$4.481 \cdot 10^{11}$	$4.332 \cdot 10^{10}$
Reaction 5.2.5	$6.485 \cdot 10^{65}$	$9.928 \cdot 10^{61}$
Reaction 5.2.6	$1.563 \cdot 10^{50}$	$2.238 \cdot 10^{47}$

From the modelling activities of the BM-T samples, complete leaching of NiO was obtained in all systems. This was, however, not the case for Ni(s) where 99 % leaching efficiency was obtained for a leaching temperature of 40 °C and 46 % at 60 °C. The decrease of the leaching efficiency at increasing temperatures can be explained by the equilibrium constant, which also decreases with an increasing leaching temperature. Modelling of the BM-U samples showed that the dissolution of $Ni_2O_3 \cdot 3H_2O$ strongly depends on the leaching temperature, as well as on the additions of reductants which correlates well with the experimental activities.

5.2.3 Manganese (Mn)

The kinetic Python model was used to calculate the initial conditions needed to secure the presence of manganese(III)oxide (Mn_2O_3) and manganese dioxide

(MnO_2) in the BM-U samples and manganese(II)oxide (MnO) in the BM-T samples.

It should be noted that from the present leaching experiments, Mn achieved overall the lowest leaching efficiency. The reactions contributing to the leaching of Mn are given in Equation 5.2.7 - Equation 5.2.12, where the first two reactions (Equation 5.2.7 and Equation 5.2.8) represent the leaching of the BM-T samples, and the last four (Equation 5.2.9, Equation 5.2.10, Equation 5.2.11 and Equation 5.2.12) represent the leaching of the BM-U samples.

$$MnO(s) + 2\,H^+(aq) \rightarrow Mn^{2+}(aq) + H_2O \qquad (5.2.7)$$

$$MnO(s) + 2\,H^+(aq) + 2\,H_2O_2(aq) \rightarrow Mn^{2+}(aq) + 3\,H_2O + O_2(g) \qquad (5.2.8)$$

$$MnO_2(s) + 2\,H^+(aq) \rightarrow Mn^{2+}(aq) + O_2(g) + H_2(g) \qquad (5.2.9)$$

$$MnO_2(s) + H_2O_2(aq) + 2\,H^+(aq) \rightarrow Mn^{2+}(aq) + O_2(g) + 2\,H_2O \qquad (5.2.10)$$

$$Mn_2O_3(s) + 6\,H^+(aq) \rightarrow 2\,Mn^{3+}(aq) + 3\,H_2O \qquad (5.2.11)$$

$$Mn_2O_3(s) + 6\,H^+(aq) + 2\,H_2O_2(aq) \rightarrow 2\,Mn^{3+}(aq) + 5\,H_2O(l) + O_2(g) \qquad (5.2.12)$$
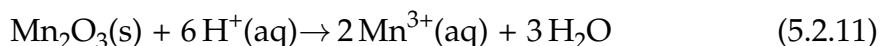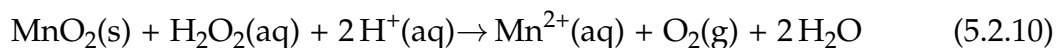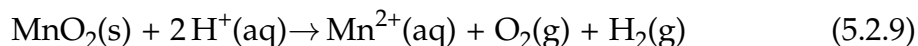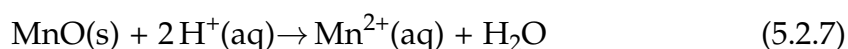
Increasing the amount of acid in the leaching system proved to make no significant difference in the leaching of Mn. There was a slight decrease in the leaching efficiency for the BM-T samples, and in the case of the BM-U samples, it resulted in a slight increase. These changes were so small that they were most likely due to experimental errors (or a systematic experimental procedure error). As previously mentioned, several signs made it reasonable to assume that the system was in surplus of acid.

The experimental leaching efficiency increased, on average, with the addition of reductant, and the modelling calculations of the equilibrium constants could support these observations. As can be seen in Table 5.2.3, the equilibrium constant increased for all manganese oxides with the addition of reductant, and these reactions were all very thermodynamically favourable. In addition, the reductant secured the reduction of the Mn^{4+} in the MnO_2 to Mn^{2+}, facilitating the leaching [34].

Increasing the leaching temperature from 40°C to 60°C proved to increase the leaching efficiency of Mn in the experiments with both BMs (8 % for the BM-U samples and 7 % for the BM-T samples). This was even though the equilibrium coefficients decreased or were relatively low. As previously mentioned, the effects of increasing the temperature on the kinetic energy are generally stronger, however, this was not experienced in the present work. With the results reported in literature by Yang *et al.* [35], it was expected that the Mn leaching efficiencies would be lower at higher temperatures. This was because Mn^{2+} was assumed to oxidise back to MnO_2 at higher temperatures due to the dissolution of O_2 gas in the leaching solution. Yang *et al.* [35] and He *et al.* [34] established that the leaching efficiency decreased at both 80 °C and 60 °C. In other words, if the present leaching system had behaved more like the one by Yang *et al.* [35], the maximum temperature would be too low to experience a decrease in leaching efficiency. Furthermore, the system was covered at all times, except at leachate extraction, to prevent evaporation of the solution, which could have limited the O dissolution.

There was no distinct difference in the leaching of the BM-U and BM-T samples in view of the overall leaching efficiency of Mn. The average equilibrium leaching efficiency for the BMs was 15 % for the BM-T samples and 17 % for the BM-U samples.

The leaching of MnO_2 proved to be thermodynamically favourable with the presence of a reductant, and the highest leaching efficiencies obtained for Mn in the present work were from these experiments for both BMs. Moreover, Makuza *et al.* [38] also discovered that higher pre-treatment temperatures could nega-

tively affect the leaching efficiency of Mn and suggest that calcine agglomeration could be the reason. In addition, Vieceli *et al.* [36] propose that increasing pre-treatment temperature could lead to oxidising conditions, which then could restrict the leaching efficiency of the metals present in the system (in this case, for Mn).

In the modelling activities corresponding to the BM-T samples, the MnO reached 100 % leaching in all experiments, though 25 minutes faster at higher temperatures (60 °C). The same was observed for Mn_2O_3 in view of the BM-U samples, which leached 100 % and faster at higher temperatures (60 °C) and with the presence of a reductant. However, the dissolution of MnO_2 proved to decrease with an increasing amount of acid. The reason for this was unknown and might be a flaw in the model and should therefore be further investigated. Furthermore, Mn_2O_3 proved to dissolve into Mn^{3+}-ions, however, the kinetic Python model did not foresee the presence of Mn^{3+} in the system. This could be because the Mn^{3+}-ions were very insoluble and would quickly form Mn_2O_3 again, and/or that the reduction of Mn^{3+} to Mn^{2+} with water, as presented in Equation 5.2.13, was thermodynamically stable under all the present leaching conditions.

$$4\,Mn^{3+}(aq) + 2\,H_2O \rightarrow 4\,Mn^{2+} + 4\,H^+(aq) + O_2(g) \tag{5.2.13}$$
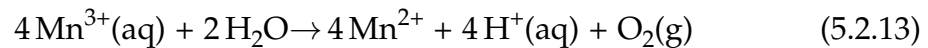
Table 5.2.3: Equilibrium constants for the relevant reactions in the leaching system of Mn at 40 °C and 60 °C

Reaction	Equilibrium constant	
	40 °C	60 °C
Reaction 5.2.7	$8.139 \cdot 10^{16}$	$5.028 \cdot 10^{15}$
Reaction 5.2.8	$3.068 \cdot 10^{51}$	$2.536 \cdot 10^{48}$
Reaction 5.2.9	$9.312 \cdot 10^{-40}$	$9.241 \cdot 10^{-37}$
Reaction 5.2.10	$2.570 \cdot 10^{17}$	$4.123 \cdot 10^{16}$
Reaction 5.2.11	$5.757 \cdot 10^{-2}$	$1.529 \cdot 10^{-3}$
Reaction 5.2.12	$2.170 \cdot 10^{33}$	$7.712 \cdot 10^{29}$
Reaction 5.2.13	$7.314 \cdot 10^{18}$	$8.923 \cdot 10^{20}$

5.2.4 Cobalt (Co)

Based on the present results, Co achieves lower leaching efficiencies than Li but generally higher than the other elements (Ni and Mn). The first two reactions below (Equation 5.2.14 and Equation 5.2.15) describe the leaching of the BM-T samples with cobalt(II)oxide (CoO) as the initial composition (where the first reaction leads to Co dissolution), and the following two reactions Equation 5.2.16 and Equation 5.2.17 describes the leaching of the BM-U samples with cobalt(III)oxide trihydrate ($Co_2O_3 \cdot 3H_2O$). The last reaction (Equation 5.2.18) shows the oxidation of Co^{+2} to Co^{+3}.

$$CoO(s) + 2H^+(aq) \rightarrow Co^{2+}(aq) + H_2O \tag{5.2.14}$$

$$CoO(s) + \frac{5}{2}H_2O_2(aq) + 3H^+(aq) \rightarrow Co^{3+}(aq) + 4H_2O(l) + O_2(g) \tag{5.2.15}$$

$$Co_2O_3 \cdot 3H_2O(aq) + 8H^+(aq) \rightarrow 4Co^{2+}(aq) + O_2(g) + 10H_2O \tag{5.2.16}$$

$$Co_2O_3 \cdot 3H_2O(aq) + H_2O_2(aq) + 4H^+(aq) \rightarrow 2Co^{2+}(aq) + O_2(g) + 6H_2O \tag{5.2.17}$$

$$2Co^{2+}(aq) + 2H^+(aq) \rightarrow 2Co^{3+}(aq) + H_2(g) \tag{5.2.18}$$
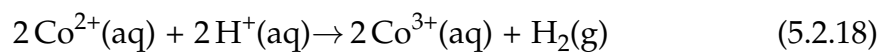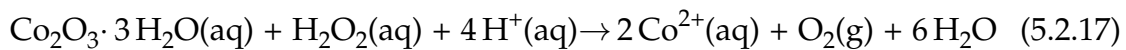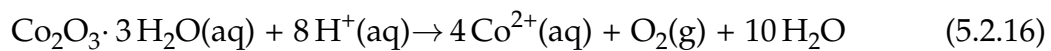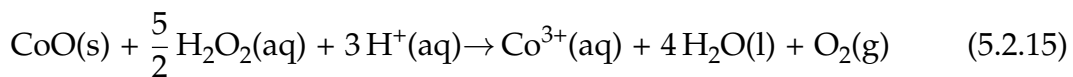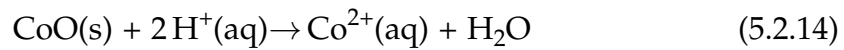
In Table 5.2.4, the model calculations of the equilibrium constants of the reactions described above are presented. As can be seen from the table, the leaching of CoO with the presence of a reductant was much higher than with just additions of acid and was hence more thermodynamically favourable. This was also observed in the experiments, where adding a reductant increased the average leaching efficiency for Co from $\sim 20\%$ to $\sim 35\%$ for the BM-T samples.

Furthermore, both the reactions taking place when leaching the BM-U samples proved that the interaction between the oxide ($Co_2O_3 \cdot 3H_2O$)), the acid, and a

reductant was thermodynamically favourable with high equilibrium constants. In the present experiments, the leaching efficiency had an average increase of $\sim$ 6 % with the addition of a reductant and $\sim$ 4 % with the addition of acid. The reductant reduced the Co^{3+} to Co^{2+}(aq), which facilitated the leaching [34]. This trend was also seen in the modelling of the BM-U samples, where the addition of a reductant seemed crucial for leaching at lower temperatures (40 °C).

The higher leaching efficiencies for Co were primarily achieved when leaching the BM-T samples, even though the BM-U samples proved to have some test conditions that resulted in higher leaching efficiencies (test conditions AO15 and AO16), as well as that the BM-T samples had the lowest leaching efficiency (test condition AO1). The average equilibrium leaching efficiencies were 27% for the BM-T samples and 19% for the BM-U samples. Since the trends were rather explicit, it could be suggested that the pre-treatment positively affected the leaching of Co.

Table 5.2.4: Equilibrium constants for the relevant reactions in the leaching system of Co at 40 °C and 60 °C

Reaction	Equilibrium constant	
	40 °C	60 °C
Reaction 5.2.14	$7.628 \cdot 10^{12}$	$6.593 \cdot 10^{11}$
Reaction 5.2.15	$5.898 \cdot 10^{43}$	$2.690 \cdot 10^{40}$
Reaction 5.2.16	$1.096 \cdot 10^{35}$	$2.073 \cdot 10^{33}$
Reaction 5.2.17	$6.429 \cdot 10^{34}$	$1.023 \cdot 10^{33}$
Reaction 5.2.18	$1.525 \cdot 10^{-64}$	$1.466 \cdot 10^{-61}$

The modelling of Co showed that the leaching of CoO reached 100 % leaching after $\sim$ 1 minute in all the leaching systems. This does, however, not correspond to the trends found in the performed experiments. A possible reason for this was that the system was suitable for leaching CoO, but since the experiments did not have as high leaching efficiencies, the trends could more easily be observed. With lower values for the test parameters, a similar trend could maybe also be observed in the modelling activities.

Temperature and additions of a reductant seemed crucial for the leaching of Co in the modelling of the BM-U samples. Acid, however, proved not to have the same impact. The same trends could be seen in the experiments, where both additions of a reductant and high temperature showed an average increase in leaching efficiency. However, an increase with additions of extra acid was not observed. As previously mentioned, the model suggested that the system was in surplus of acid.

5.3 Experimental validation

To test the reproducibility of the experiments, the test condition AO13 was replicated twice, *i.e.*, in tests AO17 and AO18. The results showed that AO17 and AO18 were closer in value to each other than to the results of test AO13, *i.e.*, they were 1-2 % lower than in the original experiment. This was believed to be because the leaching method became steadier over time and more accurate. In addition, parts of the equipment broke and got upgraded between the time of performing the original measurement (test AO13) and the duplicates (tests AO17 and AO18). The reproducibility between the two last measurements was therefore believed to show a more accurate result.

However, the leaching efficiencies in these experiments are notably lower than in the previous studies reported in literature (> 80 % for all elements [35] [36] [38]), as well as when compared with the industrially performed leaching experiments and the performed modelling activities ($\sim$ 100 %). Up to this point, the reason for this has been explained as a possible systematic error in the experimental procedure but not discussed in more detail. In view of this, it should be noted that many transferring steps existed between the original BMs and the ICP-MS analysis that could have systematically influenced the results. For example, after the BM samples were weighted, they were transferred from the container through a funnel into the round flask, and some of the BM never reached the round flask and stayed in the funnel. Furthermore, during the stirring, some of the BM got stuck up at the wall in the round flask and never dissolved into the solution. Even when the leachate samples were measured, the measuring technique was not as

accurate as the weighing of the BM and can therefore have affected the modelling calculations of leaching efficiency. In addition, part of the samples could have evaporated during the extraction. It should also be noted that the stirring was turned off during the extraction experiments and could therefore also have led to an inhomogeneous solution. With these experiences in mind, several steps could have been better executed to secure more accurate results (learning by doing).

The characterisation of the Solid Residues (see Sections D.3 and D.4) indicated that 100 % leaching of the BMs was possible. As a result, higher leaching efficiencies were expected from the performed experiments than what was reached.

5.4   Comparing models

When the leaching systems were modelled in HSC Chemistry 9, all the elements in focus in the present work reached 100 % leaching efficiency in every leaching system. Even though the kinetic Python model also predicted higher leaching efficiencies, the trends observed were similar to the ones discovered in the experiments.

The reason for the HSC Chemistry 9 model giving unrealistic results was that the model did not account for the kinetic interactions between the species during leaching but instead used the Gibbs energy minimising method to calculate the composition at equilibrium. In addition, the compositions calculated was only calculated at equilibrium, which means that it was impossible to follow the evolution in concentration with time, as well as to study the influence of the different parameter, *i.e.*, if a change in a specific parameter made the reaction go faster or slower. The time at which equilibrium was established was also never given, and it could have been longer than the 23 hours assumed in the experimental procedure. If that was the case, there could be a possibility that the leaching efficiencies for the different elements could increase further and reach complete leaching after a long time in both the experiments and in the kinetic Python model. However, this was unlikely since the leaching efficiency graphs showed a tendency to flatten out (see Figure 4.2.1 and Figure 4.2.3), indicating that the reactions had

reached equilibrium.

5.5 Contextualising the results

The report "Battery 2030 - Inventing the Sustainable Batteries of the Future" [39] is a European research initiative in battery research and development published in 2020. The working group of that project have reported on several goals in view of future battery recycling activities to meet the vision of a climate-neutral society. Some of their medium-term goals are:

- New sorting and recovery technologies for powders and components, as well as the reconditioning to new active battery-grade materials, should be demonstrated.

- The recovery rate of critical raw materials should be significantly improved relative to current processes.

- New/improved prediction and modelling tools for the reuse of materials in secondary applications should be developed.

The research performed in the present work contributes to meeting the goals mentioned above through model development and experimental parameter studies. Consequently, to reach some of the above goals within the coming years, the field will need more research for a more in-depth understanding of the leaching processes.

6 | Summary and Conclusion

The objective of the present work has been to investigate the leaching properties of two different BMs, *i.e.*, BM-U and BM-T, from spent LIBs in order to gain insight into how to optimise the process for the leaching of industrial BMs of different chemistries. The experimental work was supported by modelling activities through the commercial software HSC Chemistry 9 and a kinetic Python model partly developed in the present work.

Leaching experiments with varying temperatures and used amounts of acid and reductant were performed on untreated (BM-U) and thermally treated (BM-T) industrially produced BM samples. The BMs were characterised using SEM-EDS to investigate the O content of the cathode particles and by using ICP-MS to determine the concentration of Li, Ni, Mn, and Co, which then were used as input in the kinetic Python model for modelling the BM composition.

Leachate samples extracted during the leaching experiments were analysed with ICP-MS for the concentration of the metals in focus. The leaching systems were also modelled by using HSC Chemistry 9 and the kinetic Python model. In addition, SRs from industrially performed leaching experiments with the same BMs as those used in the present work were also characterised using SEM-EDS for comparison.

For both BMs, Li proved to be the most straightforward metal to leach and Mn the hardest, agreeing well with the present author's literature study. The experiment with the highest leaching efficiencies was test conditions AO7 with 55.7% for Li, 51.3% for Ni, 26.1% for Mn, and 53% for Co for the BM-T samples. The test conditions AO7 were also the experiment with the highest values for every

93

investigated parameter in the case of the BM-T samples, *i.e.*, 20 mL acid, 5 mL reductant, and 60 °C. The BM-U proved to have lower leaching efficiencies, and the best-performing experiment was when performing the experiments using the test conditions AO15 (20 mL acid, 5 mL reductant, and 60 °C) with 28.4% for Li, 27.7% for Ni, 28.5% for Mn, and 29.5% for Co.

The following was established and concluded in view of the different parameters adjusted during the laboratory experiments:

- An increase in the temperature and used amount of reductant increased the leaching efficiency for all metals in both BMs. However, the acid did not increase the leaching efficiency as much as expected, and it was concluded that the reason for that was the acid surplus in the solution.

- The metal recovery obtained was significantly lower than expected, with the majority of leaching efficiencies between 10 and 30%. The reason for this was concluded to be systematic errors in the experimental method used.

- The pre-treatment of the BM increased the average equilibrium leaching efficiency by around 10% for Co and Ni, > 20% for Li, and decreased by 2% for Mn. Previous studies have also shown that the leaching efficiency of Mn is limited with higher pre-treatment temperatures. In view of this, it was concluded that thermal treatment of the BM facilitates the leaching with pre-treatment temperatures lower than 800 °C in the case of Mn.

The leaching systems were also modelled using both HSC Chemistry 9 and a kinetic Python model. In the HSC Chemistry 9 calculations, every leaching system reached 100% leaching efficiency, and it was concluded that the software was inadequate in predicting the leaching efficiency. The kinetic Python model, however, predicted most of the trends observed in the experiments, but the leaching efficiencies modelled were much higher than the ones obtained in the experiments. It is difficult to conclude how accurate the Python model was since there were several possible sources of errors in the experimental method used, *e.g.*, (i) several transferring steps between BM weighing and ICP-MS analysis, (ii) imprecise measurement of the leachate samples, and (iii) leachate evaporation and BM

loss during sample extraction. Further development of the kinetic Python model would benefit from additional experimental investigations into the leaching systems in question.

Placing the present results into a societal context, *i.e.*, evaluating whether the process is economically beneficial and environmentally sustainable, would have been helpful but clearly not possible with the present results.

Based on the overall results, it can be concluded that the present results do not fulfil the recycling efficiency regulations [39], which state that the recycled content of all batteries, except for the lead-acid and nickel-cadmium batteries, by weight should reach 50%. Even though the leaching efficiencies in test conditions AO7 in mol% for the BM-T samples are mostly above 50% (55.7% for Li, 51.3% for Ni, 26.1% for Mn, and 53% for Co) in the experiments using the test conditions AO7, the weight% was below 30% (29.8% for Li, 27.7% for Ni, 12.5% for Mn, and 27.1% for Co - calculations given in Appendix C Section C.3.)

7 | Future Work

From the concluding remarks in the present work, it is apparent that further research is needed on the leaching of different BMs from LIBs to establish a more profound understanding of the behaviour of Li, Ni, Mn, and Co in view of their leaching efficiency under different conditions. For further exploration of the field, the following should be given special attention:

- Expand the present experimental matrix to test several values of the chosen parameters to further investigate the optimal leaching conditions. Especially experiments with lower acid concentrations, as acid did not significantly impact the leaching experiments.

- Investigate additional leaching variables such as stirring speed and pulp density through experiments and modelling activities to research their impact on the leaching efficiency.

- Thermal treatment of BM at several temperatures and time durations to investigate the leaching facilitation.

- Characterise the SRs after every leaching experiment with an SEM-EDS unit to better understand the cathode particles left after leaching.

- Increase the validation of the experiments by performing several parallels of each experiment and improving the characterisation routines.

- Perform experiments at several temperatures to find the lowest temperature with satisfying leaching results for energy savings.

- Extend the kinetic Python model to obtain more accurate predictions of the leaching system. The model extension should include gradual reagents ad-

dition at different time steps and relevant missing reactions, *e.g.*, precipitation reactions.

- Develop routines to externally generate ranges of kinetic coefficients to be sent to the current optimisation of the kinetic constants.

- Integrate calculations of the particle's surface area and its evolution over time in the kinetic Python model to account for multiple size fractions to improve simulation accuracy.

Bibliography

[1]   *Reduce Climate Change*. URL: https://www.fueleconomy.gov/feg/climate.shtml (visited on 08/09/2022).

[2]   *How much CO2 does a tree absorb?* URL: https://www.viessmann.co.uk/heating-advice/how-much-co2-does-tree-absorb (visited on 08/09/2022).

[3]   Ariel Cohen. *Plugging Into The Future: The Electric Vehicle Market Outlook*. Forbes. Section: Energy. URL: https://www.forbes.com/sites/arielcohen/2020/10/26/plugging-into-the-future-the-electric-vehicle-market-outlook/ (visited on 08/09/2022).

[4]   *Electric vehicles*. Deloitte Insights. URL: https://www2.deloitte.com/uk/en/insights/focus/future-of-mobility/electric-vehicle-trends-2030.html (visited on 08/09/2022).

[5]   *Over halvparten av nye personbiler er elbiler*. ssb.no. URL: https://www.ssb.no/transport-og-reiseliv/artikler-og-publikasjoner/over-halvparten-av-nye-personbiler-er-elbiler (visited on 08/09/2022).

[6]   "Global Electric Vehicle Outlook 2022". In: (2022), p. 221.

[7]   Iman Dorri. "A Literature Review of Recycling Methods for Li-ion Batteries". In: *Project thesis, NTNU, Department of Energy and Process Engineering* (Dec. 2021).

[8]   *5 ways to make the electric vehicle battery more sustainable*. World Economic Forum. URL: https://www.weforum.org/agenda/2021/05/electric-vehicle-battery-recycling-circular-economy/ (visited on 08/09/2022).

[9]   B. Kennedy, D. Patterson, and S. Camilleri. "Use of lithium-ion batteries in electric vehicles". In: *Journal of Power Sources* 90.2 (Oct. 2000), pp. 156–

162. ISSN: 03787753. DOI: 10.1016/S0378-7753(00)00402-X. URL: https://linkinghub.elsevier.com/retrieve/pii/S037877530000402X (visited on 05/16/2022).

[10] James Arambarri et al. "Lithium ion car batteries: Present analysis and future predictions". In: *Environmental Engineering Research* 24.4 (Feb. 15, 2019), pp. 699–710. ISSN: 1226-1025, 2005-968X. DOI: 10.4491/eer.2018.383. URL: http://eeer.org/journal/view.php?doi=10.4491/eer.2018.383 (visited on 06/11/2022).

[11] Ivar Gunvaldsen, Steinar Mathiesen, and Knut A. Rosvold. *batteri*. In: *Store norske leksikon*. Jan. 1, 2022. URL: http://snl.no/batteri (visited on 04/26/2022).

[12] Mario Pagliaro and Francesco Meneguzzo. *Lithium Battery Reusing and Recycling: A Circular Economy Insight*. preprint. CHEMISTRY, May 5, 2019. DOI: 10.20944/preprints201905.0012.v1. URL: https://www.preprints.org/manuscript/201905.0012/v1 (visited on 05/23/2022).

[13] Jakob Sandstad. *galvanisk element*. In: *Store norske leksikon*. Dec. 13, 2020. URL: http://snl.no/galvanisk_element (visited on 04/10/2022).

[14] Øyvind Grøn. *elektrisk strøm*. In: *Store norske leksikon*. Aug. 24, 2021. URL: http://snl.no/elektrisk_str%C3%B8m (visited on 04/26/2022).

[15] Jie Deng et al. "Electric Vehicles Batteries: Requirements and Challenges". In: *Joule* 4.3 (Mar. 2020), pp. 511–515. ISSN: 25424351. DOI: 10.1016/j.joule.2020.01.013. URL: https://linkinghub.elsevier.com/retrieve/pii/S254243512030043X (visited on 05/24/2022).

[16] Xiaopeng Chen et al. "An overview of lithium-ion batteries for electric vehicles". In: *2012 10th International Power & Energy Conference (IPEC)*. 2012 10th International Power & Energy Conference (IPEC). Ho Chi Minh City: IEEE, Nov. 2012, pp. 230–235. DOI: 10.1109/ASSCC.2012.6523269. URL: http://ieeexplore.ieee.org/document/6523269/ (visited on 05/08/2022).

[17] W.J. Rankin. *Minerals, Metals and Sustainability - Meeting Future Material Needs*. CRC Press, 2011.

[18] Mengyuan Chen et al. "Recycling End-of-Life Electric Vehicle Lithium-Ion Batteries". In: *Joule* 3.11 (Nov. 2019), pp. 2622–2646. ISSN: 25424351. DOI:

`10.1016/j.joule.2019.09.014`. URL: `https://linkinghub.elsevier.com/retrieve/pii/S254243511930474X` (visited on 05/07/2022).

[19] Condé Nast. "The spiralling environmental cost of our lithium battery addiction". In: *Wired UK* (). Section: tags. ISSN: 1357-0978. URL: `https://www.wired.co.uk/article/lithium-batteries-environment-impact` (visited on 12/10/2021).

[20] *"They can't escape the dust"*. Amnesty International. May 6, 2020. URL: `https://www.amnesty.org/en/latest/news/2020/05/drc-alarming-research-harm-from-cobalt-mine-abuses/` (visited on 12/10/2021).

[21] Antonella Accardo et al. "Life Cycle Assessment of an NMC Battery for Application to Electric Light-Duty Commercial Vehicles and Comparison with a Sodium-Nickel-Chloride Battery". In: *Applied Sciences* 11.3 (Jan. 27, 2021), p. 1160. ISSN: 2076-3417. DOI: `10.3390/app11031160`. URL: `https://www.mdpi.com/2076-3417/11/3/1160` (visited on 05/15/2022).

[22] Yangtao Liu et al. "Current and future lithium-ion battery manufacturing". In: *iScience* 24.4 (Apr. 2021), p. 102332. ISSN: 25890042. DOI: `10.1016/j.isci.2021.102332`. URL: `https://linkinghub.elsevier.com/retrieve/pii/S258900422100300X` (visited on 05/20/2022).

[23] Antti Väyrynen and Justin Salminen. "Lithium ion battery production". In: *The Journal of Chemical Thermodynamics* 46 (Mar. 2012), pp. 80–85. ISSN: 00219614. DOI: `10.1016/j.jct.2011.09.005`. URL: `https://linkinghub.elsevier.com/retrieve/pii/S0021961411003090` (visited on 05/15/2022).

[24] Saeed Rahimpour Golroudbary, Daniel Calisaya-Azpilcueta, and Andrzej Kraslawski. "The Life Cycle of Energy Consumption and Greenhouse Gas Emissions from Critical Minerals Recycling: Case of Lithium-ion Batteries". In: *Procedia CIRP*. 26th CIRP Conference on Life Cycle Engineering (LCE) Purdue University, West Lafayette, IN, USA May 7-9, 2019 80 (Jan. 1, 2019), pp. 316–321. ISSN: 2212-8271. DOI: `10.1016/j.procir.2019.01.003`. URL: `https://www.sciencedirect.com/science/article/pii/S2212827119300058` (visited on 12/11/2021).

[25] Linda Gaines et al. "Direct Recycling R&D at the ReCell Center". In: (2021), p. 18.

[26] S. Ramachandra Rao. *Resource Recovery and Recycling from Metallurgical Wastes*. Vol. 7. Waste Management Series. Elsevier, 2006. ISBN: 978-0-08-045131-2. DOI: `10.1016/S0713-2743(06)X8083-2`. URL: `https://linkinghub.elsevier.com/retrieve/pii/S0713274306X80832` (visited on 05/08/2022).

[27] "Umicore - Integrated Annual Report 2021". In: (2021), p. 241. URL: `https://www.umicore.com/storage/group/integrated-annual-report-2021.pdf`.

[28] Dr Christian Hagelüken and A Greinerstraat. "Recycling of Electronic Scrap at Umicore Precious Metals Refining". In: (2006), p. 9.

[29] Velázquez-Martínez et al. "A Critical Review of Lithium-Ion Battery Recycling Processes from a Circular Economy Perspective". In: *Batteries* 5.4 (Nov. 5, 2019), p. 68. ISSN: 2313-0105. DOI: `10.3390/batteries5040068`. URL: `https://www.mdpi.com/2313-0105/5/4/68` (visited on 08/18/2022).

[30] J. Hjelen. *Scanning elektron-mikroskopi*. Metallurgisk Institutt, NTH: SINTEF, Avdeling for metallurgi.

[31] W. B. White, S. M. Johnson, and G. B. Dantzig. "Chemical Equilibrium in Complex Mixtures". In: *The Journal of Chemical Physics* 28.5 (May 1958), pp. 751–755. ISSN: 0021-9606, 1089-7690. DOI: `10.1063/1.1744264`. URL: `http://aip.scitation.org/doi/10.1063/1.1744264` (visited on 08/04/2022).

[32] Petri Kobylin, Lena Furta, and Danil Vilaev. *Equilibrium Module - Description of Menus and Options*. Nov. 12, 2020.

[33] *General Python FAQ — Python 3.10.5 documentation*. URL: `https://docs.python.org/3/faq/general.html` (visited on 06/20/2022).

[34] Li-Po He et al. "Leaching process for recovering valuable metals from the LiNi1/3Co1/3Mn1/3O2 cathode of lithium-ion batteries". In: *Waste Management* 64 (June 1, 2017), pp. 171–181. ISSN: 0956-053X. DOI: `10.1016/j.wasman.2017.02.011`. URL: `https://www.sciencedirect.com/science/article/pii/S0956053X17300533` (visited on 11/18/2021).

[35] Jian Yang et al. "Reductive acid leaching of valuable metals from spent lithium-ion batteries using hydrazine sulfate as reductant". In: *Transactions of Nonferrous Metals Society of China* 30.8 (Aug. 2020), pp. 2256–2264. ISSN:

10036326. DOI: `10.1016/S1003-6326(20)65376-6`. URL: `https://linkinghub.elsevier.com/retrieve/pii/S1003632620653766` (visited on 08/02/2022).

[36]   Nathália Vieceli et al. "Hydrometallurgical recycling of EV lithium-ion batteries: Effects of incineration on the leaching efficiency of metals using sulfuric acid". In: *Waste Management* 125 (Apr. 2021), pp. 192–203. ISSN: 0956053X. DOI: `10.1016/j.wasman.2021.02.039`. URL: `https://linkinghub.elsevier.com/retrieve/pii/S0956053X21001082` (visited on 08/02/2022).

[37]   Amalie My Olsen. "Leaching of Pre-treated Li-ion Batteries, Database Integration and Modelling". In: (), p. 39.

[38]   Brian Makuza et al. "Dry Grinding - Carbonated Ultrasound-Assisted Water Leaching of Carbothermally Reduced Lithium-Ion Battery Black Mass Towards Enhanced Selective Extraction of Lithium and Recovery of High-Value Metals". In: *Resources, Conservation and Recycling* 174 (Nov. 1, 2021), p. 105784. ISSN: 0921-3449. DOI: `10.1016/j.resconrec.2021.105784`. URL: `https://www.sciencedirect.com/science/article/pii/S0921344921003931` (visited on 11/18/2021).

[39]   Kristina Edström et al. *Battery 2030: Inventing the Sustainable Batteries of the Future*. 2020.

Appendix

A | Experimental preparation

A.1 Weighted BMs

The BM weight in each leaching experiment is given in Table A.1.1.

Table A.1.1: The weighted BM of each experiment

Test ID	Mass [g]
AO1	1.0083
AO2	1.0016
AO3	1.0079
AO4	1.0046
AO5	0.9991
AO6	1.0045
AO7	1.0068
AO8	1.0007
AO9	1.0049
AO10	1.0040
AO11	1.0021
AO12	1.0060
AO13	1.0085
AO14	1.0016
AO15	1.0090
AO16	1.0064
AO17	1.0029
AO18	1.0047

A.2   Preparation of acid solution

Table A.2.1 shows the physical properties of H_2SO_4 which is used in the calculation for preparation of the H_2SO_4 solution.

Table A.2.1: Physical properties of H_2SO_4

Total volume [L]	Molar weight [g/mol]	Density [g/mL]	Concentration [M]
V_{tot}	$Mm_{H_2SO_4}$	$\rho_{H_2SO_4}$	$c_{H_2SO_4}$
0.50	98.10	1.84	2.00

The amount of acid needed to be added are given in the equation below:

$$V_{H_2SO_4} = V_{tot} \cdot c_{H_2SO_4} \cdot \frac{Mm_{H_2SO_4}}{\rho_{H_2SO_4}} \tag{A.2.1}$$

Inserting the values from the table, the resulting volume is 53.32 mL. The equipment available at the lab is not that precise, so the resulting volume of sulfuric acid added was 54 mL. By rearranging Equation A.2.1 and inserting the values of properties, calculations gives the resulting concentration to be 2.03 mol/L.

A.3   Preparation of reductant solution

The desired concentration of H_2O_2 was 2.5 M. To calculate the needed volume for a 2.5 M reductant solution with a total volume of 0.2 L, values from Table A.3.1 was used in the equation below,

$$c_1 \cdot V_1 = c_2 \cdot V_2 \tag{A.3.1}$$

Rearranging gives,

$$V_{H_2O_2} = \frac{c_{tot} \cdot V_{tot}}{c_{H_2O_2}} \tag{A.3.2}$$

and the volume of H_2O_2 needed was calculated to 51.02 mL.

Table A.3.1: Physical properties of H_2O_2

Total volume [L]	Concentration [mol/L]
V_{tot}	$c_{H_2O_2}$
0.2	9.8

B | Temperature and pH evolution during leaching

B.1 Experiments performed on the BM-U

Figure B.1.1 shows the temperature and pH evolution in the experiments performed on the BM-U.

B.2 Experiments performed on BM-T

Figure B.2.1 shows the temperature and pH evolution in the experiments performed on the BM-T.
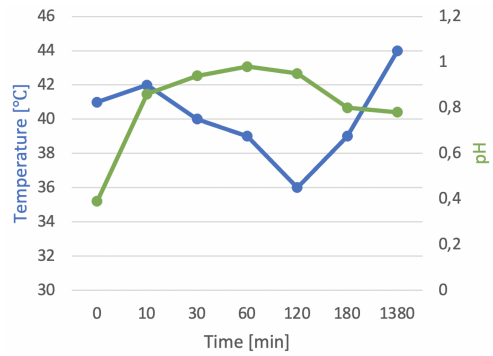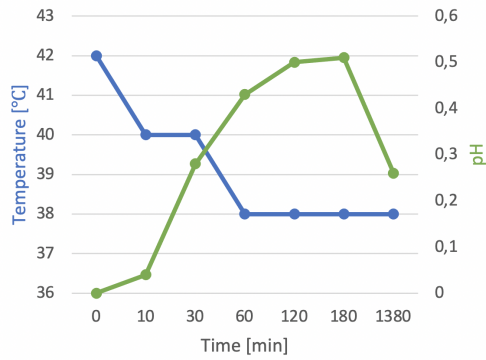
(a) Temperature and pH evolution of the experiments with leaching conditions AO9

(b) Temperature and pH evolution of the experiments with leaching conditions AO10
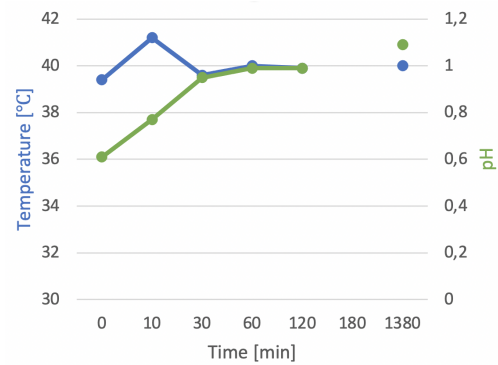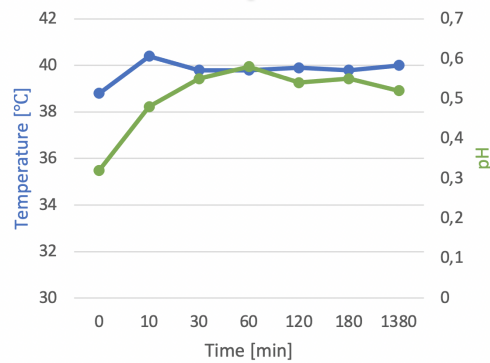
(c) Temperature and pH evolution of the experiments with leaching conditions AO11

(d) Temperature and pH evolution of the experiments with leaching conditions AO12
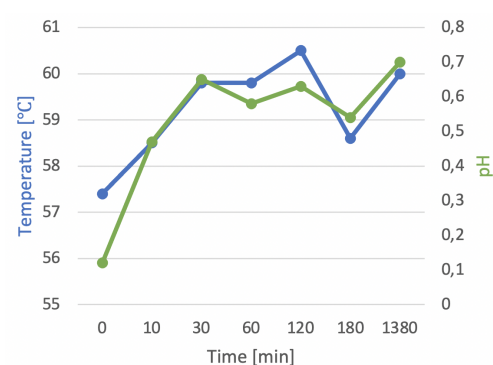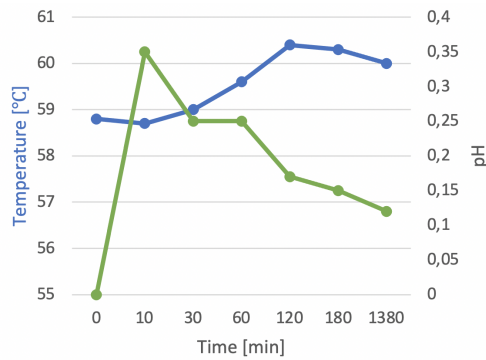
(e) Temperature and pH evolution of the experiments with leaching conditions AO13

(f) Temperature and pH evolution of the experiments with leaching conditions AO14
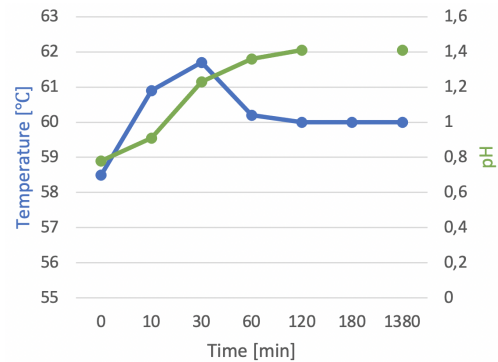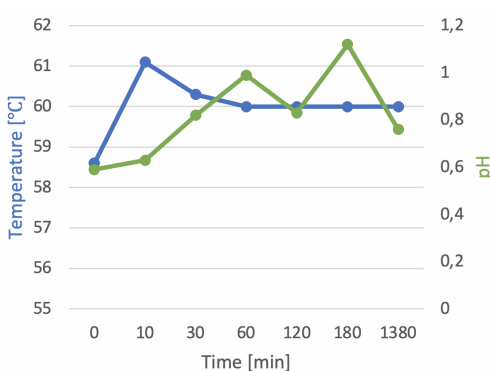
(g) Temperature and pH evolution of the experiments with leaching conditions AO15

(h) Temperature and pH evolution of the experiments with leaching conditions AO16

Figure B.1.1: Temperature and pH evolution in the leaching experiments performed on the BM-U.
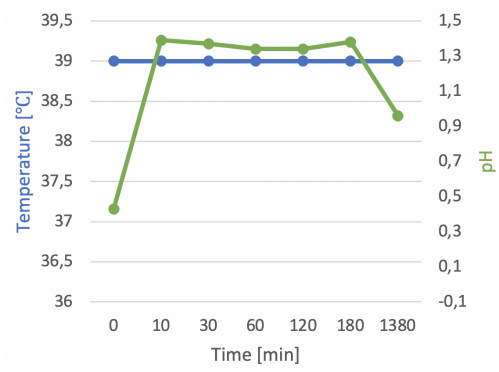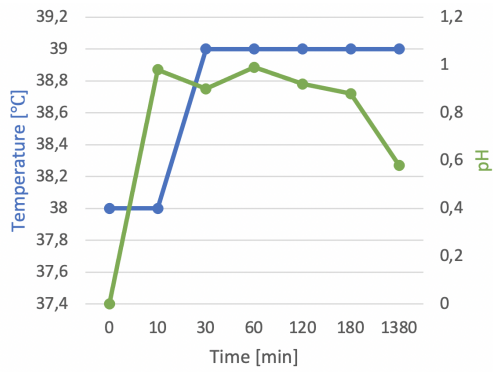
(a) Temperature and pH evolution of the experiments with leaching conditions AO1

(b) Temperature and pH evolution of the experiments with leaching conditions AO2
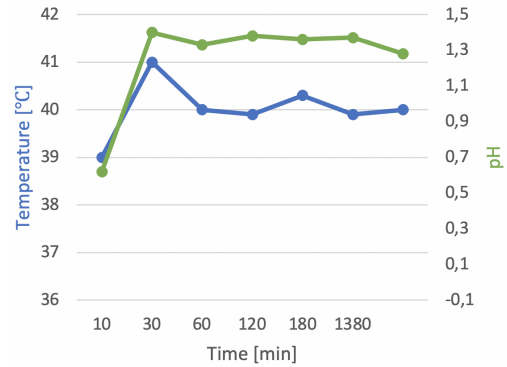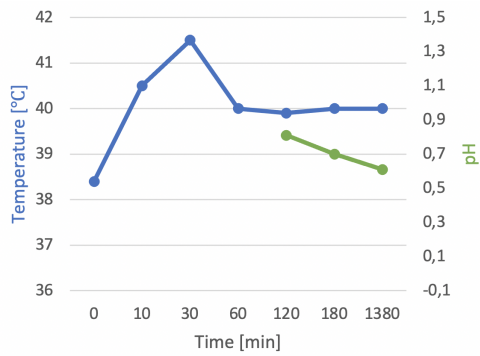
(c) Temperature and pH evolution of the experiments with leaching conditions AO3

(d) Temperature and pH evolution of the experiments with leaching conditions AO4
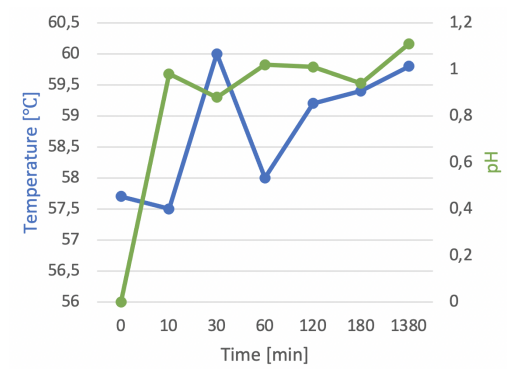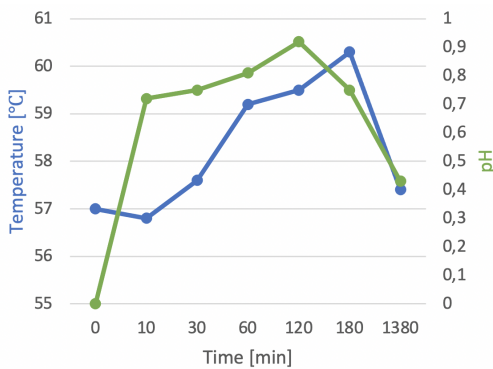
(e) Temperature and pH evolution of the experiments with leaching conditions AO5

(f) Temperature and pH evolution of the experiments with leaching conditions AO6
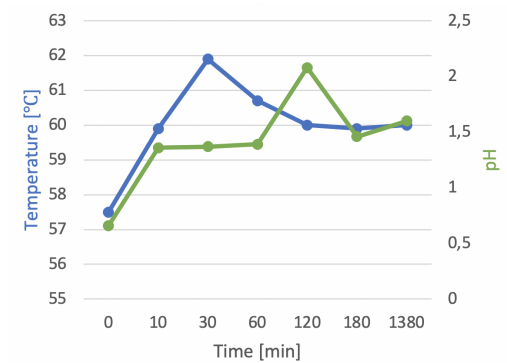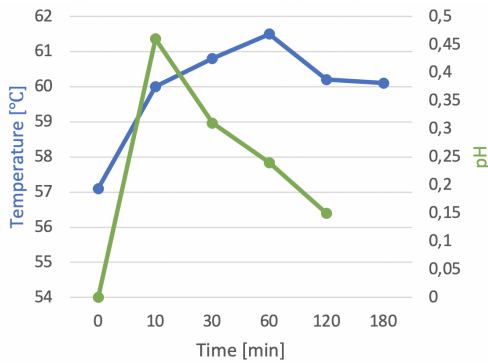
(g) Temperature and pH evolution of the experiments with leaching conditions AO7

(h) Temperature and pH evolution of the experiments with leaching conditions AO8

Figure B.2.1: Temperature and pH evolution in the leaching experiments performed on the BM-T.

C | Leachate calculations

C.1 ICP-MS results

The ICP-MS results provided by ALS Global are given in Table C.1.1.

Experiment		Element [µg/L]			
TestID	Time [min]	Co	Mn	Ni	Li
	10	616000	280000	1960000	1260000
	30	264000	270000	2540000	1210000
AO1	60	263000	303000	2670000	1220000
	120	213000	291000	2890000	1250000
	180	180000	311000	3750000	1240000
	1380	47900	348000	4400000	1290000
	10	1130000	3260000	169000	1330000
	30	1450000	3230000	2100000	1230000
AO2	60	1790000	3390000	3020000	1360000
	120	1760000	3130000	3170000	1240000
	180	2210000	3270000	3790000	1250000
	1380	2330000	3330000	4040000	1300000
	10	2130000	3320000	3440000	1240000
	30	2040000	3180000	3590000	1280000
AO3	60	2240000	3330000	3670000	1280000
	120	2120000	3330000	3780000	1280000
	180	2320000	3420000	3790000	1300000
	1380	2390000	3600000	4140000	1400000

	10	1680000	2770000	2940000	1130000
	30	2090000	3260000	3380000	1190000
AO4	60	1890000	3040000	3430000	1200000
	120	2420000	3560000	3820000	1340000
	180	1990000	3110000	3530000	1210000
	1380	2320000	3400000	3770000	1300000
	10	1320000	3200000	1960000	1250000
	30	1720000	3590000	2320000	1310000
AO5	60	1910000	3960000	2910000	1500000
	120	1700000	3290000	3190000	1380000
	180	2080000	3480000	3600000	1360000
	1380	2760000	3730000	5030000	1460000
	10	1290000	3250000	2020000	1300000
	30	2040000	4460000	3090000	1810000
AO6	60	1990000	4260000	3150000	1670000
	120	1900000	3680000	3030000	1420000
	180	1910000	3500000	3460000	1450000
	1380	2950000	4010000	5270000	1510000
	10	2140000	3280000	3640000	1280000
	30	2280000	3450000	3720000	1300000
AO7	60	2260000	3450000	3840000	1290000
	120	2560000	4010000	4880000	1670000
	180	2520000	3660000	4100000	1380000
	1380	12300000	16400000	23800000	7950000
	10	1900000	3050000	3210000	1160000
	30	2290000	3320000	3570000	1240000
AO8	60	2140000	3310000	3670000	1300000
	120	2160000	3260000	3700000	1280000
	180	2180000	3340000	3820000	1340000
	1380	2820000	3860000	4410000	1420000
	10	616000	280000	1960000	1260000
AO9					

	30	264000	270000	2540000	1210000
	60	263000	303000	2670000	1220000
	120	213000	291000	2890000	1250000
	180	180000	311000	3750000	1240000
	1380	47900	348000	4400000	1290000
	10	1130000	3260000	1690000	1330000
	30	1450000	3230000	2100000	1230000
AO10	60	1790000	3390000	3020000	1360000
	120	1760000	3130000	3170000	1240000
	180	2210000	3270000	3790000	1250000
	1380	2330000	3330000	4040000	1300000
	10	2130000	3320000	3440000	1240000
	30	2040000	3180000	3590000	1280000
AO11	60	2240000	3330000	3670000	1280000
	120	2120000	3330000	3780000	1280000
	180	2320000	3420000	3790000	1300000
	1380	2390000	3600000	4140000	1400000
	10	1680000	2770000	2940000	1130000
	30	2090000	3260000	3380000	1190000
AO12	60	1890000	3040000	3430000	1200000
	120	2420000	3560000	3820000	1340000
	180	1990000	3110000	3530000	1210000
	1380	2320000	3400000	3770000	1300000
	10	768000	1160000	1460000	950000
	30	847000	1230000	1500000	917000
AO13	60	904000	1380000	1780000	1020000
	120	1160000	1680000	2090000	1030000
	180	1150000	1740000	2320000	1070000
	1380	2120000	3030000	3720000	1650000
	10	623000	959000	1140000	747000
	30	-	-	-	
AO14	60	704000	1050000	1330000	832000

	120	1130000	1670000	2110000	1110000
	180	1170000	1760000	2200000	1060000
	1380	1510000	2260000	2880000	1190000
AO15	10	918000	1430000	1790000	635000
	30	1850000	2670000	3230000	1020000
	60	1860000	2680000	3300000	1090000
	120	1900000	2790000	3460000	1140000
	180	1760000	2720000	3480000	1150000
	1380	2120000	3030000	3720000	1190000
AO16	10	405000	618000	780000	311000
	30	1250000	1960000	2500000	851000
	60	1710000	2550000	3080000	1030000
	120	1580000	2490000	3130000	1050000
	180	1780000	2610000	3240000	1100000
	1380	1950000	2870000	3590000	1180000
AO17	10	127000	195000	235000	170000
	30	734000	1090000	1330000	829000
	60	927000	1380000	1700000	975000
	120	1130000	1670000	2100000	1040000
	180	1440000	1990000	2370000	1080000
	1380	1990000	2970000	3630000	1400000
AO18	10	659000	973000	1200000	752000
	30	787000	1150000	1420000	850000
	60	765000	1190000	1560000	889000
	120	1100000	1590000	1920000	948000
	180	1130000	1670000	2140000	997000
	1380	1580000	2350000	2920000	1120000

Table C.1.1: The ICP-MS results from ALS Global given in µg/L.

C.2 Calculating leaching efficiency

The equations used for calculating the moles of each element i from the ICP-MS results is given below:

$$n_i = \frac{c_i \cdot V}{Mm_i} = \frac{\mu[g/L] \cdot m[L]}{[g/mol]} = 10^{-9} mol$$

For the calculation of leaching efficiency, the equation below was used:

$$\text{leaching efficiency AOX}_i = \Sigma_{i-1}(\text{leaching efficiency}) + \frac{n_{i,leachate}}{n_{i,BM}} * 100\%$$

C.3 Calculation of weight% of the experiment with leching conditions AO7

The weight percentage of leached element are calculated form the molar mass and the content in the BM before leaching and the sum of elemental content from the leachate samples extracted during leaching. The calculation is given below:

$$weight\% = \frac{n_{i,after} \cdot Mm_i}{n_{i,before} \cdot Mm_i} \cdot 100\%$$

The values used in the calculations and the resulting weight% are given in Table C.3.1.

Table C.3.1: Leaching efficiency in weight percentage from the experiment with leaching conditions AO7, and the properties used for calculation.

Element	Li	Ni	Mn	Co
Molar mass [g/mol]	6.94	58,69	54.93	58.93
Content before leaching [mol]	0.0077	0,0029	0.0048	0,0015
Content before leaching [mol]	0.0023	0,0008	0.0006	0,0004
Leaching efficiency [weight%]	29.8%	27.7%	12.5%	27.1%

D | Chemical mapping of the BMs and SRs with SEM-EDS

D.1 Chemical mapping of the BM-U
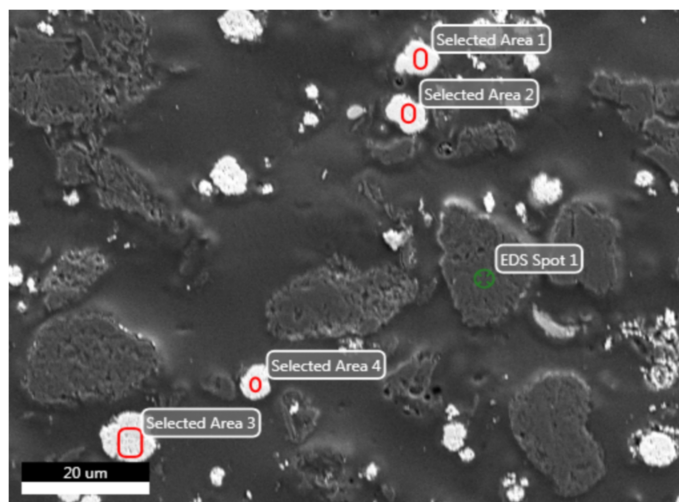
(a) BM-U: Area 1. Overview of Selected Areas and EDS Spots.
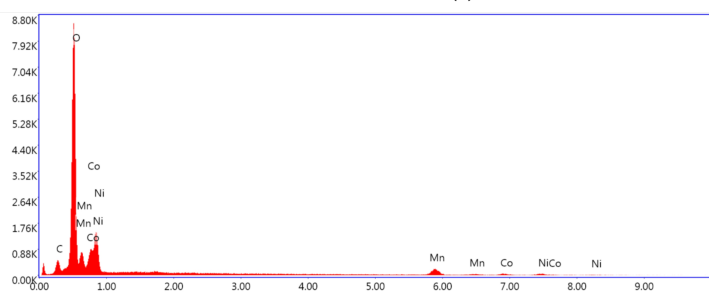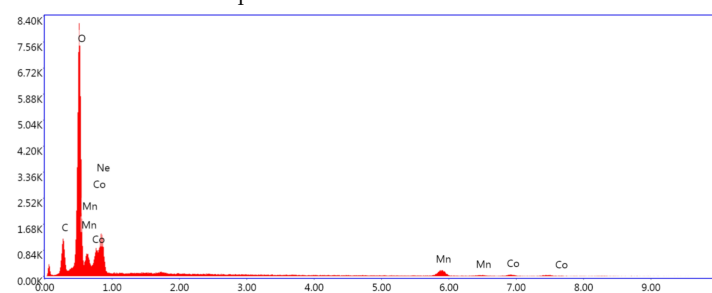
(b) Mass specter: Selected Area 1

(c) Mass specter: Selected Area 2
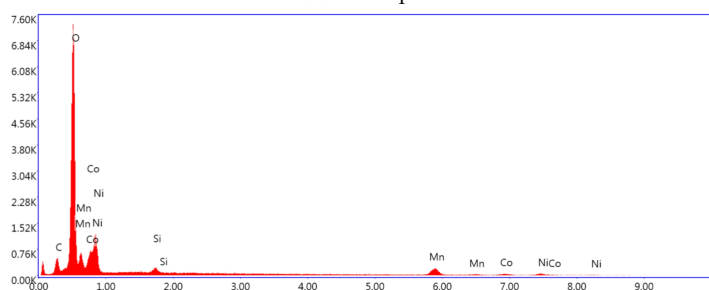
(d) Mass specter: Selected Area 3
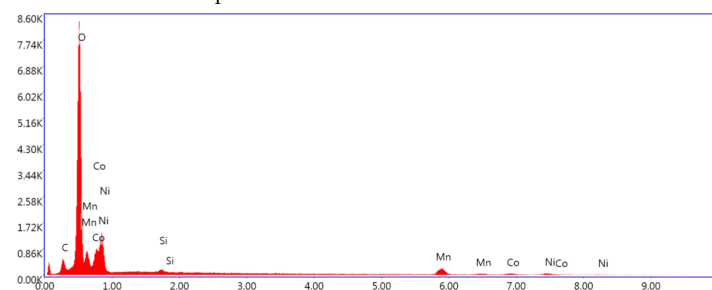
(e) Mass specter: Selected Area 4
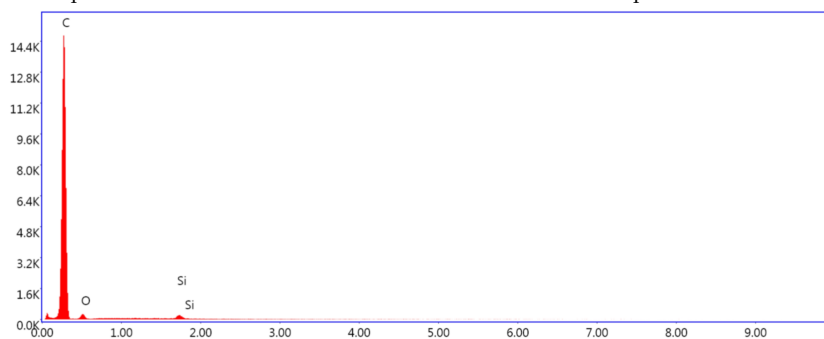
(f) Mass specter: EDS Spot 1

Figure D.1.1: BM-U: Area 1. Overview of Selected Areas and EDS Spots and mass specter over the respective Selected Areas / EDS Spots
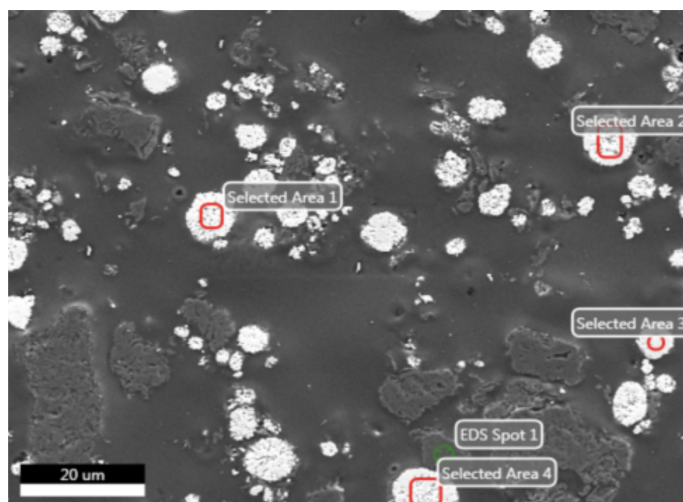
(a) BM-U: Area 2. Overview of Selected Areas and EDS Spots.
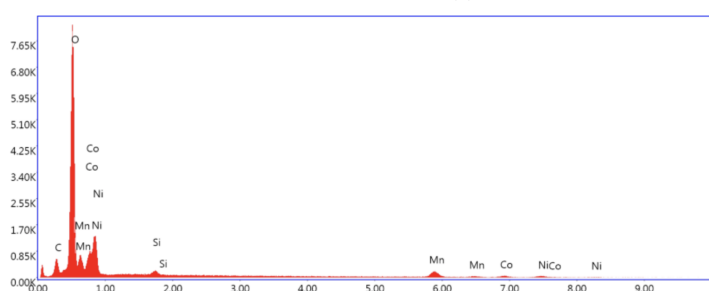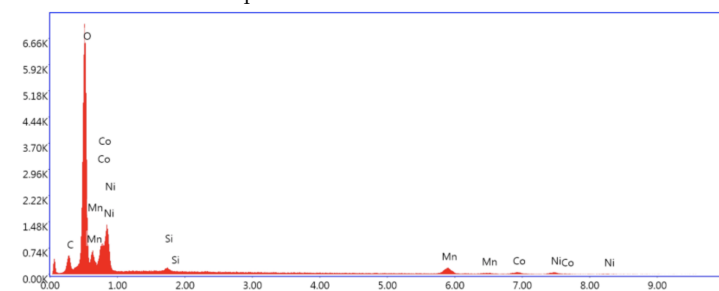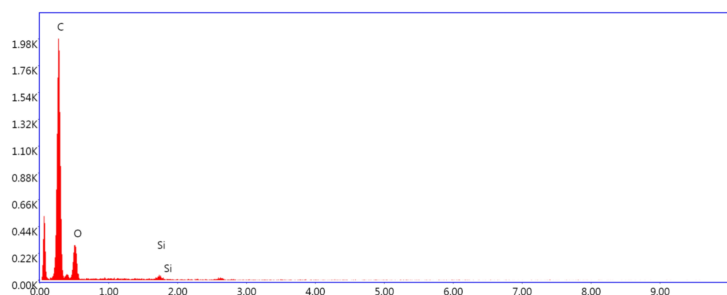

(b) Mass specter: Selected Area 1

(c) Mass specter: Selected Area 2
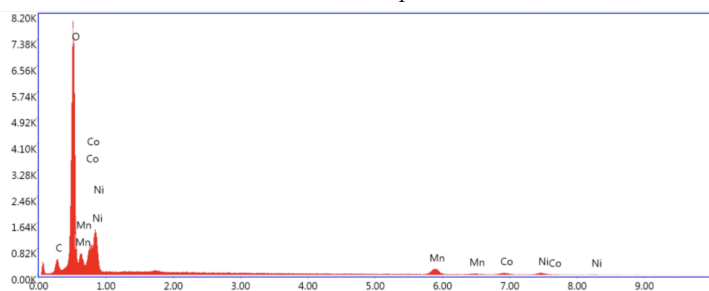
(d) Mass specter: Selected Area 3
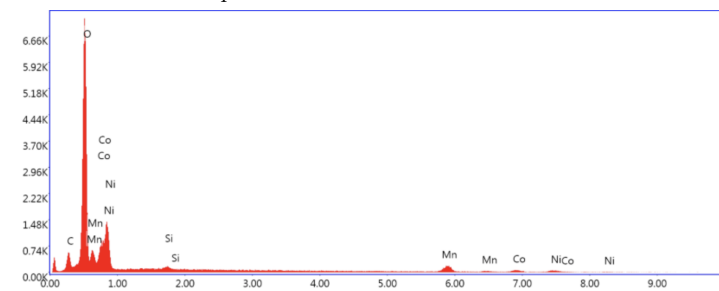
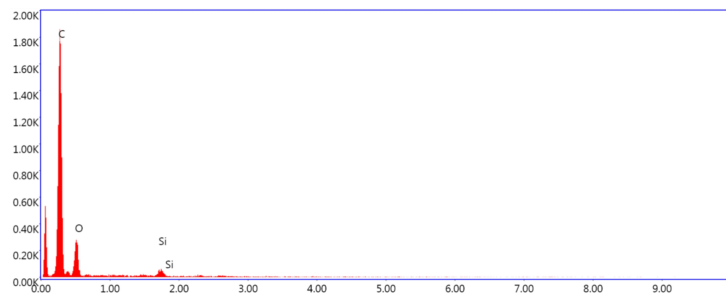(e) Mass specter: Selected Area 4
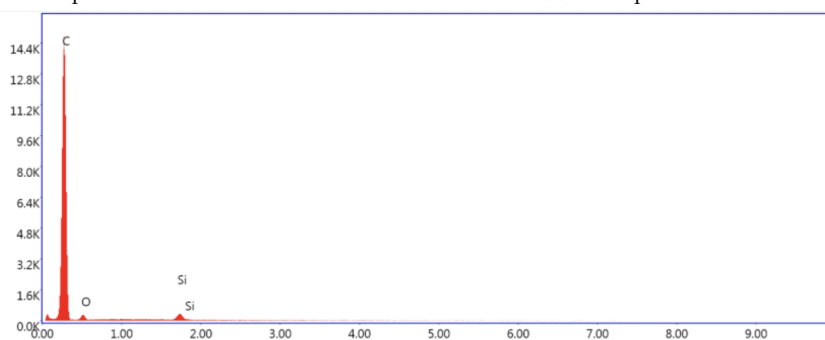
(f) Mass specter: EDS Spot 1

Figure D.1.2: BM-U: Area 2. Overview of Selected Areas and EDS Spots and mass specter over the respective Selected Areas / EDS Spots
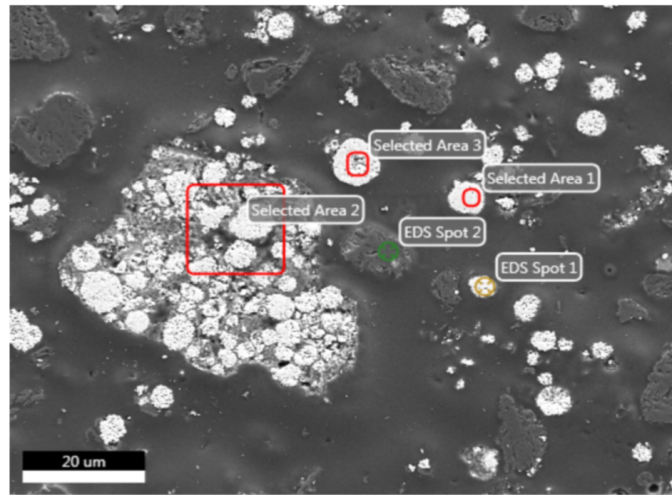
(a) BM-U: Area 3. Overview of Selected Areas and EDS Spots.
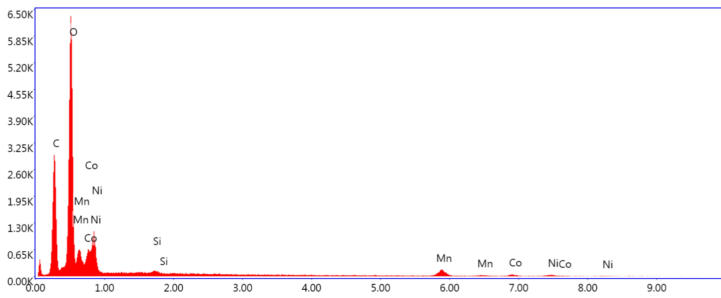
(b) Mass specter: Selected Area 1
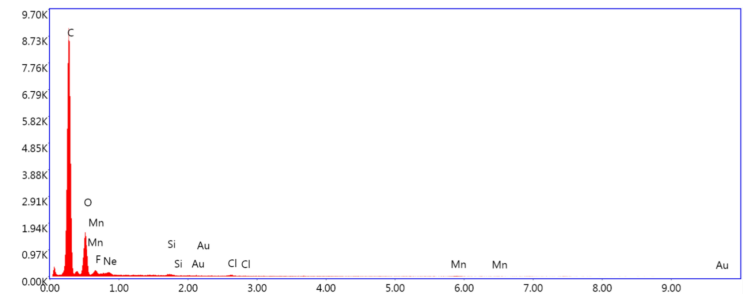
(c) Mass specter: Selected Area 2
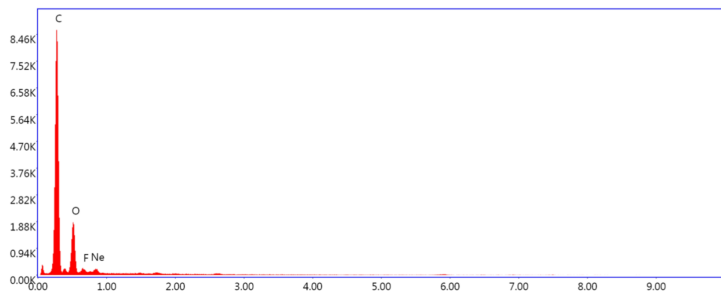
(d) Mass specter: Selected Area 3
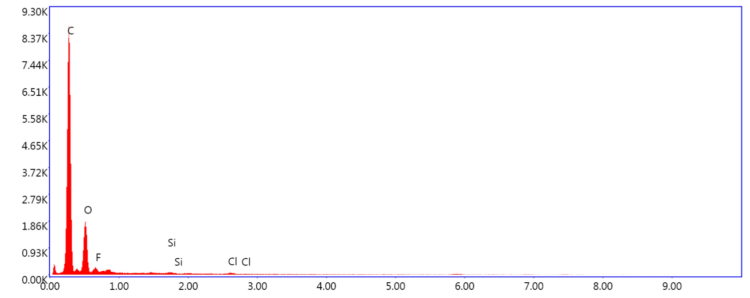
(e) Mass specter: EDS Spot 1
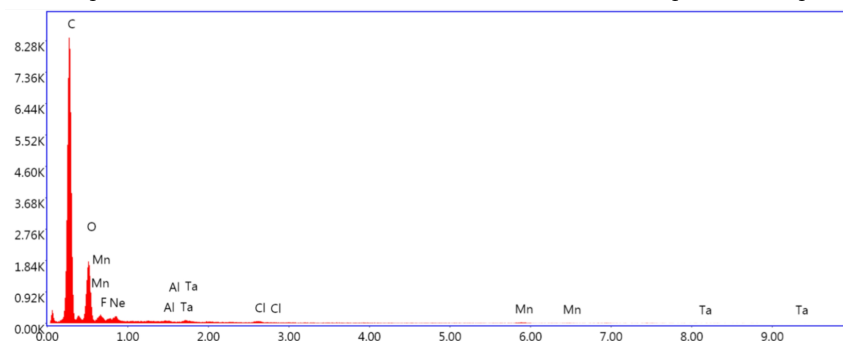
(f) Mass specter: EDS Spot 2

Figure D.1.3: BM-U: Area 3. Overview of Selected Areas and EDS Spots and mass specter over the respective Selected Areas / EDS Spots
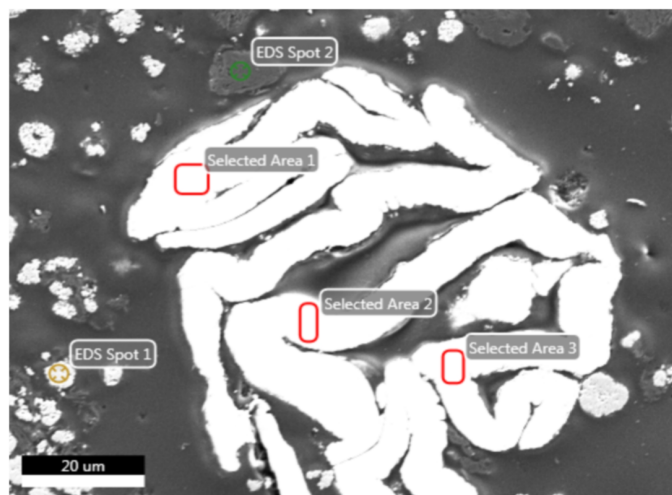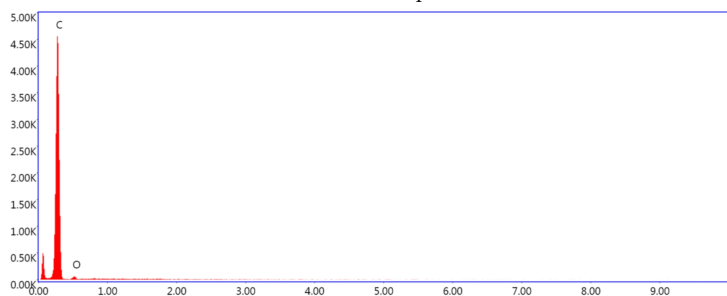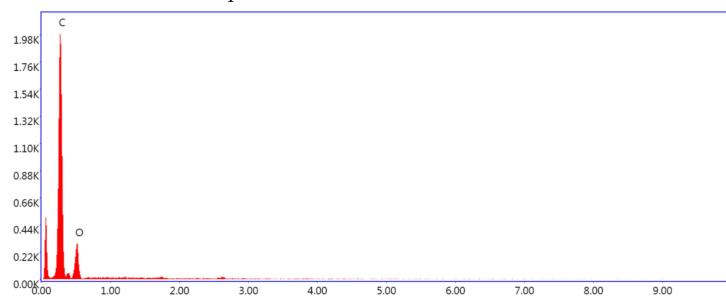
(a) BM-U: Area 3. Overview of Selected Areas and EDS Spots.
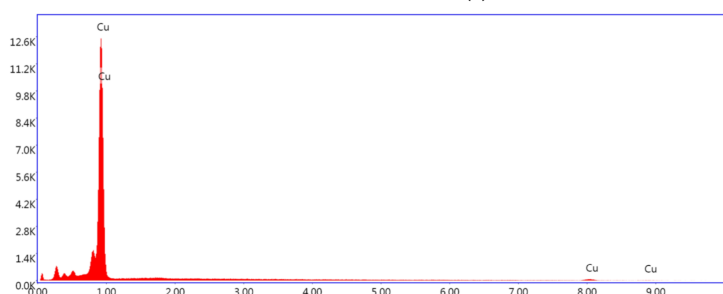
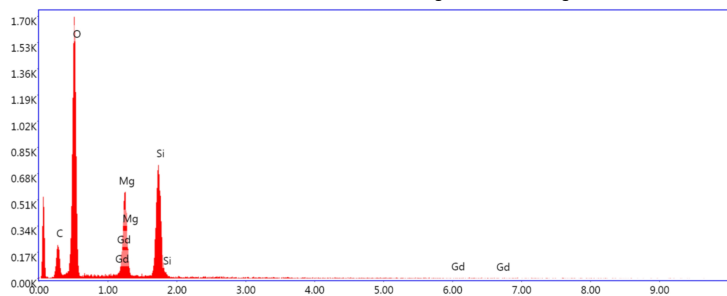**(b)** Mass specter: Selected Area 1
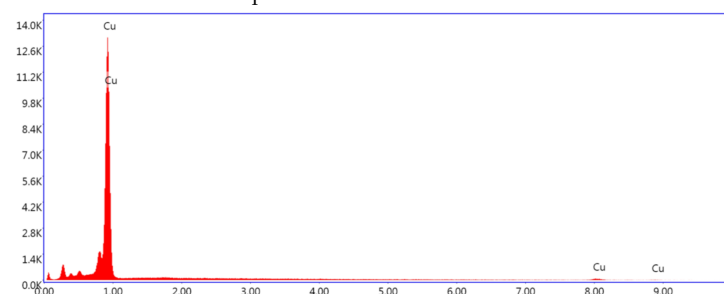
(c) Mass specter: Selected Area 2
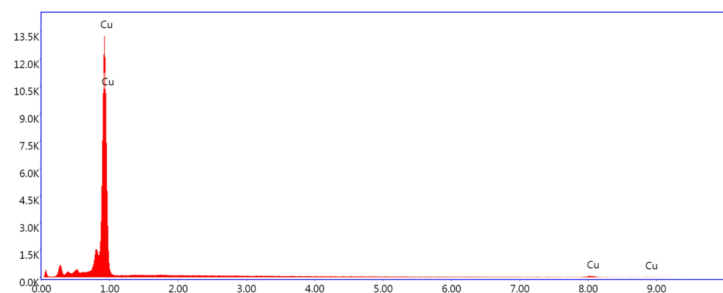
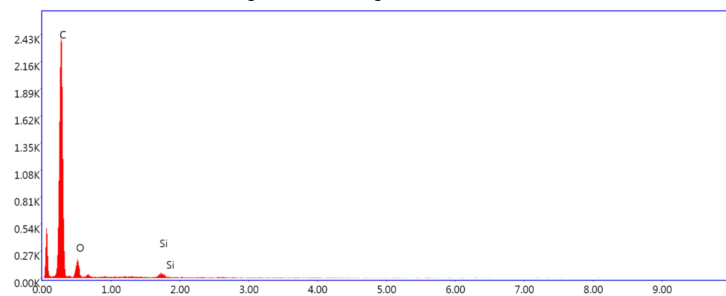**(d)** Mass specter: Selected Area 3
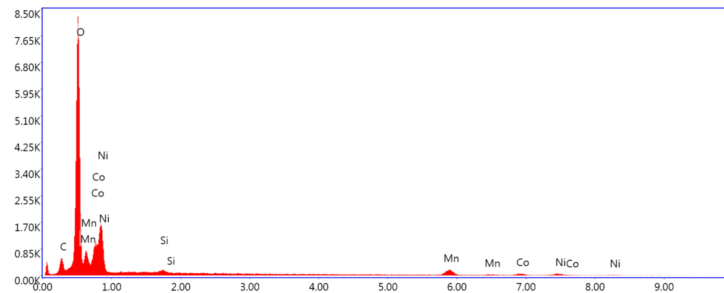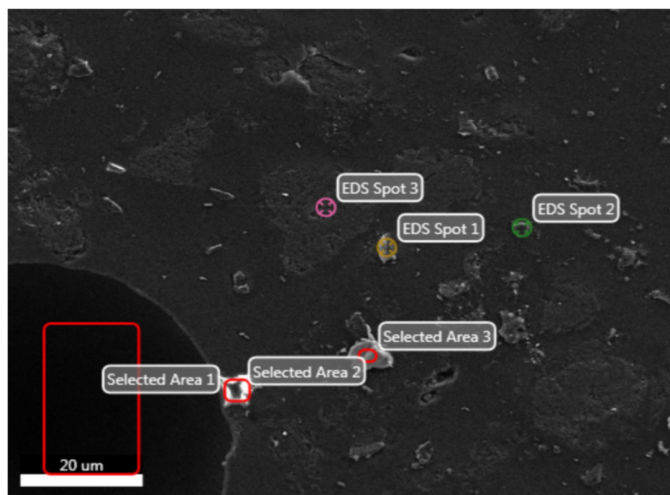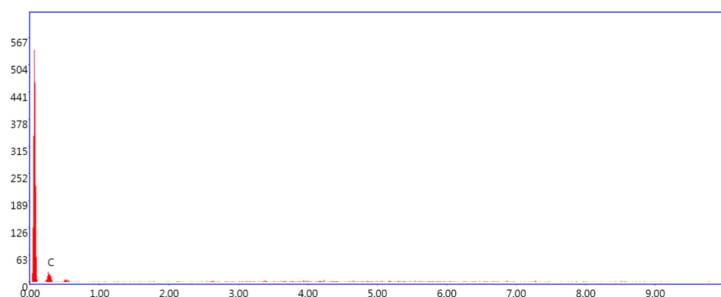

(e) Mass specter: EDS Spot 1
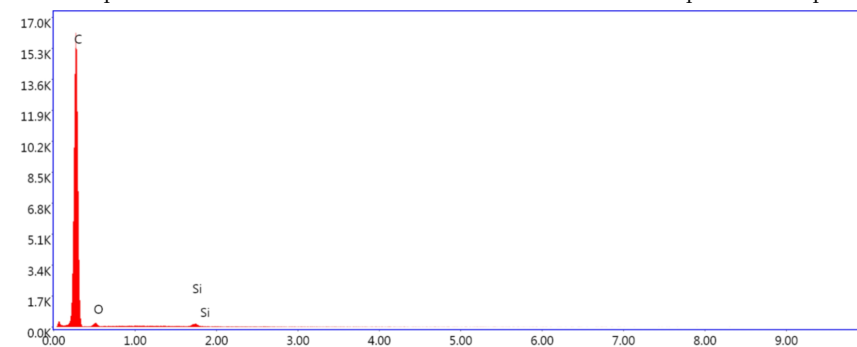
(f) Mass specter: EDS Spot 2

Figure D.1.4: BM-U: Area 4. Overview of Selected Areas and EDS Spots and mass specter over the respective Selected Areas / EDS Spots
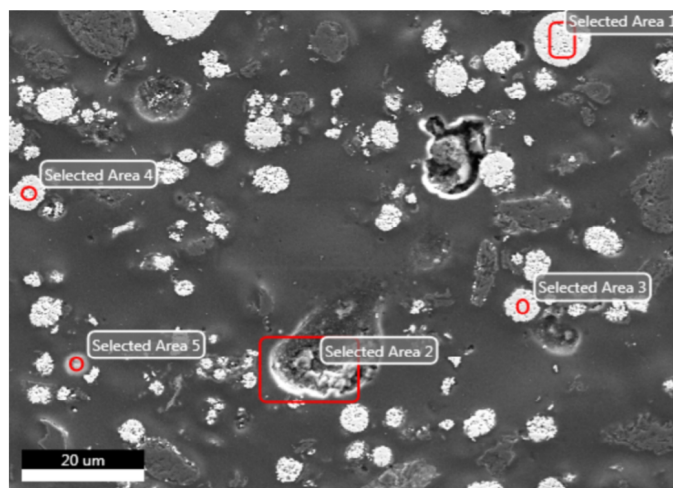
(a) BM-U: Area 5. Overview of Selected Areas and EDS Spots.
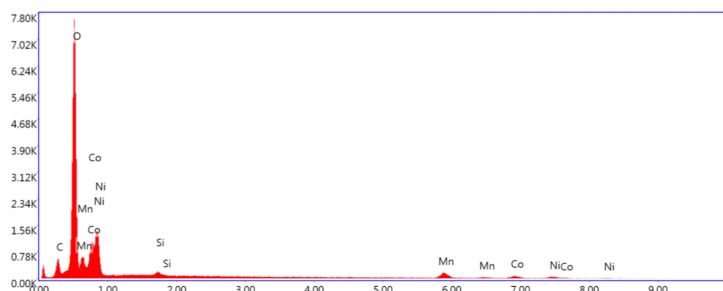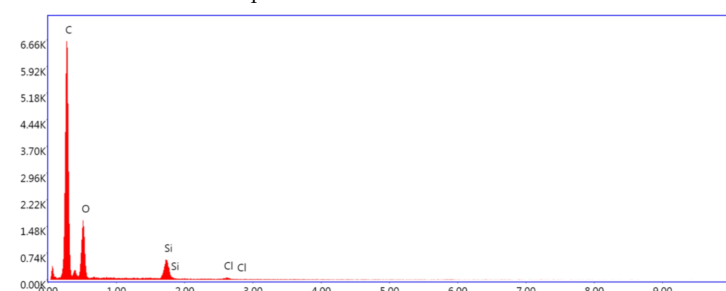
(b) Mass specter: Selected Area 1

(c) Mass specter: Selected Area 2
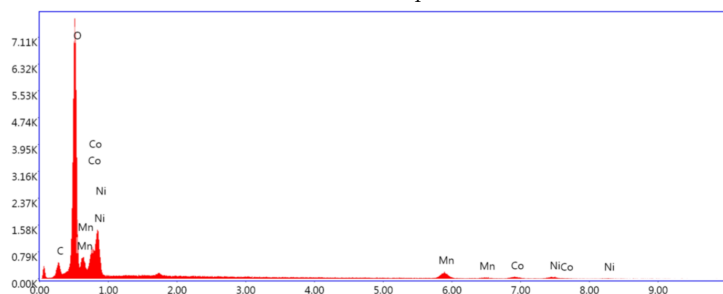
(d) Mass specter: Selected Area 3
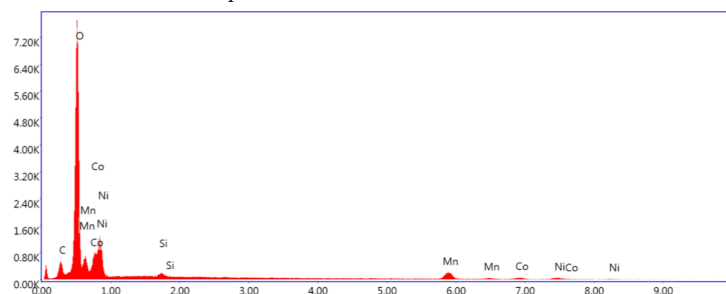
(e) Mass specter: Selected Area 4
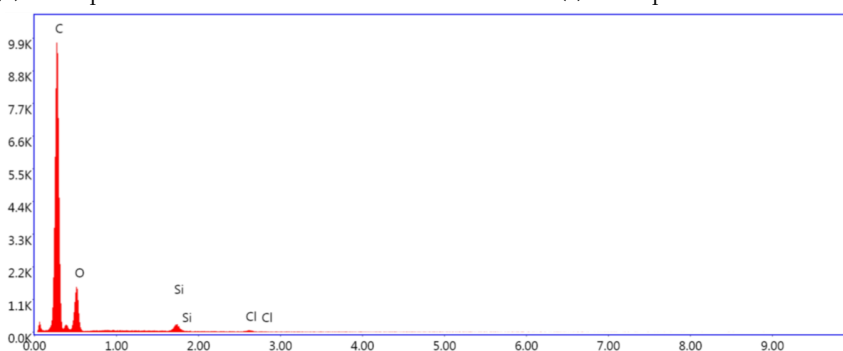
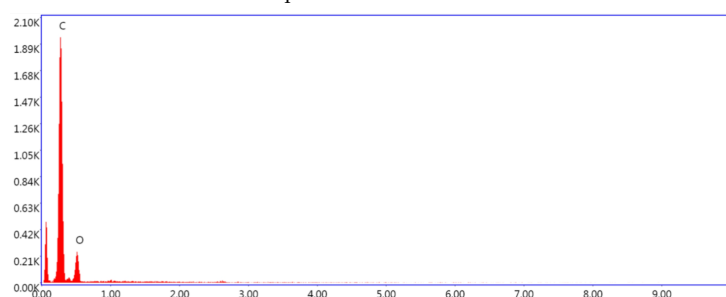**(f)** Mass specter: Selected Area 5

Figure D.1.5: BM-U: Area 5. Overview of Selected Areas and EDS Spots and mass specter over the respective Selected Areas / EDS Spots
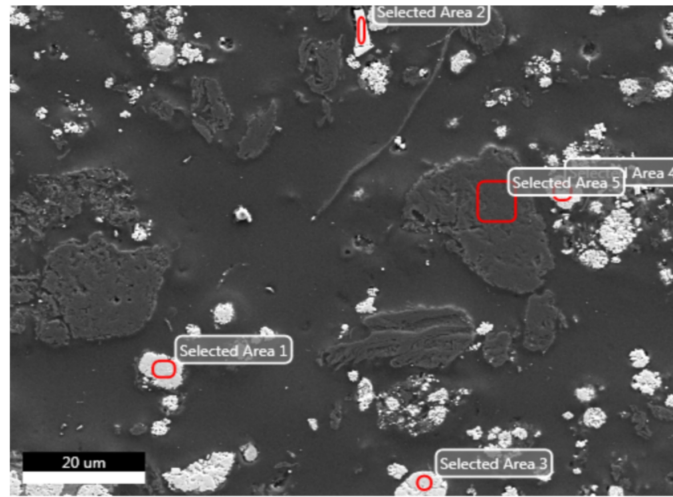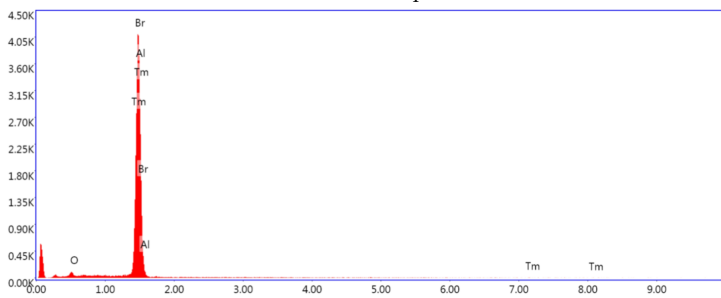
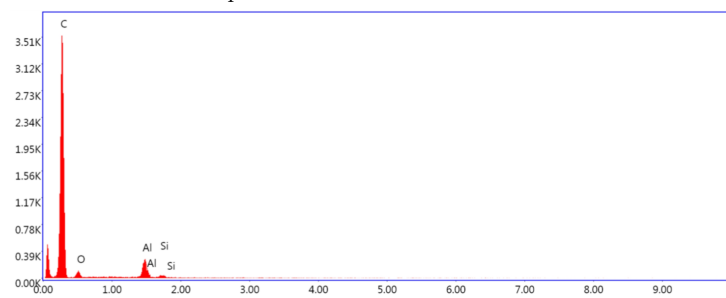**(a)** BM-U: Area 6. Overview of Selected Areas and EDS Spots.
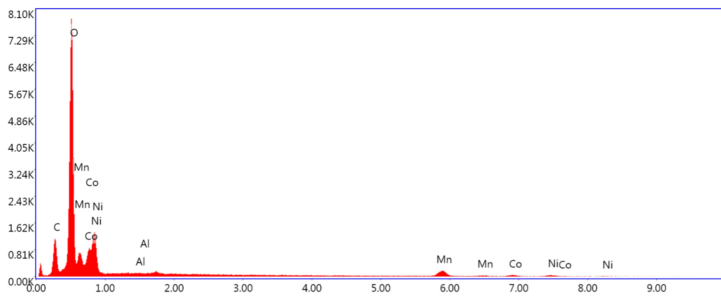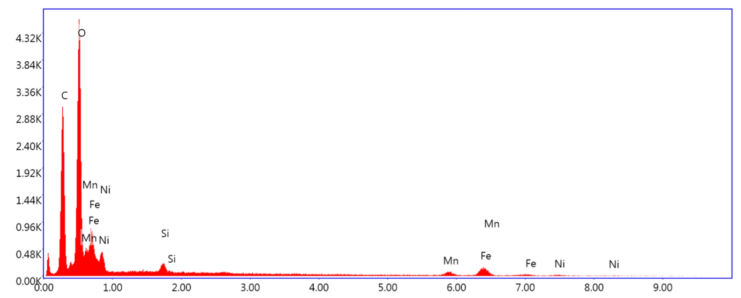
(b) Mass specter: Selected Area 1

(c) Mass specter: Selected Area 2
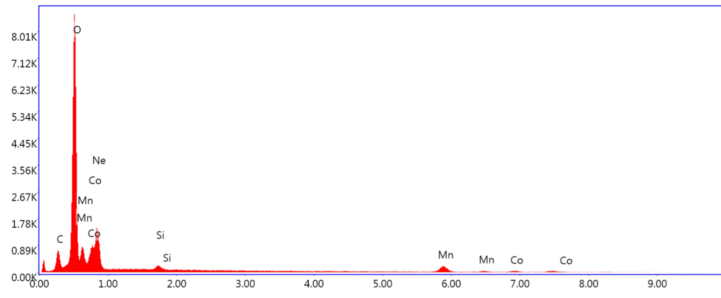
(d) Mass specter: Selected Area 3
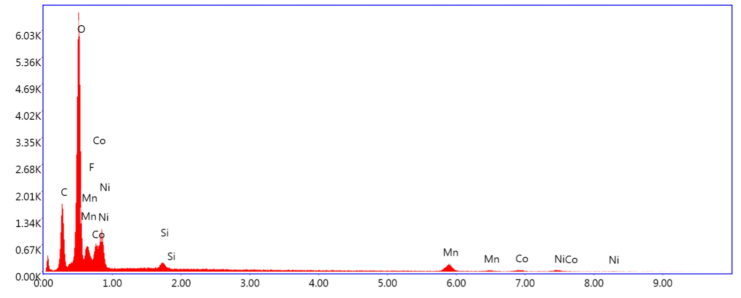
(e) Mass specter: Selected Area 4
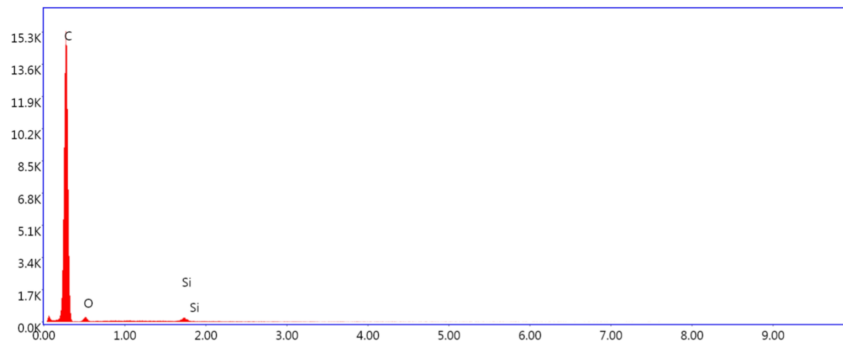
(f) Mass specter: Selected Area 5

Figure D.1.6: BM-U: Area 6. Overview of Selected Areas and EDS Spots and mass specter over the respective Selected Areas / EDS Spots

D.2 Chemical mapping of the BM-T
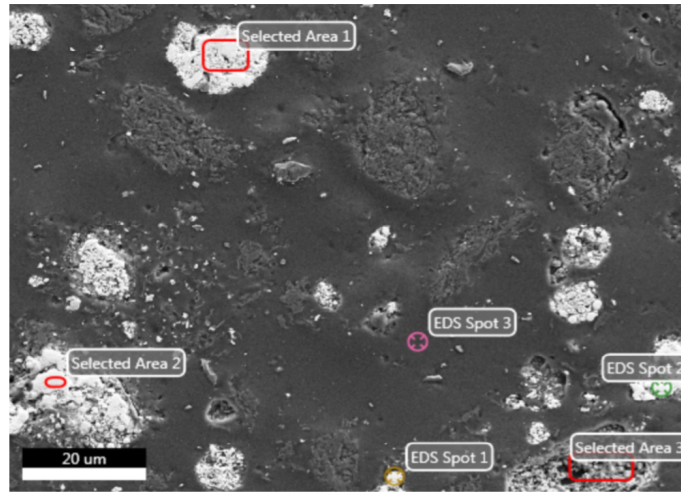
(a) BM-T: Area 1. Overview of Selective Areas and EDS Spots.
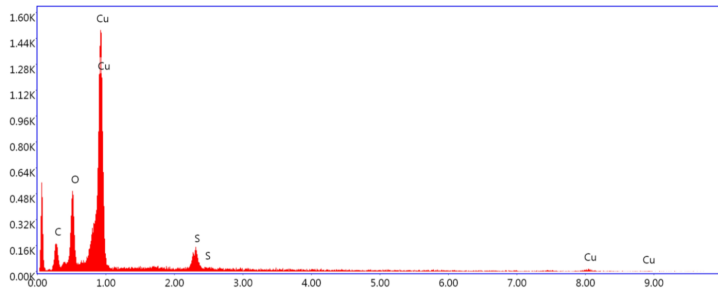
(b) Mass specter: Selective Area 1
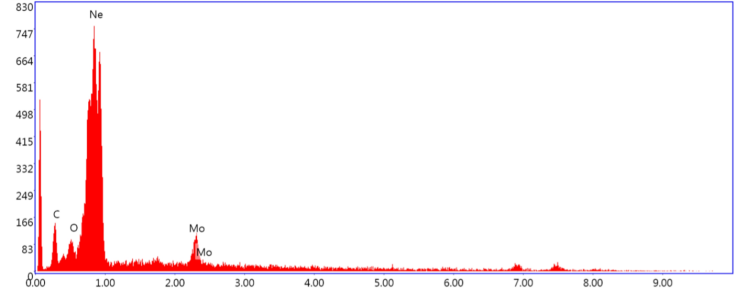
(c) Mass specter: Selective Area 2
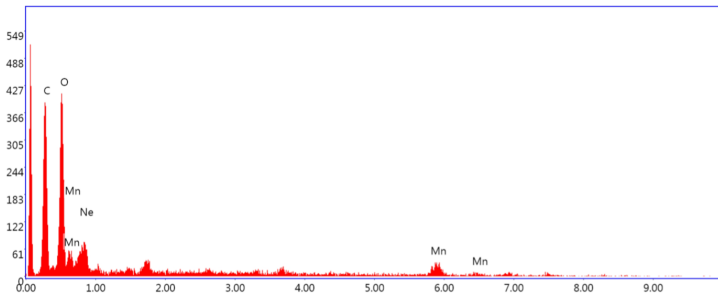
(d) Mass specter: Selective Area 3
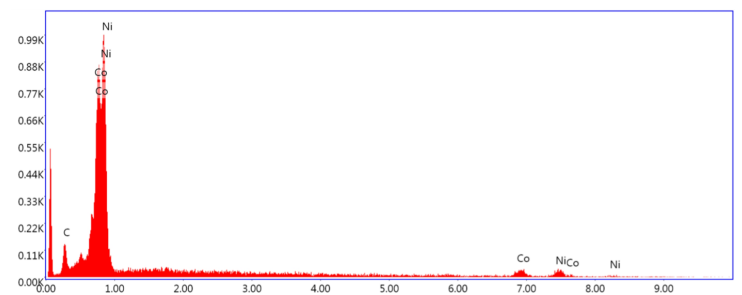
(e) Mass specter: EDS Spot 1
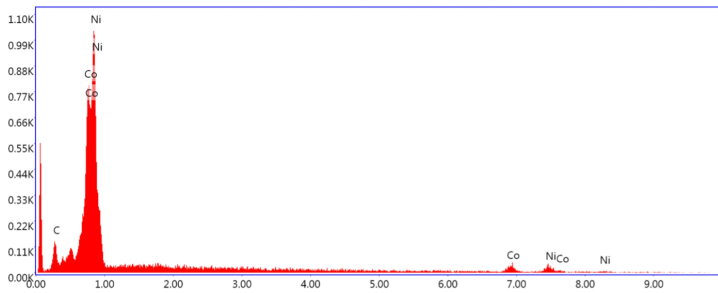
(f) Mass specter: EDS Spot 2
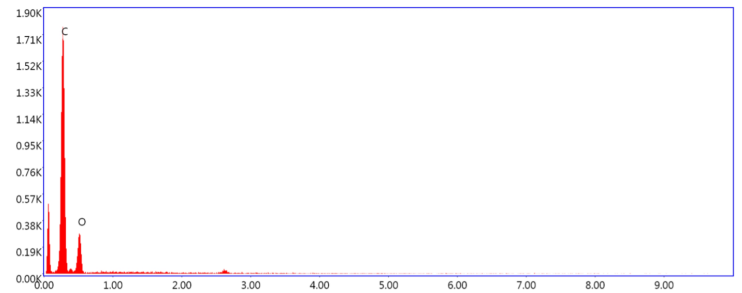
(g) Mass specter: EDS Spot 3

Figure D.2.1: BM-U: Area 1. Overview of Selective Areas and EDS Spots and mass specter over the respective Selective Area / EDS Spot
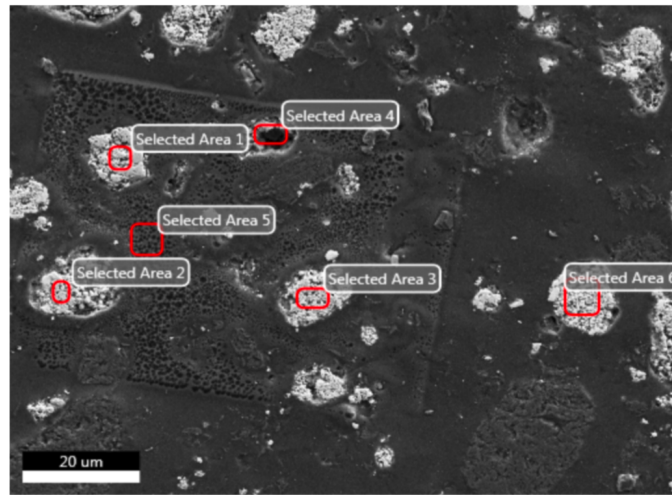
(a) BM-T: Area 2. Overview of Selective Areas and EDS Spots.
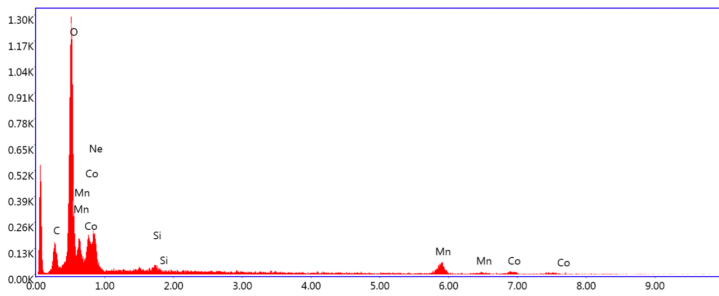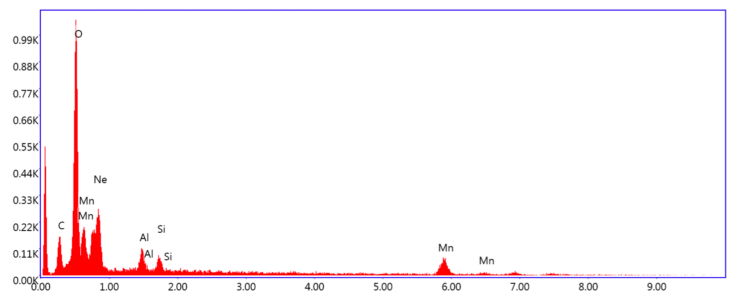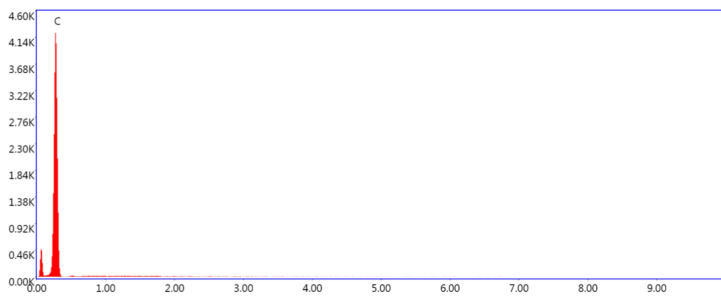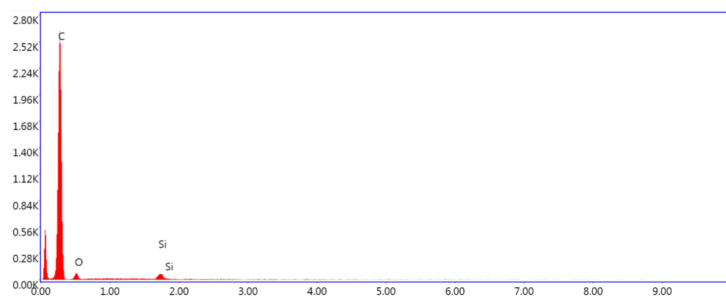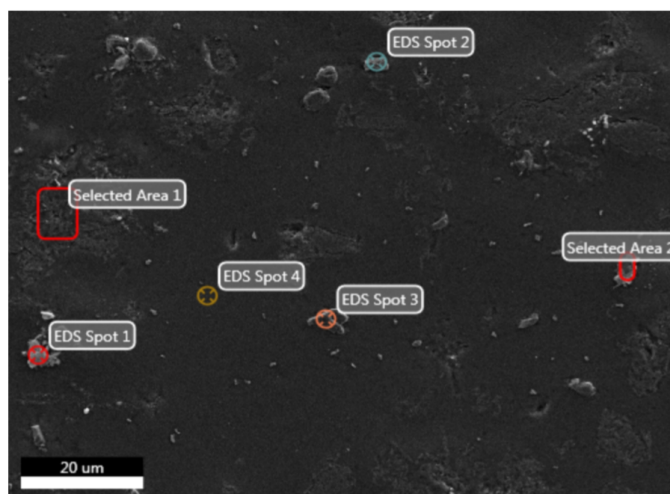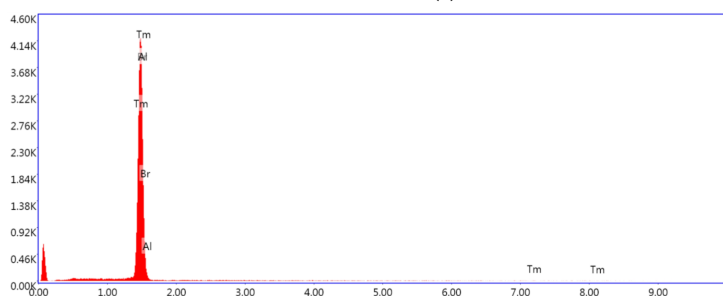

(b) Mass specter: Selected Area 1

(c) Mass specter: Selected Area 2
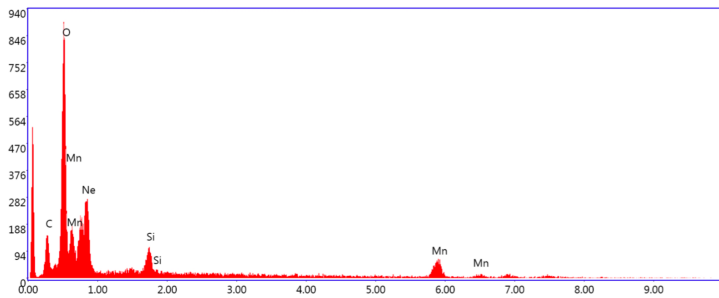
(d) Mass specter: Selected Area 3
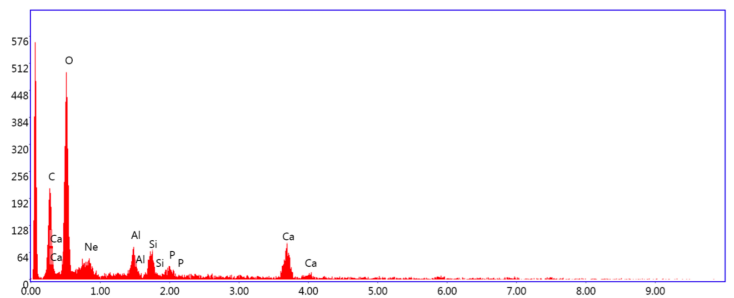
(e) Mass specter: Selected Area 4
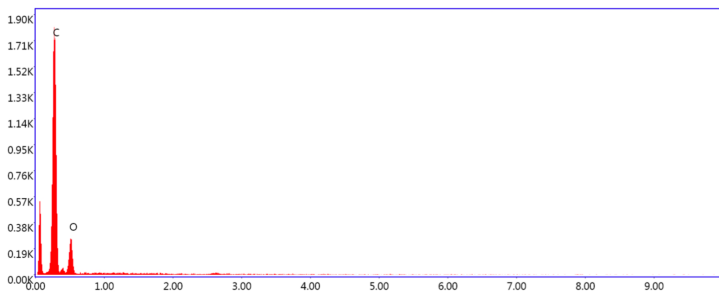
(f) Mass specter: Selected Area 5
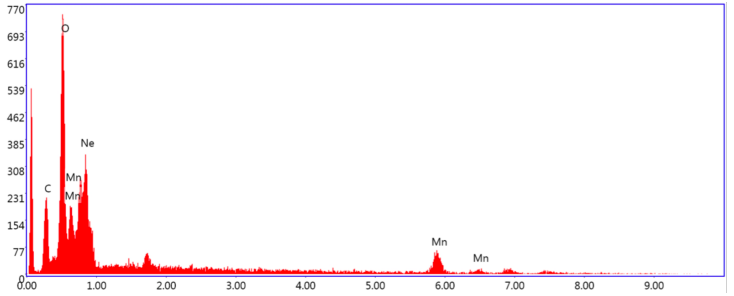
(g) Mass specter: Selected Area 6

Figure D.2.2: BM-T: Area 2. Overview of Selective Areas and mass specter over the respective Selected Area
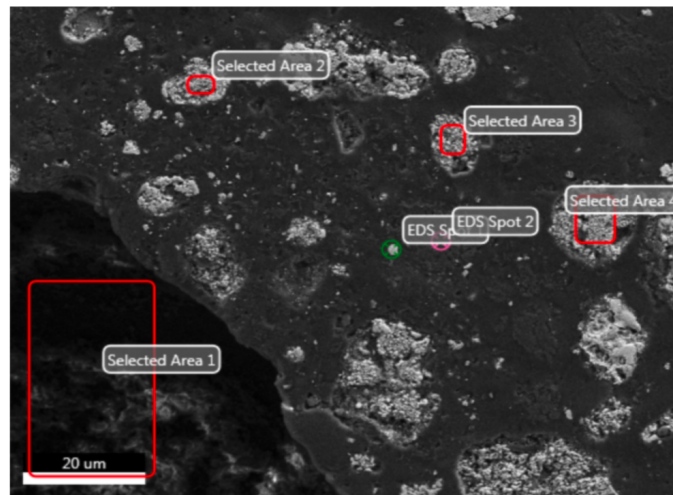
(a) BM-T: Area 3. Overview of Selective Areas and EDS Spots.
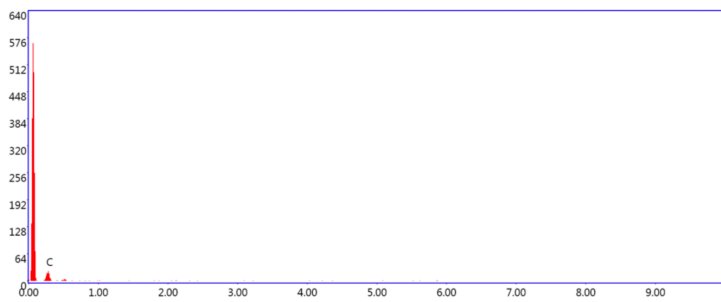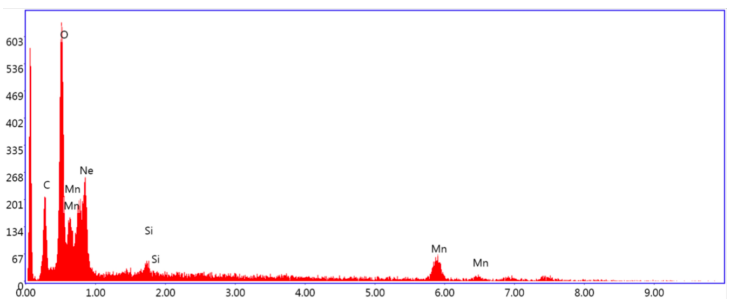
(b) Mass specter: Selected Area 1

(c) Mass specter: Selected Area 2
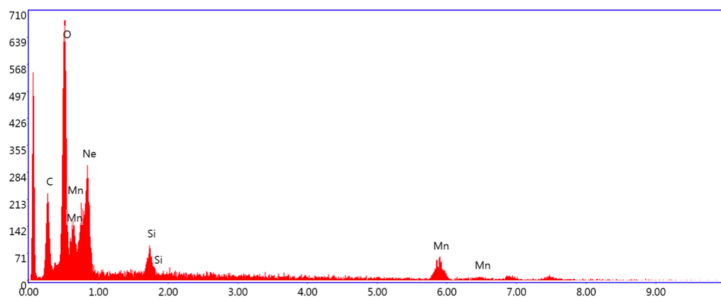
(d) Mass specter: Selected Area 3
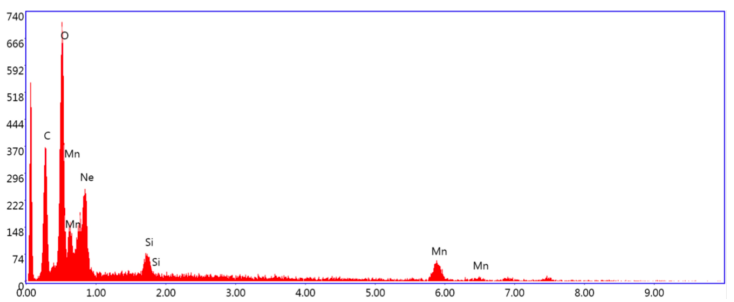
(e) Mass specter: Selected Area 4
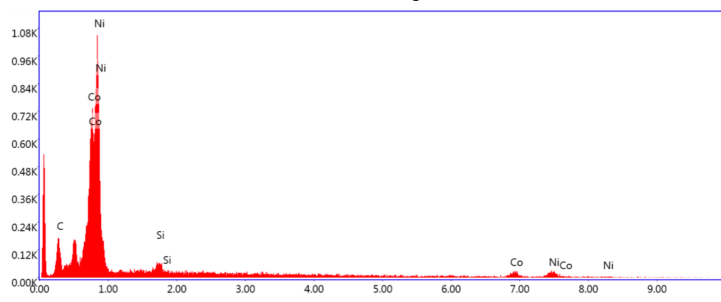
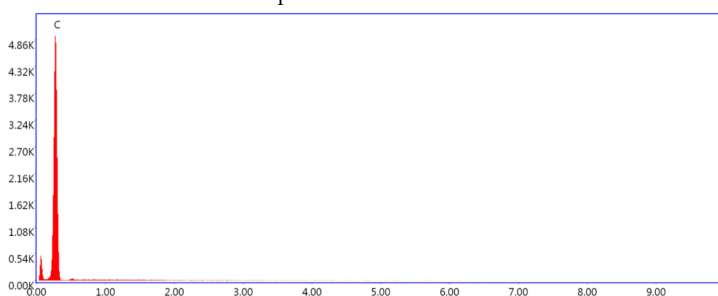**(f)** Mass specter: EDS Spot 1
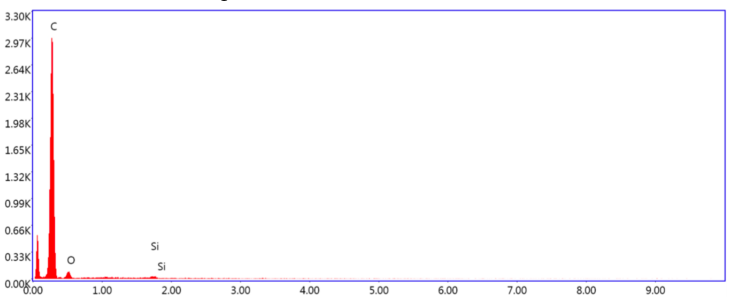
(g) Mass specter: EDS Spot 2

Figure D.2.3: BM-T: Area 3. Overview of Selective Areas and EDS Spots and mass specter over the respective Selective Areas / EDS Spots
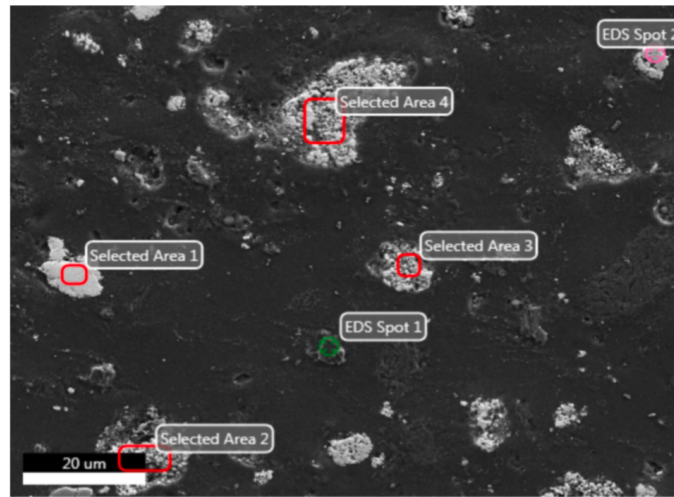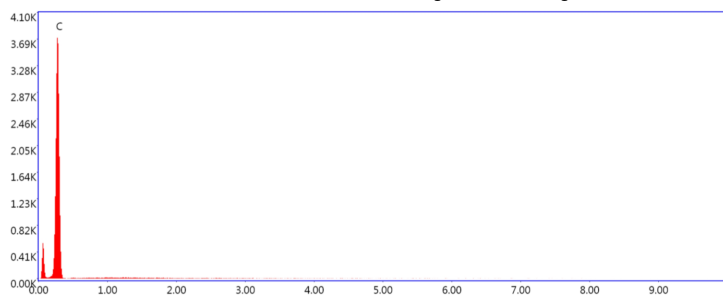
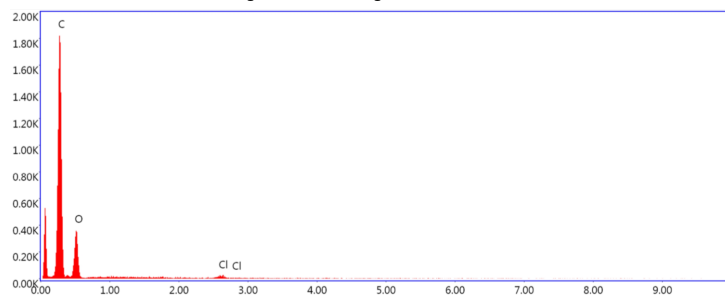**(a)** BM-T: Area 4. Overview of Selective Areas and EDS Spots.
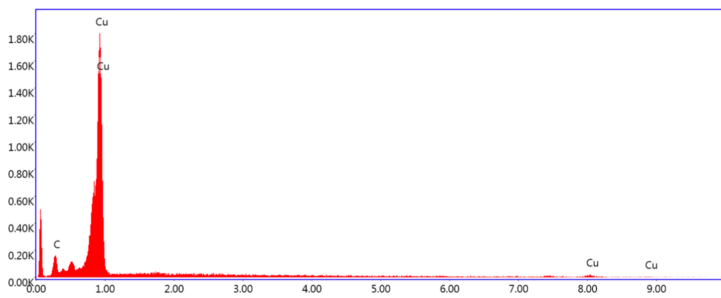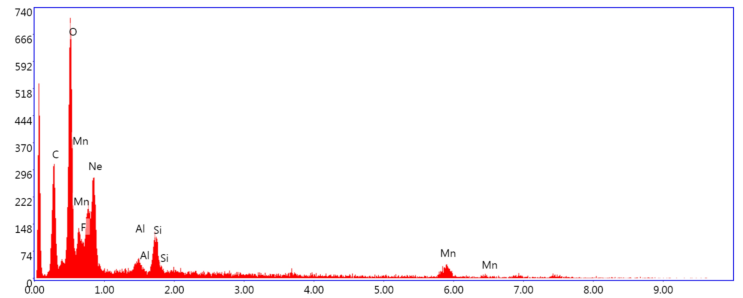
(b) Mass specter: Selected Area 1

(c) Mass specter: Selected Area 2
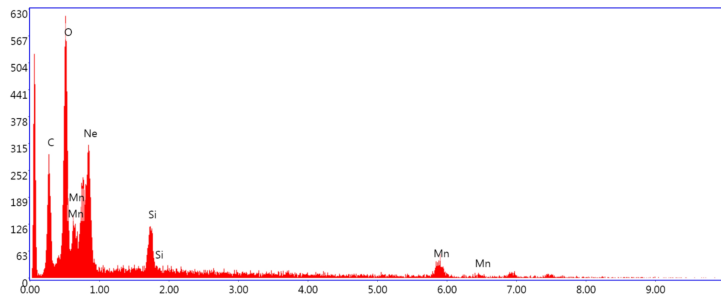
(d) Mass specter: Selected Area 3
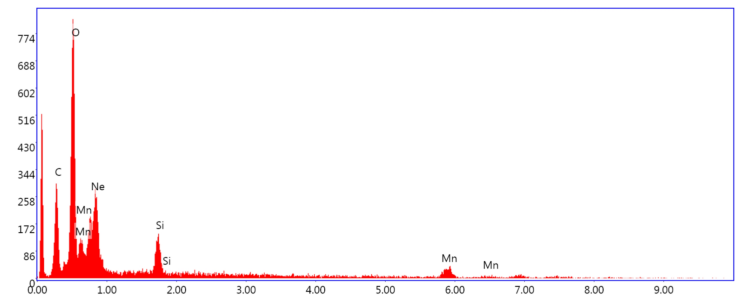
(e) Mass specter: Selected Area 4
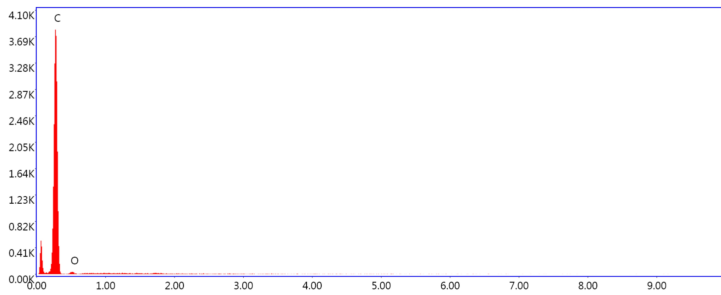
(f) Mass specter: EDS Spot 1
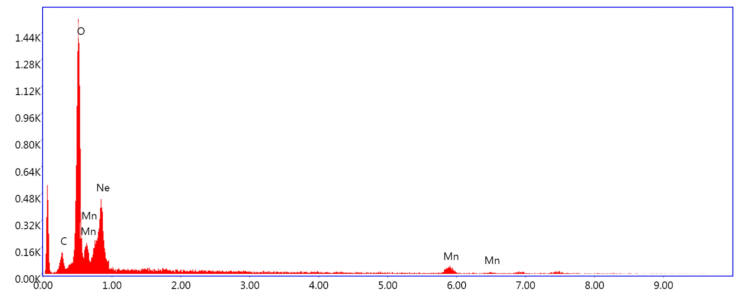
(g) Mass specter: EDS Spot 2

Figure D.2.4: BM-T: Area 4. Overview of Selective Areas and EDS Spots and mass specter over the respective Selective Areas / EDS Spots
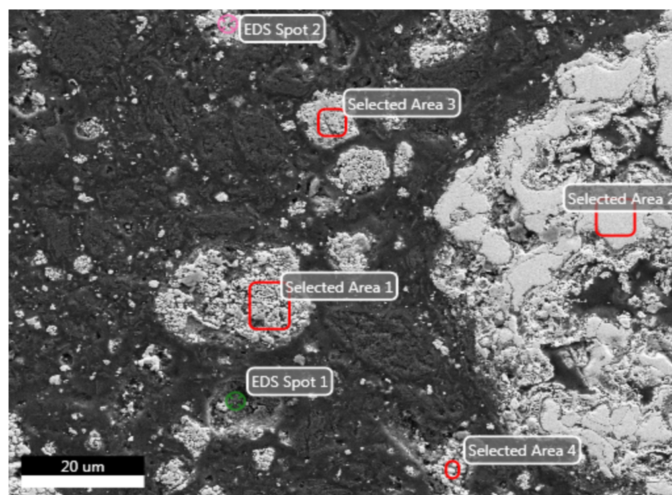
(a) BM-T: Area 5. Overview of Selective Areas and EDS Spots.
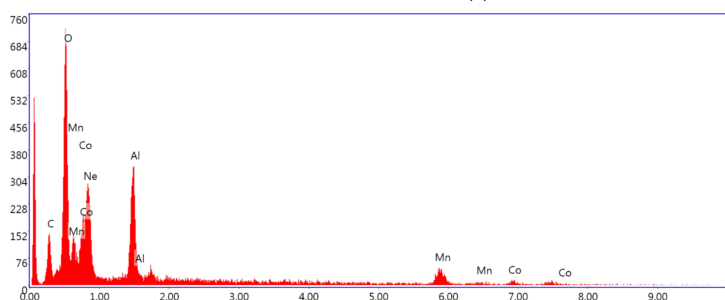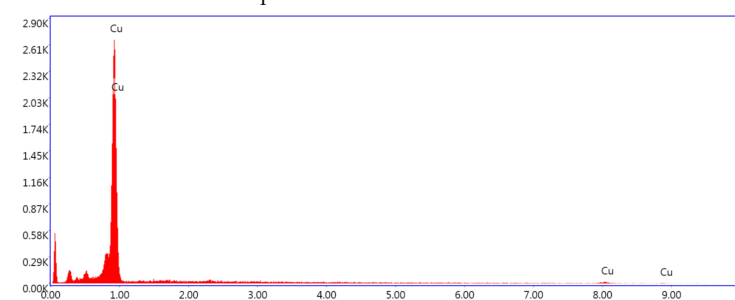
(b) Mass specter: Selected Area 1

(c) Mass specter: Selected Area 2
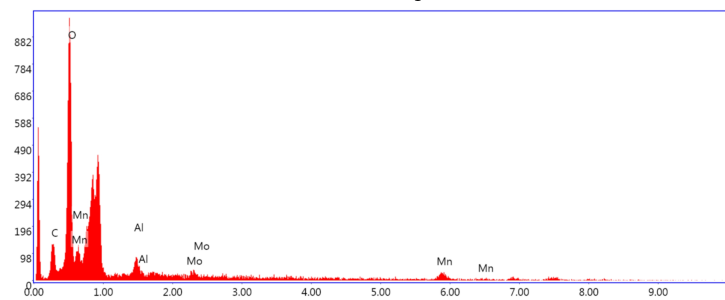
(d) Mass specter: Selected Area 3
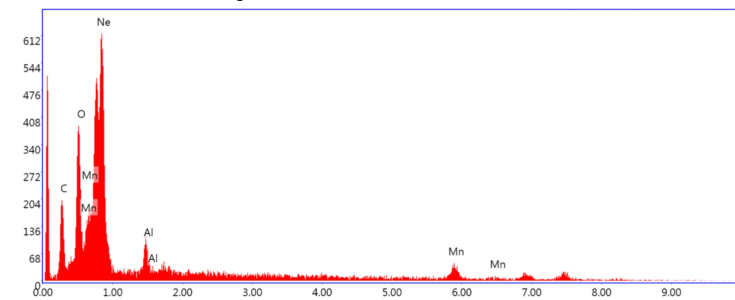
(e) Mass specter: Selected Area 4
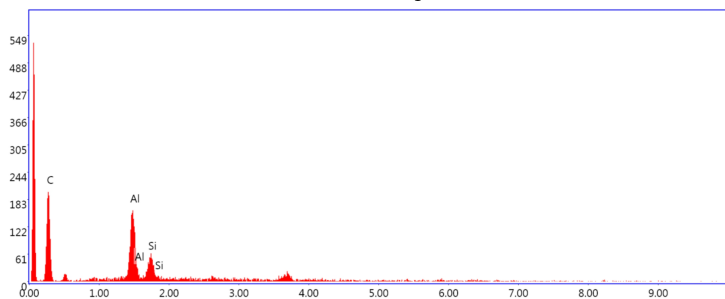
(f) Mass specter: EDS Spot 1
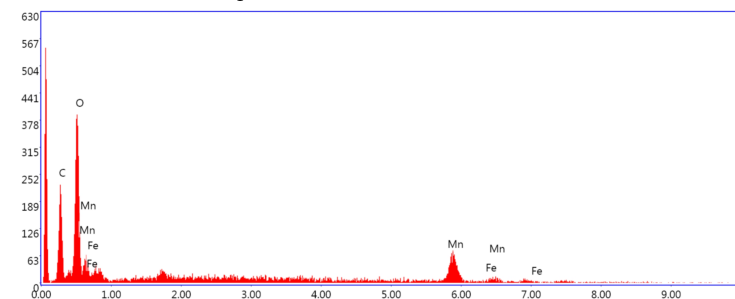
(g) Mass specter: EDS Spot 2

Figure D.2.5: BM-T: Area 5. Overview of Selective Areas and EDS Spots and mass specter over the respective Selective Areas / EDS Spots.
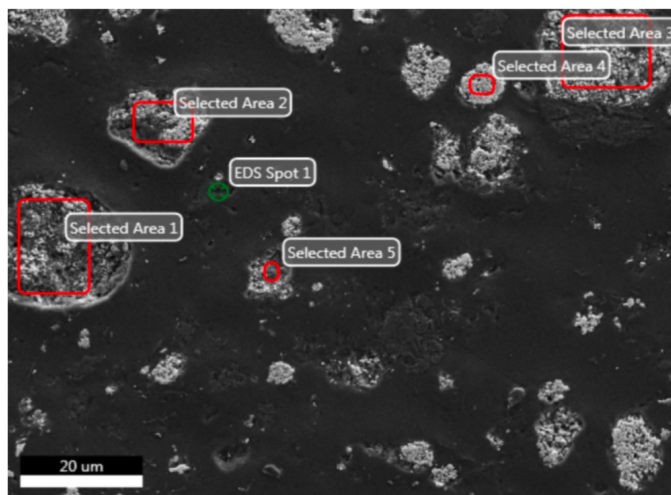
(a) BM-T: Area 6. Overview of Selective Areas and EDS Spots.
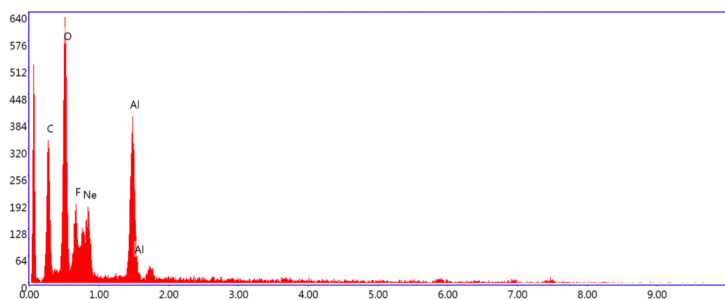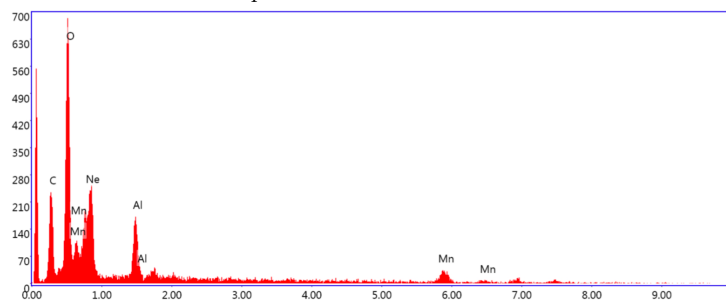
(b) Mass specter: Selected Area 1

(c) Mass specter: Selected Area 2
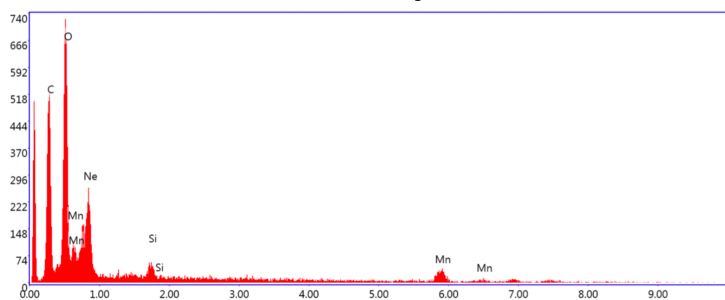
(d) Mass specter: Selected Area 3
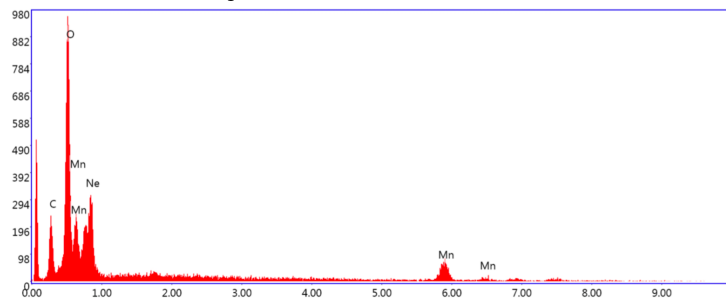
(e) Mass specter: Selected Area 4
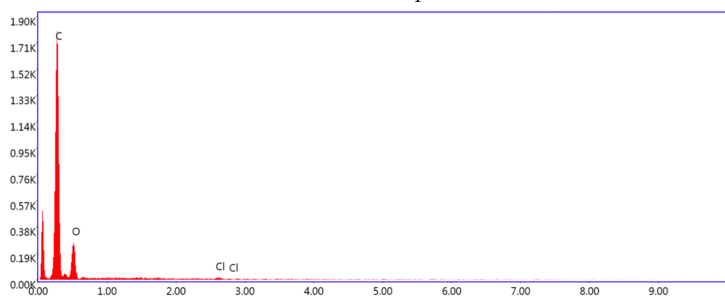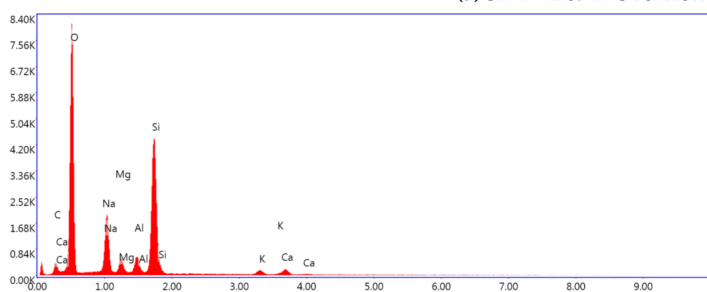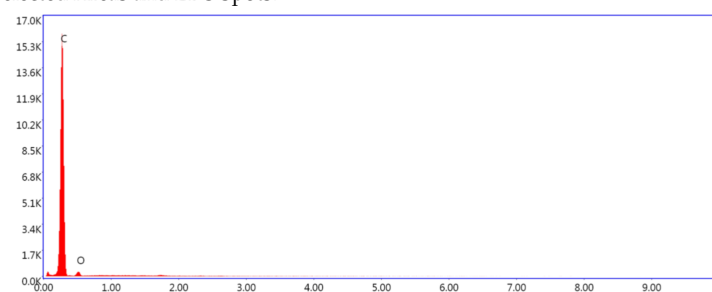

(f) Mass specter: EDS Spot 1
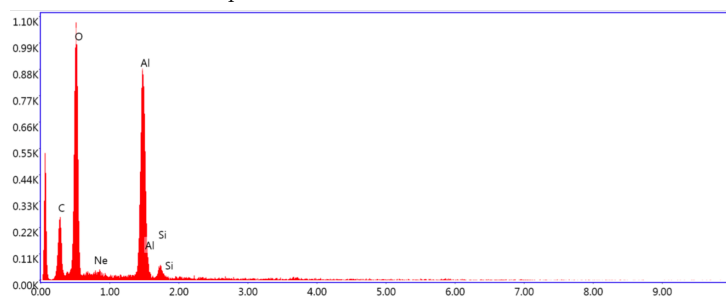
(g) Mass specter: Selected Area 5

Figure D.2.6: BM-T: Area 6. Overview of Selective Areas and EDS Spots and mass specter over the respective Selective Areas / EDS Spots
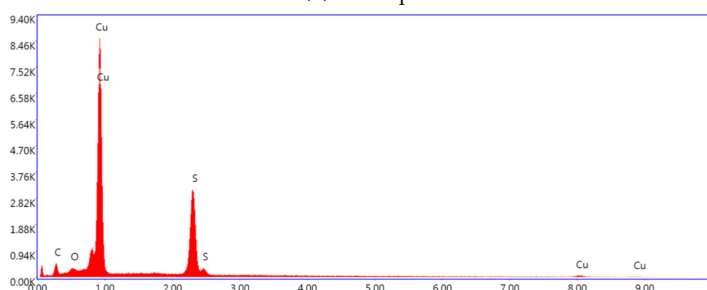
D.3 Chemical mapping of the SR-U
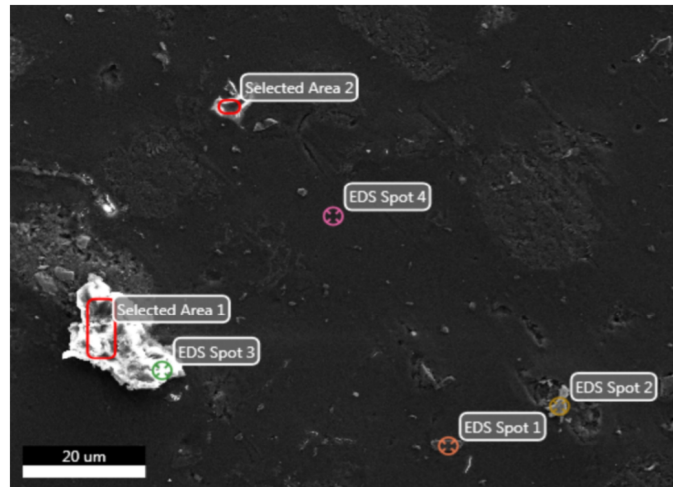
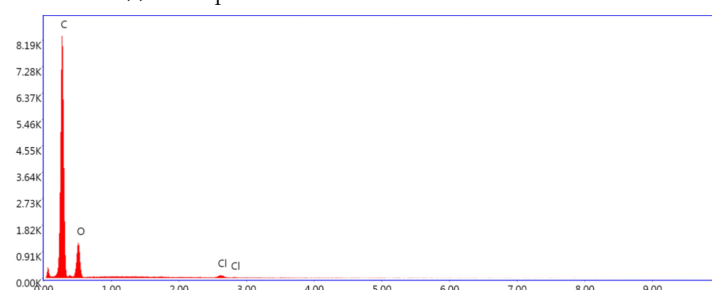**(a)** SR-U: Area 1. Overview of Selected Areas and EDS Spots.
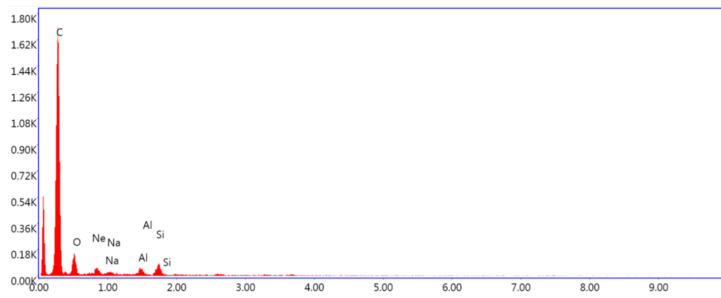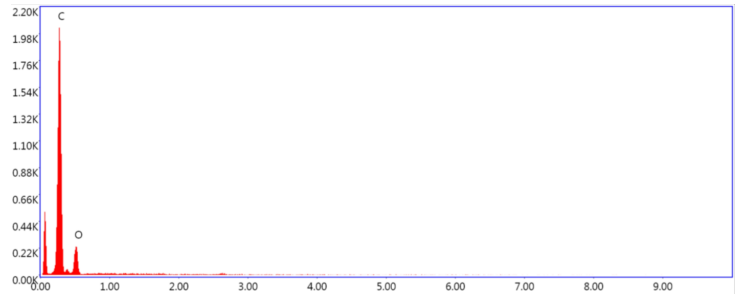
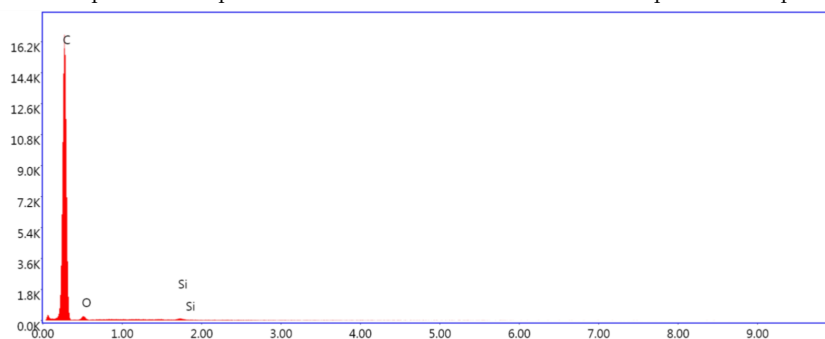**(b)** Mass specter: Selected Area 1

(c) Mass specter: Selected Area 2
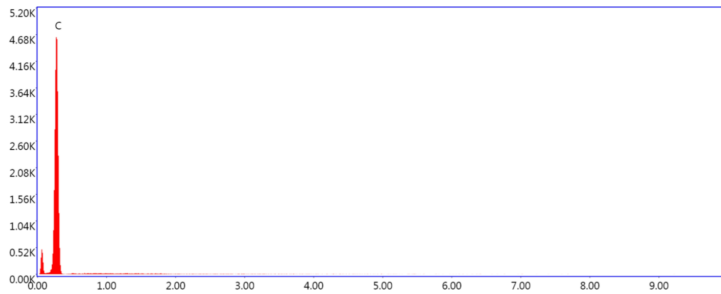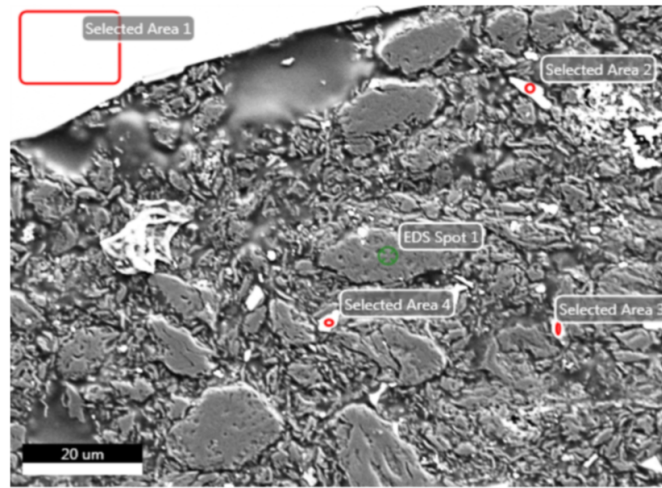

(d) Mass specter: EDS Spot 1
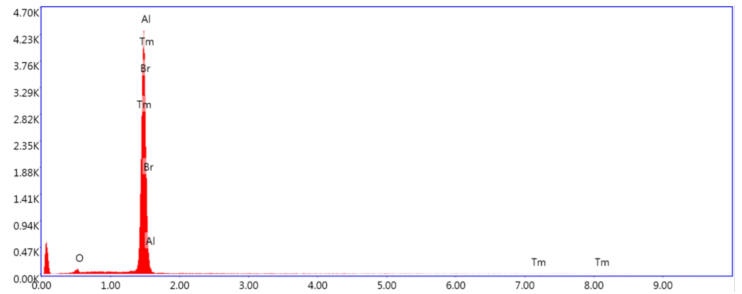
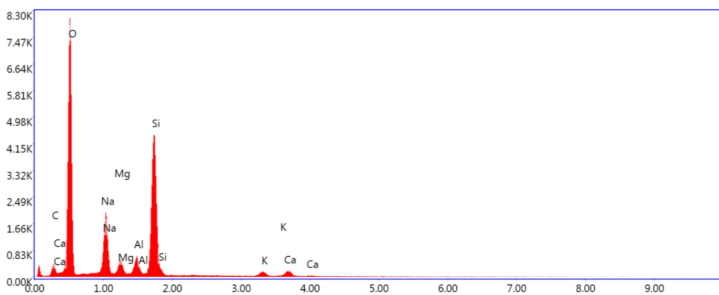**(e)** Mass specter: EDS Spot 2
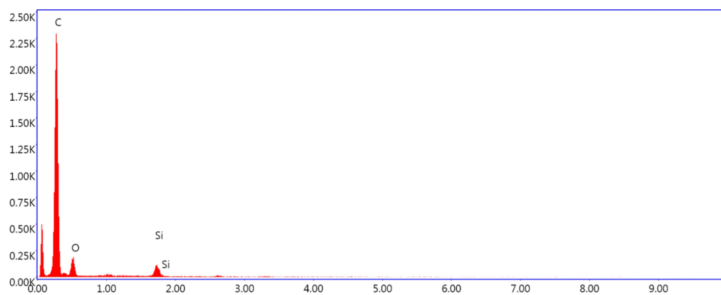
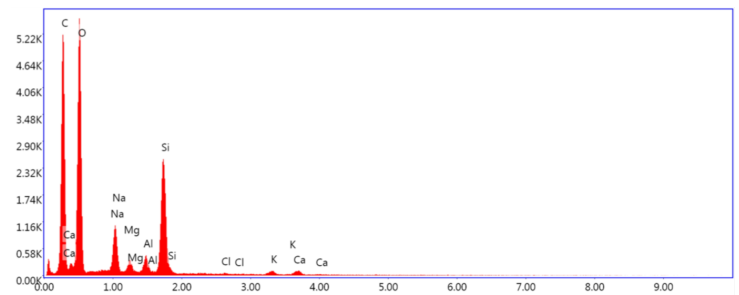**(f)** Mass specter: EDS Spot 3
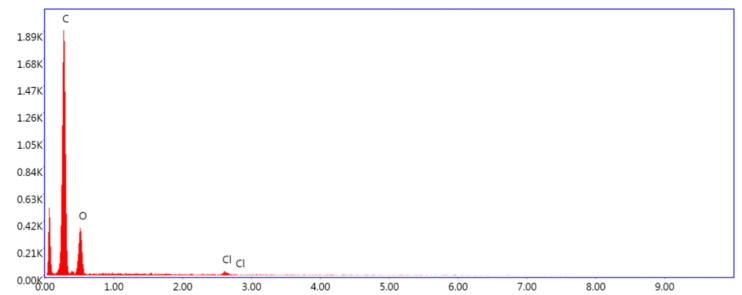
(g) Mass specter: EDS Spot 4

Figure D.3.1: SR-U: Area 1. Overview of EDS areas and spots and mass specter over the respective Selected Area/EDS Spot
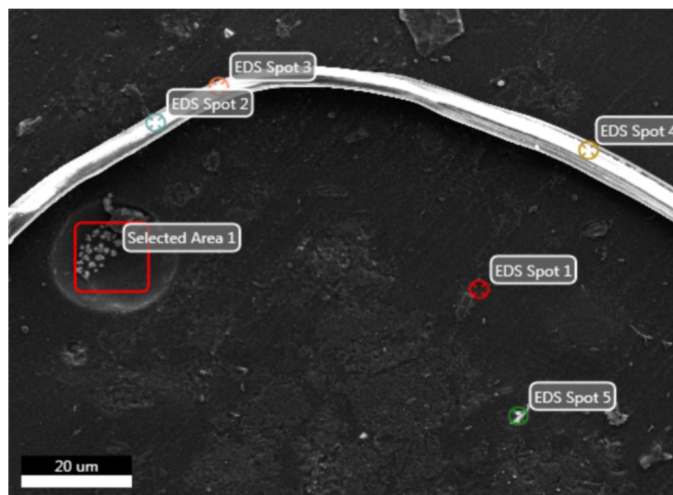
(a) SR-U: Area 2. Overview of Selected Areas and EDS Spots.
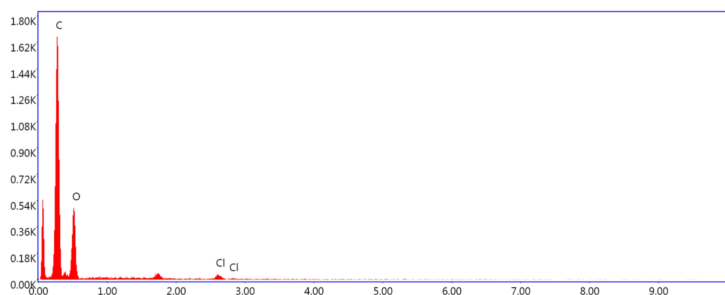
(b) Mass specter: EDS Spot 1
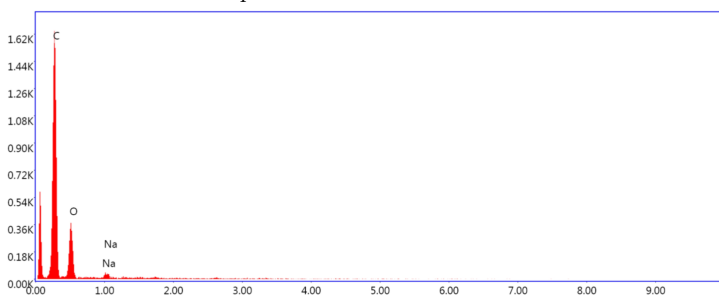
(c) Mass specter: EDS Spot 2
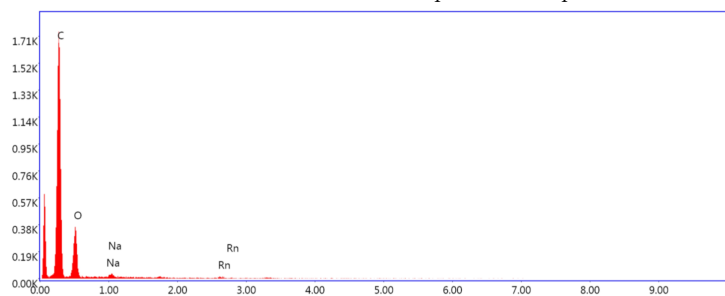
(d) Mass specter: EDS Spot 3
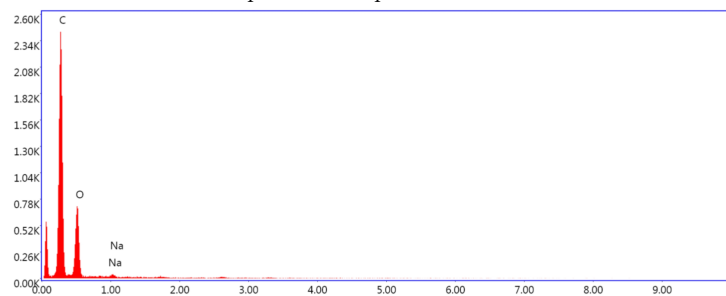
(e) Mass specter: EDS Spot 4
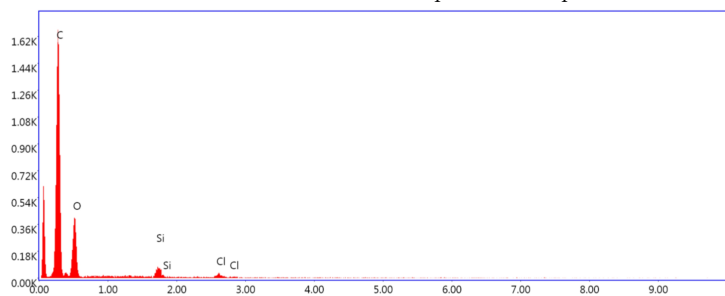
(f) Mass specter: EDS Spot 5
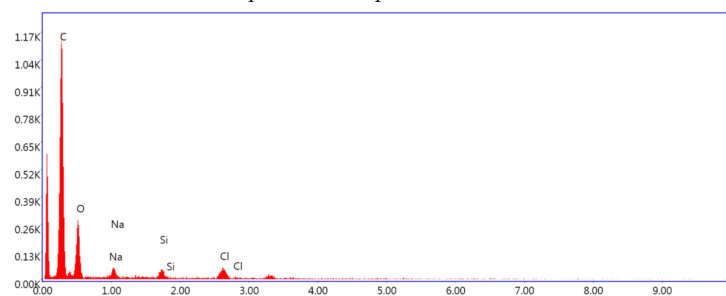
(g) Mass specter: Selected Area 1

Figure D.3.2: SR-U: Area 2. Overview of EDS areas and spots and mass specter over the respective Selected Area/ EDS Spot
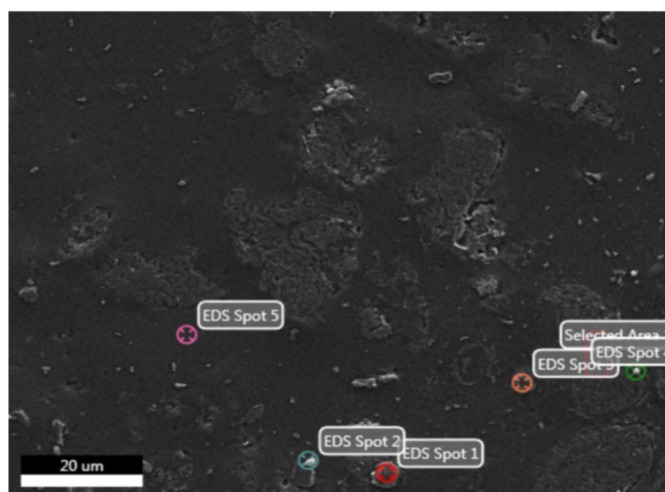
(a) Solid residue: Area 3. Overview of Selected Areas and EDS Spots.
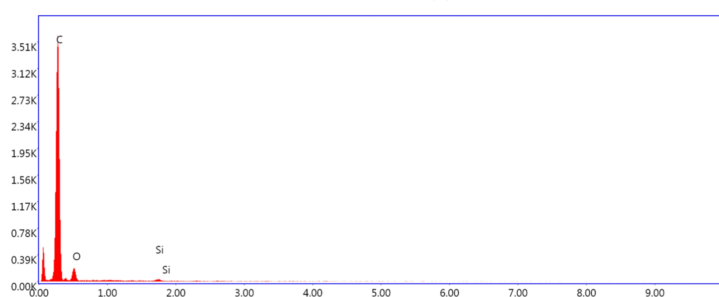
(b) Mass specter: EDS Spot 1
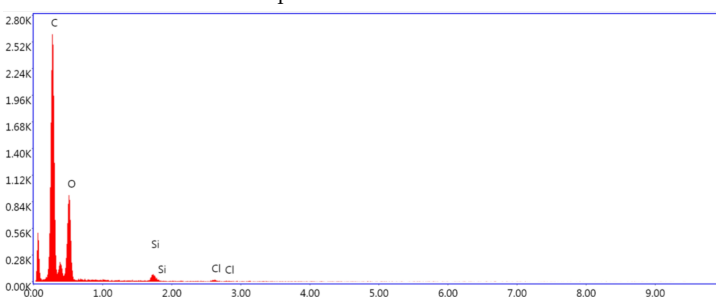
(c) Mass specter: EDS Spot 2
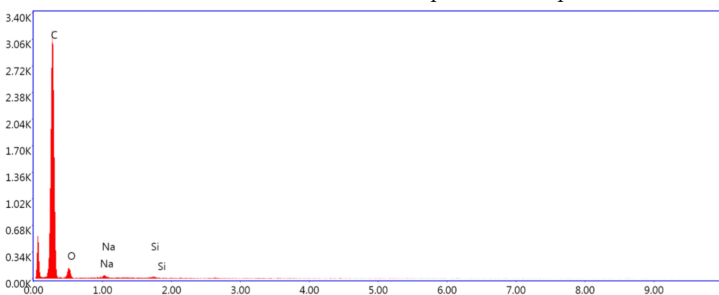
(d) Mass specter: EDS Spot 3
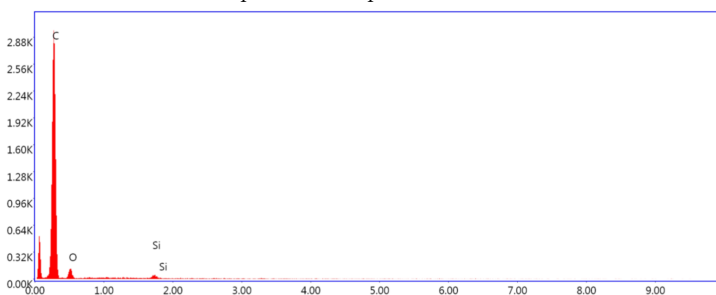
(e) Mass specter: Selected Area 1
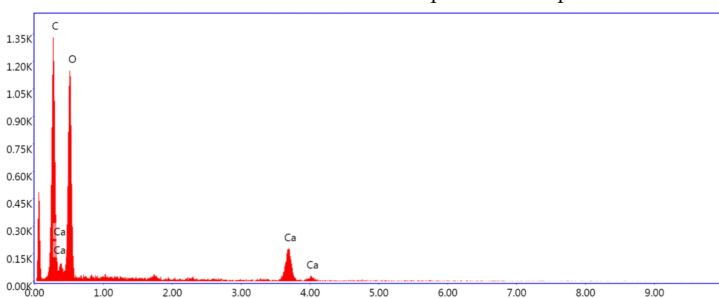
(f) Mass specter: EDS Spot 4
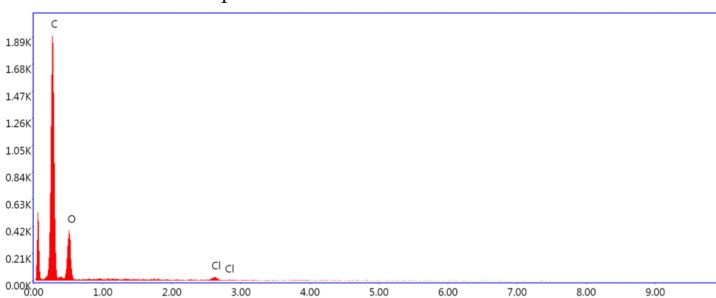
(g) Mass specter: EDS Spot 5

Figure D.3.3: SR-U: Area 3. Overview of Selected Areas and EDS Spots and mass specter over the respective Selected Area / EDS Spot
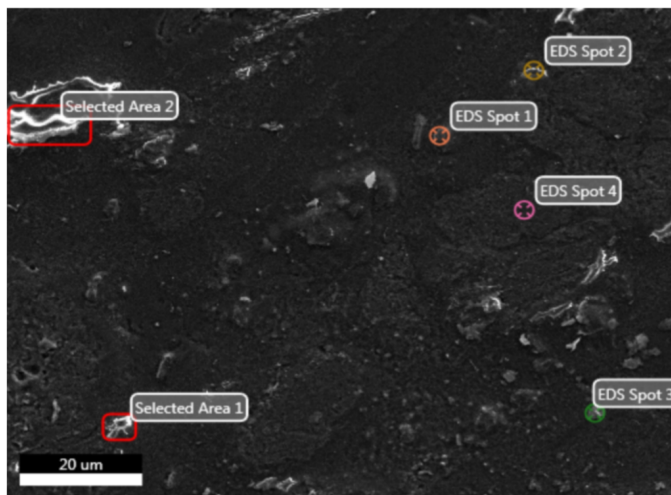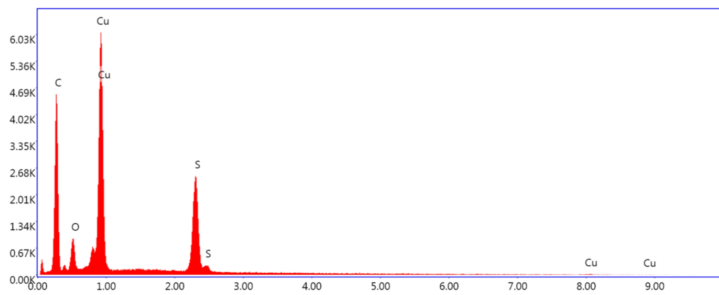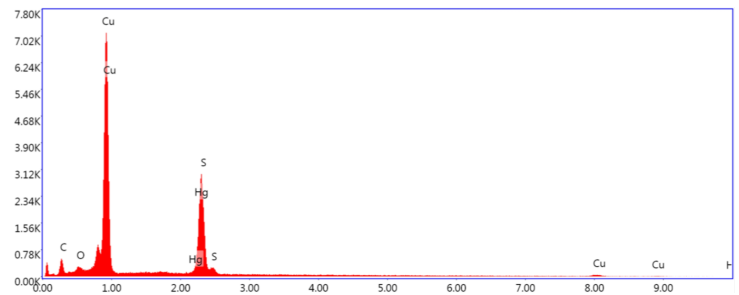
(a) Solid residue: Area 4. Overview of Selected Areas and EDS Spots.
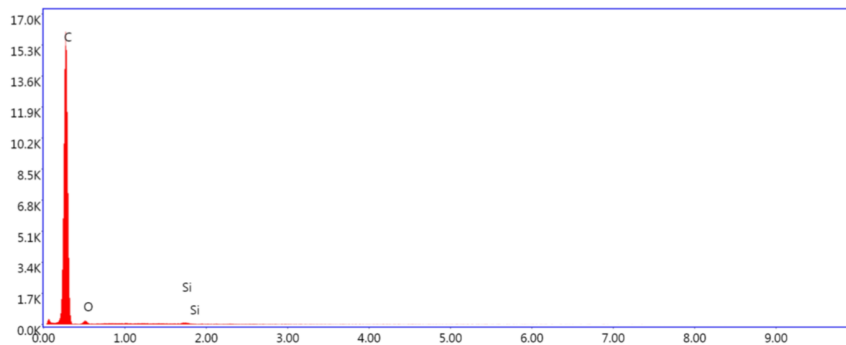

(b) Mass specter: Selected Area 1

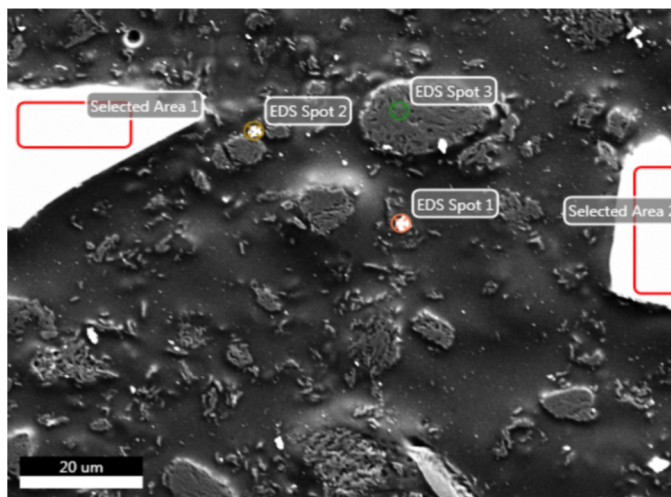**(c)** Mass specter: Selected Area 2

(d) Mass specter: EDS Spot 1

(e) Mass specter: EDS Spot 2

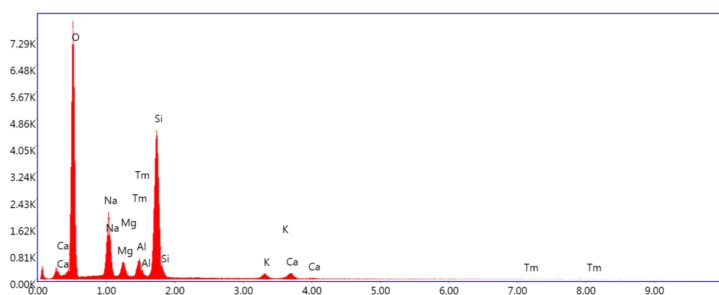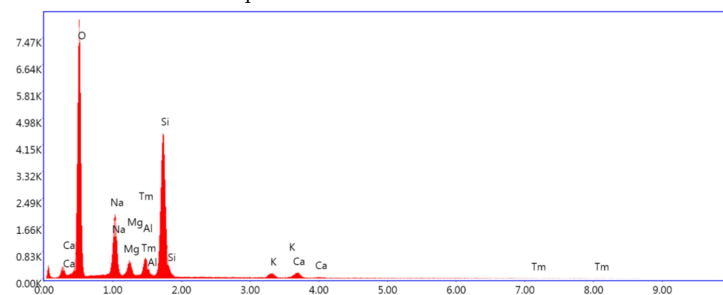**(f)** Mass specter: EDS Spot 3

(g) Mass specter: EDS Spot 4

Figure D.3.4: SR-U: Area 4. Overview of Selected Areas and EDS Spots and mass specter over the respective Selected Area/ EDS Spot

(a) Solid residue: Area 5. Overview of Selected Areas and EDS Spots.

(b) Mass specter: Selected Area 1

(c) Mass specter: Selected Area 2

(d) Mass specter: Selected Area 3

(e) Mass specter: EDS Spot 1

(f) Mass specter: EDS Spot 2

(g) Mass specter: EDS Spot 3

Figure D.3.5: SR-U: Area 5. Overview of Selected Areas and EDS Spots and mass specter over the respective Selected Area/ EDS Spots
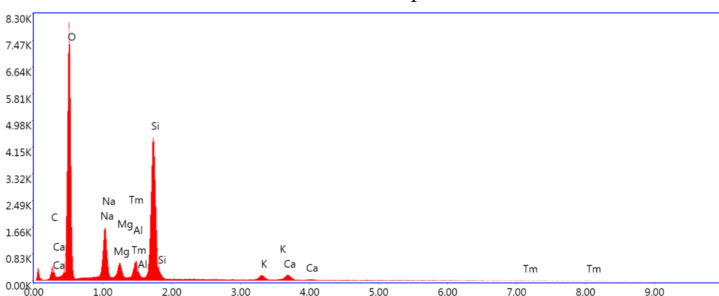
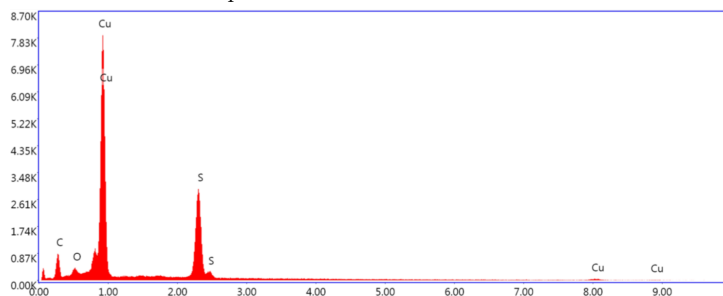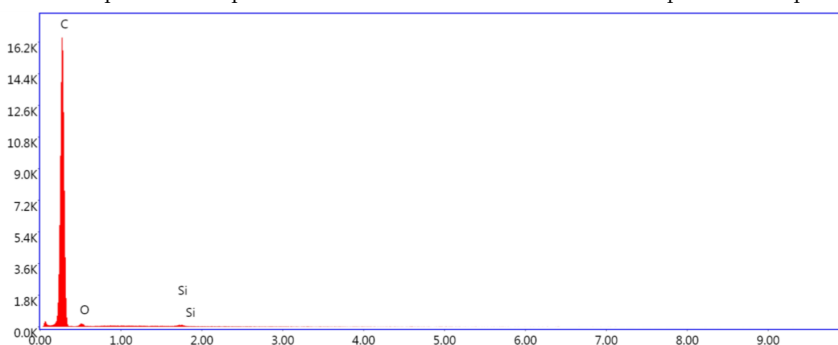**(a)** Solid residue: Area 6. Overview of Selected Areas and EDS Spots.

(b) Mass specter: EDS Spot 1

(c) Mass specter: EDS Spot 2

(d) Mass specter: EDS Spot 3

(e) Mass specter: EDS Spot 4
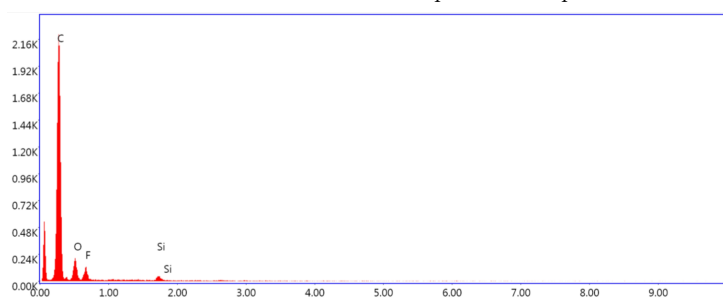
(f) Mass specter: Selected Area 1
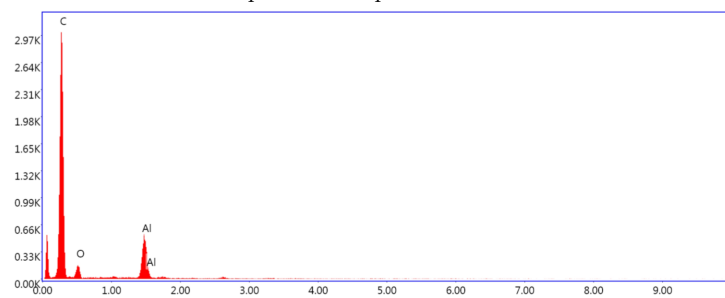
(g) Mass specter: Selected Area 2

Figure D.3.6: SR-U: Area 6. Overview of Selected Areas and EDS Spots and mass specter over the respective Selected Area / EDS Spot

D.4   Chemical mapping of the SR-T
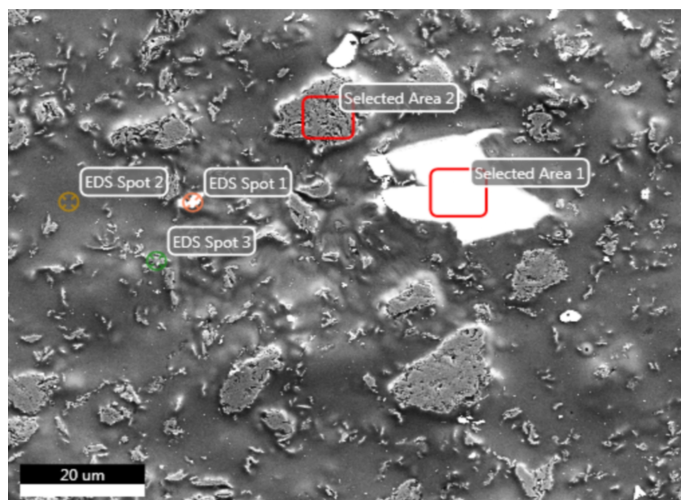
(a) SR-T: Area 1. Overview of Selected Areas and EDS Spots.

(b) Mass specter: Selected Area 1

(c) Mass specter: Selected Area 2
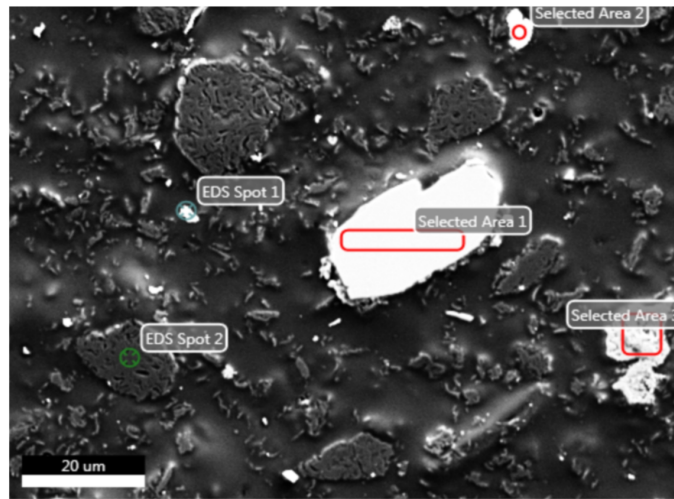

(d) Mass specter: EDS Spot 1
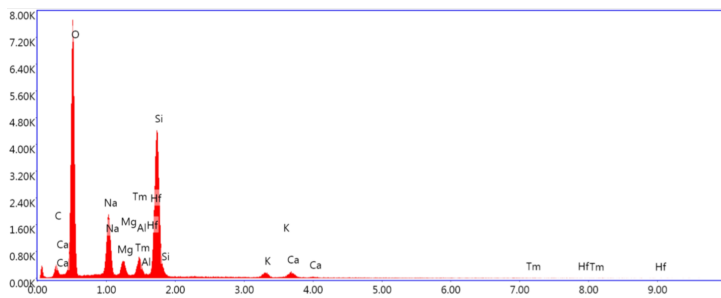

(e) Mass specter: EDS Spot 2

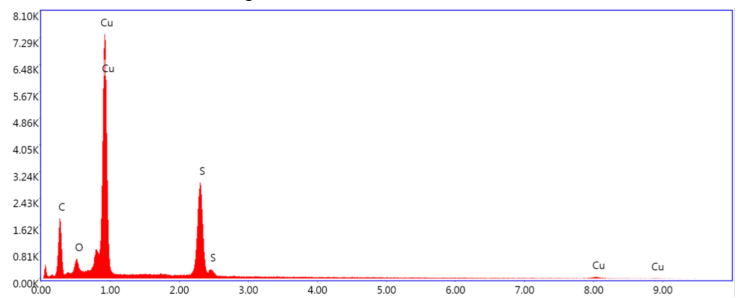

(f) Mass specter: EDS Spot 3

Figure D.4.1: SR-T: Area 1. Overview of Selected Areas and EDS Spots and mass specter over the respective Selected Areas / EDS Spots
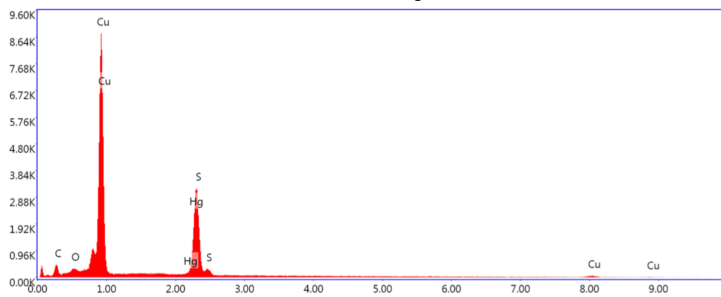
(a) SR-T: Area 1. Overview of Selected Areas and EDS Spots.

(b) Mass specter: Selected Area 1

(c) Mass specter: Selected Area 2

(d) Mass specter: Selected Area 3

(e) Mass specter: Selected Area 4

(f) Mass specter: EDS Spot 1

Figure D.4.2: SR-T: Area 2. Overview of Selected Areas and EDS Spots and mass specter over the respective Selected Areas / EDS Spots

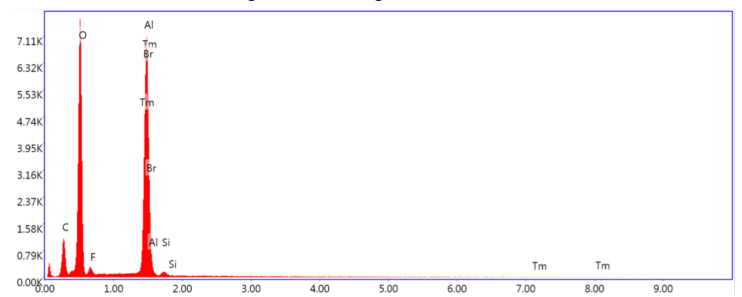(a) SR-T: Area 3. Overview of Selected Areas and EDS Spots.
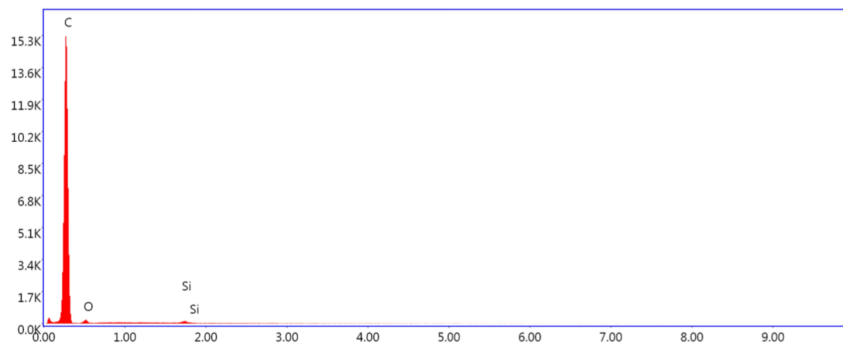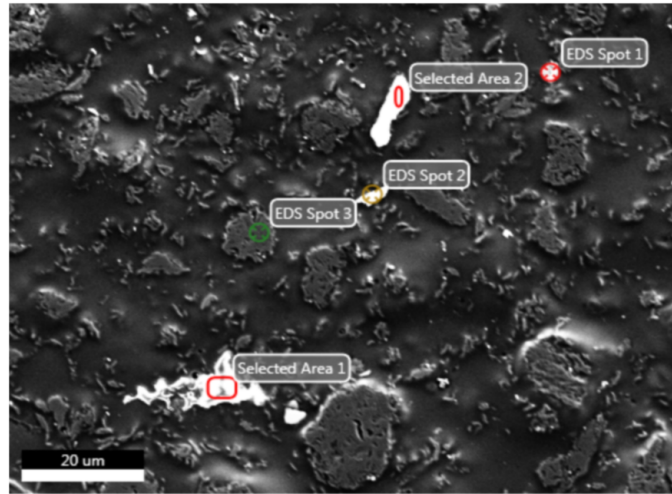

(b) Mass specter: Selected Area 1

(c) Mass specter: Selected Area 2

(d) Mass specter: EDS Spot 1

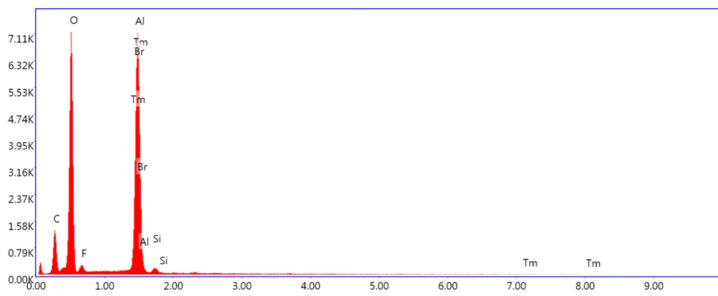(e) Mass specter: EDS Spot 2

(f) Mass specter: EDS Spot 3

Figure D.4.3: SR-T: Area 3. Overview of Selected Areas and EDS Spots and mass specter over the respective Selected Areas / EDS Spots

(a) SR-T: Area 4. Overview of Selected Areas and EDS Spots.

(b) Mass specter: Selected Area 1

(c) Mass specter: EDS Spot 1

(d) Mass specter: Selected Area 2

(e) Mass specter: Selected Area 3

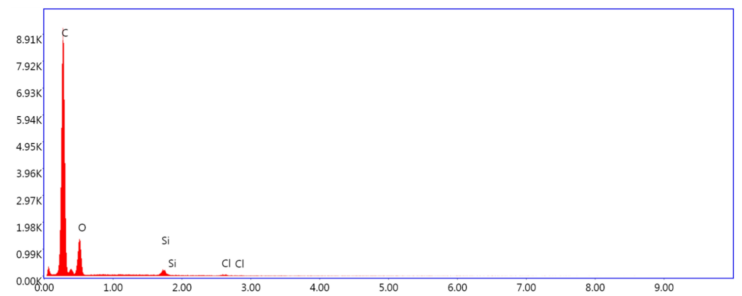**(f)** Mass specter: EDS Spot 2

Figure D.4.4: SR-T: Area 4. Overview of Selected Areas and EDS Spots and mass specter over the respective Selected Areas / EDS Spots
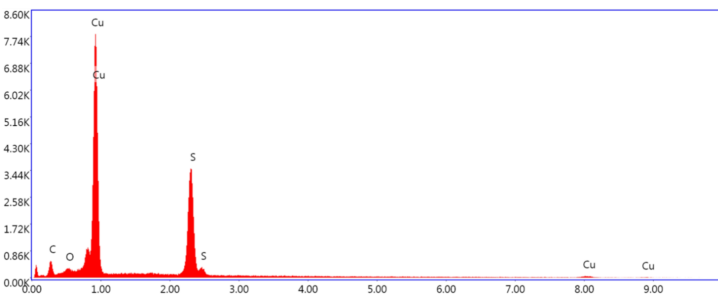
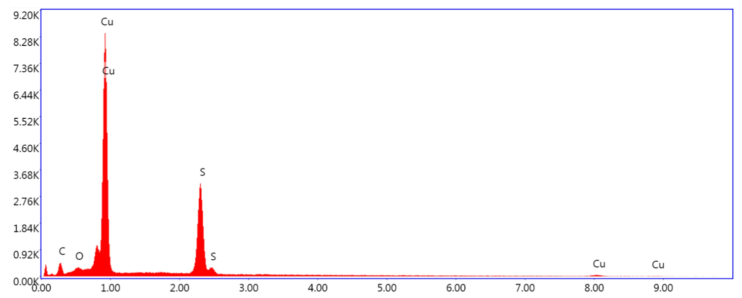**(a)** SR-T: Area 5. Overview of Selected Areas and EDS Spots.
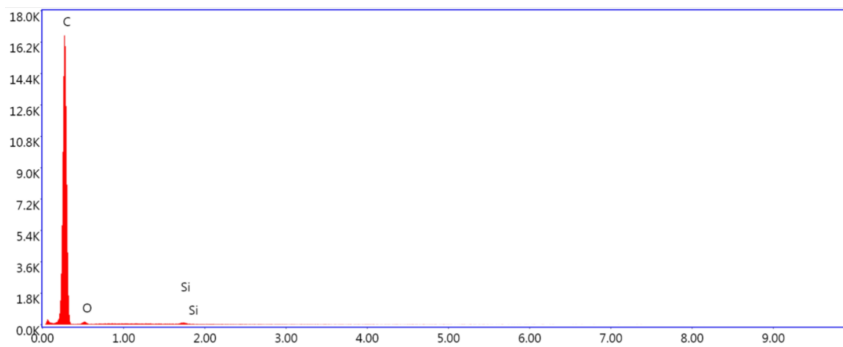

(b) Mass specter: EDS Spot 1

(c) Mass specter: Selected Area 1

(d) Mass specter: Selected Area 2

(e) Mass specter: EDS Spot 2

(f) Mass specter: EDS Spot 3

Figure D.4.5: SR-T: Area 5. Overview of Selected Areas and EDS Spots and mass specter over the respective Selected Areas / EDS Spots

(a) SR-T: Area 5. Overview of EDS areas and spots.

(b) Mass specter: Selected Area 1

(c) Mass specter: EDS Spot 1

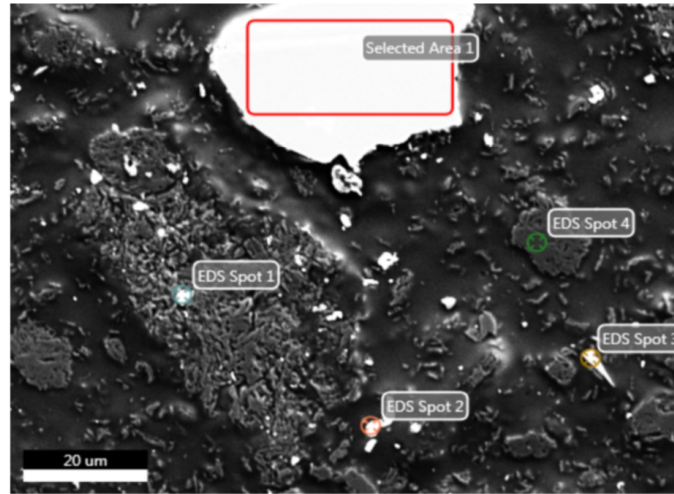**(d)** Mass specter: EDS Spot 2

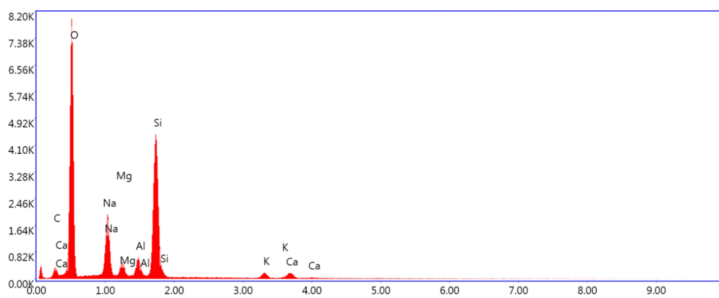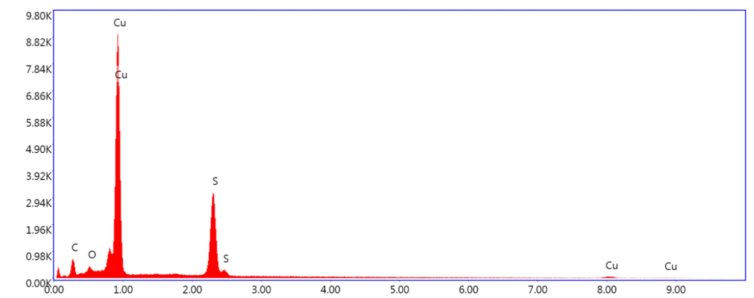**(e)** Mass specter: EDS Spot 3

(f) Mass specter: EDS Spot 4

Figure D.4.6: SR-T: Area 6. Overview of Selected Areas and EDS Spots and mass specter over the respective Selected Areas / EDS Spots
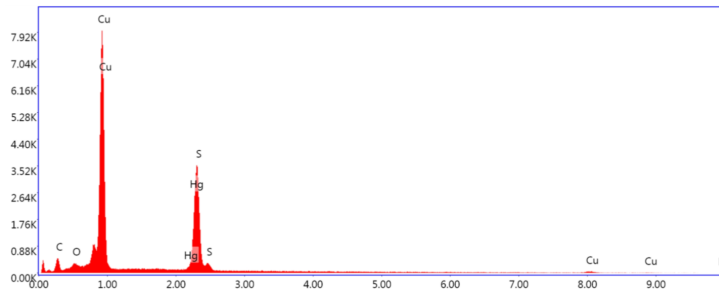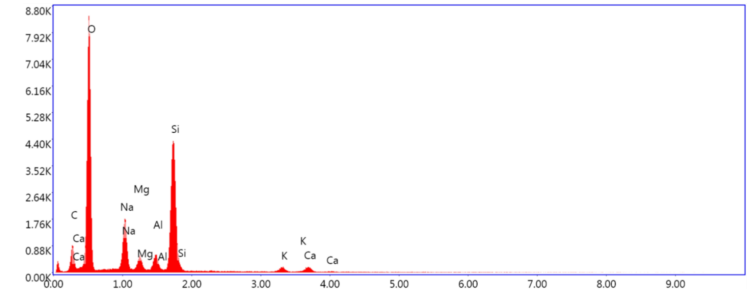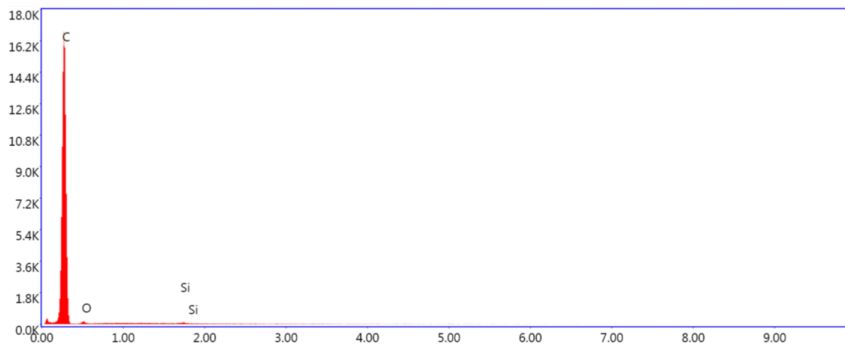
E | Risk assessment

Unit/Institute:	IMA						Date:	02/02/2022	
Responsible line manager (name):	Einar Hjorthol						Revised:		
Responsible for activities being risk assessed (name):	Amalie My Olsen								
Participants in the risk assement (names):	Amalie My Olsen, Ragnhild Elizabeth Aune, Daniel Perez Clos, Robert Fritzsch and Hannes Zedel								
Available contact person(s) during lab work (name):	Ragnhild Elizabeth Aune, Daniel Perez Clos, Robert Fritzsch and Hannes Zedel								

Activity / process	Unwanted incident	Existing risk reducing measures	Probability (P)	Consequence (C) Evaluate the categories individualley. *Health should always be evaluated.*				Risk value (P x C)	Risk reducing measures - suggestions	Residual risk after measures being implemented (S x K)
			(1-5)	Health (1-5)	Material values (1-5)	Environment (1-5)	Reputation (1-5)		Measures reducing the	
Sample preparation - making epoxy (EpoFix Resin og Hardener)	Epofix resin: give allergic reaction, serious eyeirritation and poisonous for life in water. Epofix hardener: dangerous if swallowed or with skin contact, give serious etching damage on skin and eye, can give allergic reaction on skin, can damage life in water.	Gloves, glasses and fumehood	1	2				2		
Sample preparation - polishing	Can cut fingers	Be careful to not touch the machin while it´s working	1	2				2		
Sample preparation - black mass/ solid residue powder	Nanoparticle content (below 2 wt%) - can be a breathable hazard	Use gloves, glasses and work in fumehood	1	1				1		
Leaching experiments of black mass	Nanoparticle content (below 2 wt%) - can be a breathable hazard	Use gloves, glasses and work in fumehood	1	1						
	Hydrogenperoxide: Dangerous if swallowed. Damaging to the eyes. Can irritate mucous membranes.	Use glasses and fumehood to prevent inhalation.	1	2				2		
	Sulfuric acid: Highly corrosive. Storng reaction with water and alcohol.	Do not add water to the acid. Use gloves and glasses.	1	2				2		
	Mixing water and acid: If water is added to the acid it can begin to boil and splash concentrated acid causing damage to the skin, clothes and eyes.	Always add the acid to water and preferably in small amounts. Juse gloves, glasses and lab coat.	1	2				2		

Amalie My Olsen

Leaching and Modelling of LIB BM for Metal Recovery

NTNU
Norwegian University of
Science and Technology